

104

CLASSIFICATION CHANGED
TO Unclassified
BY DD254 R.F. Rodger
DATE 16 August 1985
G. Patterson
7-15-87

WIND TUNNEL INVESTIGATION OF
THE FLUCTUATING PRESSURES ON THE SURFACE
OF A SATURN I VEHICLE, 2.75% MODEL (U)

AUGUST 1963
DOUGLAS REPORT SM-44148

MISSILE & SPACE SYSTEMS DIVISION
DOUGLAS AIRCRAFT COMPANY, INC.
SANTA MONICA/CALIFORNIA

FACILITY FORM 602

N70-76126	(THRU)
(ACCESSION NUMBER)	NONE
149	(CODE)
(PAGES)	
CR-113275	(CATEGORY)
(NASA CR OR TMX OR AD NUMBER)	



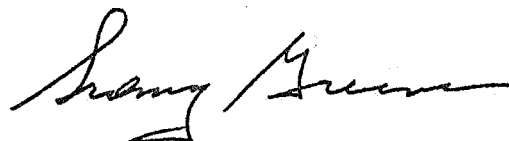
CONFIDENTIAL

WIND TUNNEL INVESTIGATION
OF THE FLUCTUATING PRESSURES ON THE SURFACE
OF A SATURN I VEHICLE, 2.75% MODEL (U)

AUGUST 1963
DOUGLAS REPORT SM-44148

PREPARED BY: C.M. AILMAN
ACOUSTICS AND STRUCTURAL DYNAMICS

PREPARED FOR:
NATIONAL AERONAUTICS AND
SPACE ADMINISTRATION
UNDER NASA CONTRACT NAS7-1



APPROVED BY: S. GREENE
CHIEF, S-IV SYSTEMS ENGINEERING

REPLACEMENT OF THIS DOCUMENT BY AN UNCLASSIFIED PERSON IS PROHIBITED BY LAW

12 YEAR

DOUGLAS MISSILE & SPACE SYSTEMS DIVISION

~~CONFIDENTIAL~~

ABSTRACT

A wind tunnel test was performed to measure the fluctuating pressures at the surface of a 2.75% model of the Saturn I vehicle -- SA5 configuration (as of October, 1962). Overall levels and octave band spectrum shapes are reported and analyzed for 10 Mach numbers (0.8 - 3.5) at various angles of attack (from -8° to $+8^{\circ}$). Details of the test plan and procedures as well as descriptions of the various calibrations which were necessary are included. Extrapolation to full-scale conditions indicate considerable boundary layer energy is available over a wide frequency range during forty to fifty seconds of the proposed Saturn exit trajectory. Further studies are therefore warranted to determine the extent of structural response to boundary layer excitation -- this aspect not being covered in the report.

CONFIDENTIAL

PREFACE

This document constitutes the final report of phase one of the 2.75% model scale Saturn wind tunnel test, and covers the study of fluctuating pressures at the surface of the model. It is partial fulfillment of Scope Change 124 of NAS7-1 contract. The test was performed by Douglas personnel in the Douglas Aerophysics Laboratory, El Segundo, California.

CONFIDENTIAL

TABLE OF CONTENTS

	<u>Page</u>
ABSTRACT	iii
PREFACE	v
1.0 INTRODUCTION	1
2.0 TEST APPARATUS	3
2.1 Facilities	3
2.2 Models	4
2.3 Instrumentation	4
3.0 TEST PROCEDURES	7
3.1 Test Conditions	7
3.2 Calibrations and Resultant Corrections	8
3.2.1 Wind Tunnel	8
3.2.2 Transducers	9
3.2.3 Amplifiers	10
3.2.4 Systems	10
3.2.5 Recorders	11
3.2.6 Data Reduction Equipment	11
3.3 Precision of Measurements	11
3.4 Data Reduction	12
4.0 ANALYSIS OF RESULTS	13
4.1 Spatial Distribution of FPL's	13
4.2 Repeatability	15
4.3 Angle of Attack Dependency	17
4.4 Spectra	19
4.5 Explanation of the Low FPL's	20
4.6 Comparison With Other Measurements	21
4.7 Static Pressure Data	24

TABLE OF CONTENTS (Cont'd)

	<u>Page</u>
5.0 CONCLUSIONS	27
REFERENCES	29
APPENDIX A	31

LIST OF ILLUSTRATIONS

<u>Figure Number</u>		<u>Page</u>
1	A Rigid 2.75% Saturn I Model Without Protuberances . . .	34
2	Detachable Protrusions for the Saturn Model	35
3	Detachable Apollo Abort Tower and Escape Rocket Model .	36
4	Complete Model of the Saturn I Vehicle (2.75%)	37
5	The Flight Vehicle Modified by a 20° Fairing at the SI/S-IV Juncture	38
6	Geometry of the Atlantic Research Model ID 80-M1 Transducer	39
7	Location of the Measurements for Phase I of the 2.75% Model Saturn I Wind Tunnel Pressure Test	40
8	Rear View of the Flat Plate Showing the Fairing Over the Transducer Case and Lead	41
9	Hemisphere Used to Calibrate the Wind Tunnel	42
10	Apparent Noise Levels in the Center of the Douglas Aerophysics Lab 4' x 4' Trisonic Tunnel	43
11 through 18	Apparent Wind Tunnel Noise Spectrum Shapes	44
19	Typical ID 80-M1 Vibration Response at 1G RMS Sine Wave Input	52
20	Vibration Sensitivity of the ID 80-M1's to a 2G Sine Wave Input	53
21 through 48	Overall Fluctuating Pressure Level Distribution Over the 2.75% Saturn Model	54
49	Repeatability of the Data on the A Configuration	82
50	Repeatability of the Data on the B Configuration	83
51	Comparison of Two Transducers 180° Apart at Station Number 1637 for Different Configurations	84
52 through 55	Shock on the Forward Interstage of the S-IV Stage . . .	85

LIST OF ILLUSTRATIONS (Cont.)

<u>Figure Number</u>		<u>Page</u>
56 through 63	Variation of Spectrum Shape with Angle of Attack α . . .	89
64	Overall Fluctuating Pressure Level Distribution in Fin Plane II of Configuration A vs. Mach Number	105
65	Overall Fluctuating Pressure Level Distribution in Fin Plane II of Configuration B vs. Mach Number	106
66	Overall Fluctuating Pressure Level Distribution in Fin Plane II of Configuration C vs. Mach Number	107
67 through 69	Shadowgraph of the B Configuration	108
70 through 75	Variation of Spectrum Shape with Angle of Attack	111
76	Percent of Model Fluctuating Pressure Measurements Greater than the Apparent Noise Levels of the Wind Tunnel	123
77 through 82	Non-Dimensionalized Uncorrected Spectra of the Pressure at the Surface for "Well-Behaved" Model Flow	124
83	Time History of SA-4 Fluctuating Pressure Levels and Comparison with 2.75% Scale Model Wind Tunnel Measurements	130
84	Shadowgraph Showing the Influence of the Hydrogen Chill Down Duct at Mach 1.6	131
85	Comparison of SA-4 Flight Data and 2.75% Scale Model Wind Tunnel Data During Max q	132
86	Comparison of SA-4 Measurement at Maximum Levels with 2.75% Model Scale Data	133
87 through 91	Comparison of Static Pressure Coefficients Measured On Saturn I Models	134
92	Typical Pressure Calibration of an LD 80-M1	139
93	Diffraction Correction Curves	140

1.0 INTRODUCTION

Preliminary estimates of in-flight fluctuating pressure levels near certain protuberances at the exterior surface of the Saturn I space vehicle indicated the possibility of an extremely severe environment. Since no precise measurements were available from similar areas of other vehicles, and in the absence of theoretical methods, it was deemed advisable to perform a detailed study based upon a model scale test in a wind tunnel.

The study was funded by NASA and was planned and executed by the Douglas Aircraft Company with the cooperative support of the Experimental Aerodynamics Section of the Aeroballistics Division of the Marshall Space Flight Center at Huntsville, Alabama. The test was performed in the Douglas Aerophysics Laboratory's 4' x 4' trisonic wind tunnel in November of 1962.

This document discusses the preparation, performance, and results of phase one of the model scale wind tunnel test (measurement of the fluctuating pressure at the surface of a 2.75% scale Saturn vehicle). A data supplement is available on request which quotes the actual data obtained and the corrections for calibrations, the recorder attenuator settings, and the data for any invalidated runs.

0 TEST APPARATUS

2.1 Facilities

The Douglas Trisonic wind tunnel is a well equipped facility with adequate shop equipment and personnel to properly maintain and modify a model (ref. 1). The four foot tunnel has two interchangeable test sections, either of which may be installed in less than eight hours. The supersonic section is 60 inches in length and the transonic 144 inches in length. Each of the test sections contains two 30 inch clear view windows arranged on the model centerline so that shadowgraphs or schlieren photographs may be made. Film processing is done at the tunnel so that the results may be viewed between runs. The model support structure is so arranged that a pitch range of -15° to $+25^{\circ}$ and rolls up to 185° can be accomplished without opening the tunnel.

The attachment of the model to the model support structure is done by a hollow cylindrical sting, allowing the leads from the model instrumentation to be routed out of the tunnel without being exposed to the tunnel airflow.

The static pressure tap leads are routed to a pressure scanning switch which allows the selection of preset groups of pressure points to be read simultaneously. This information is then routed to an automatic recording system. This recording system receives data from various kinds of sensors and prepares punched cards detailing the measured static pressures, tunnel total pressures, tunnel temperature, free stream pressure, Reynolds number, and dynamic pressure (q) of the flow, as well as angles of attack and roll. Leads carrying electrical signals from the fluctuating pressure transducers mounted in the model are routed to rack mounted amplifiers located below the test section of the tunnel, where the signals may be controlled for level. From the output of the amplifiers the signals are fed to tape recorders located, with the automatic recording equipment, in the tunnel control room. Further details of these test mechanics are given in ref. 2.

2.2 Models

For this fluctuating pressure test, three configurations were examined. One basic model was constructed which incorporated sufficient versatility to suffice for each of the different configurations studied. The model was a 2.75% rigid model of the Saturn I vehicle consisting of two calibers of the S-I stage, the S-IV stage, the guidance and control package, and the Apollo nose cone (see Figure 1). Attachable to the basic model were all the protrusions on the vehicle such as retro rockets, camera packs, hydrogen chill down ducts, ullage rockets, antenna panel, etc., as well as the abort tower on top of the vehicle (see Figures 2 and 3).

The first configuration tested (configuration A) was the basic model devoid of all protrusions except for the abort tower and rocket which were attached (Figure 1). The second configuration (configuration B) was composed of the basic model plus every external part, fairing, or protrusion characteristic of the SA5 flight vehicle as its design was fixed in October of 1962 (including the wedge shaped fairings for the exposed I beam ends, see Figure 4). The third and last configuration (configuration C) tested during this first phase of a Saturn vehicle pressure study, was the configuration B modified by a 20° fairing covering the SI/S-IV juncture (see Figure 5).

The only other model modification made which was not discussed above, was incorporated in the B configuration studies. This further change consisted of checking the effects in fluctuating pressure levels over the whole surface of the model of (1) a disc with a diameter 2-1/2 times that of the abort rocket placed near the rocket's tail (see Figure 3) and (2) of varying the angle of the abort rocket's tail fairing. The results of these tests are discussed in Part IV of this report.

2.3 Instrumentation

The instrumentation system used to measure and record the fluctuating pressure data on the models consisted of the following items (see ref. 3):

- 45 Model ID80-M1 Atlantic Research Transducers
- 3 Model 6006 Columbia Research Amplifiers (18 channels)
- 3 Model 6003 Columbia Research Amplifiers (9 channels)
- 45 Model CFP-IN-30 Extension Probes
- 1 Ampex Model CP100 Tape Recorder - 14 track
- 1 Sangamo Model 471RB Tape Recorder - 14 track

This system was the result of an intensive search of the equipment available in each category, and in the case of the transducers, an instrumentation development program.

By surveying the commercially available transducers, it was determined that a transducer embodying the following characteristics did not exist:

1. Small diaphragm area to prevent pressure cancellation of small high frequency eddies
2. High natural frequency of resonance
3. Adequate sensitivity
4. Capability of handling large amplitude fluctuations
5. Suitable encasement to allow flush mounting in the model and close center to center spacing between adjacent transducers.

Several companies expressed a willingness to develop such a transducer if the Douglas Company would provide assistance; however, time did not permit this type of program.

Several companies proposed modifications to existing transducers. Three of these companies were requested to submit samples of the units they proposed to modify, and these sample units were tested and evaluated. Two of these transducers were piezo-electric, the third was an RF suppressed carrier capacitance type. The modifications necessary to each unit were detailed by Douglas. These consisted basically of a reduction of diaphragm area, raising the natural frequency of resonance, and a reduction of overall size. As a consequence of the evaluation, it was decided not to proceed with the modification of the capacitance type transducer because, in order to achieve the overall reduction in size necessary, the RF carrier frequency would have to be shifted. This would have entailed modification of the electronics package as well as the transducer,

which would have been expensive and time consuming. A parallel development of the remaining two piezo-electric transducers was instigated by the Douglas Company in close cooperation with the two companies involved. Several approaches to the solution of the problems were discussed with each of the companies. Prototype units were fabricated and tested until a satisfactory solution was achieved. The Atlantic Research Corporation at Alexandria, Va., following the suggestions advanced by the Douglas Company, was successful in modifying their model ID80 transducer to meet most of the objectives desired. Forty five of the new transducers, bearing model number ID80-M1 were ordered for the test. The transducers were $3/8$ inches in overall diameter, with a $3/8 \times 24$ threaded external case (see Figure 6). The sensing element was a lead zirconate crystal approximately .060 inches in diameter.

With the selection of the transducer completed, the amplifier requirements were determined. A data search was made, and where available, samples of amplifiers were obtained and tested. Size not being a major consideration, there was considerable choice available. It had earlier been determined that with 43 transducers installed, it would not be possible to locate the amplifiers internally in the model.

The final choice was a Columbia Research Laboratories Model Series 6000 amplifier along with a thirty foot low-loss driven shield extension probe designed to operate with the amplifier. This choice allowed the location of the amplifiers outside the wind tunnel test section with a total loss due to cabling of 6 db (compensation for this 6 db loss was made by correcting the equivalent voltage response of the transducer).

~~CONFIDENTIAL~~

3.0 TEST PROCEDURES

3.1 Test Conditions

Each of the three configurations described in Section 2.2 above, was tested at nine angles of attack at each of nine Mach numbers. The angles were -8° , -6° , -4° , -2° , 0° , $+2^{\circ}$, $+4^{\circ}$, $+6^{\circ}$, and $+8^{\circ}$; the Mach numbers were 0.8, 0.9, 0.95, 1.00, 1.05, 1.2, 1.6, 1.8, and 2.0. In addition, configuration B was tested at 0° and $+2^{\circ}$ for a Mach number of 3.5 and for a 45° roll at Mach number 1.6 (for all the prescribed nine angles of attack).

Five shadowgraphs were taken during most runs at the angle of attack positions -8° , -4° , 0° , $+4^{\circ}$, and $+8^{\circ}$. Two fourteen-track tape recorders provided twenty-four simultaneous data tracks during each run (the other four tracks being used for synchronization and voice cueing) on which fluctuating pressure information measured at the surface of the model was recorded (see Figure 7 for model measurement locations). Thirteen static pressure transducers were also in operation for each run. Two vibration pickups were mounted in the model so that any contribution from mechanical excitation in the recorded pressure data would become evident. Wind tunnel data were measured and recorded separately, providing basic data such as free stream pressure, Reynolds number, temperature, Mach number, and pitch, yaw and roll angles of the model (see ref. 2).

Easy access to the model, its many attachments and/or its internal instrumentation was available at any time. Daily calibrations and constant visual checks monitored the physical aspects of the test in addition to the data monitoring.

Duplicability and data checks show validity of a considerable quantity of the data. Further elaboration of this statement is contained in section 4.0 (analysis of results).

~~CONFIDENTIAL~~

3.2 Calibrations and Resultant Corrections

To ensure data accuracy, several different calibration techniques had to be employed for this test. These calibrations are enumerated and discussed below.

3.2.1 Wind Tunnel

It was necessary to determine the apparent noise of the wind tunnel in the vicinity of the model measurement positions, but without the model mounted in the tunnel. Such a calibration enables one to differentiate between (1) a measurement of fluctuating pressure levels at the surface of the model induced by the turbulent boundary layer (itself produced by the presence of the model) and, (2) a fluctuating pressure level partially or predominately induced by the apparent wind tunnel noise. This apparent wind tunnel noise includes the direct and reflected acoustic pressures as well as pressure fluctuations induced by turbulence in the flow.

There are two different basic techniques by which the levels of the apparent noise in a wind tunnel can be measured. In the first case, a small housing for the sensing transducer is constructed so as to cause a minimum influence on the flow over the sensing element (see Figure 8). To keep the sensing element in laminar flow, the transducer is mounted near the leading edge of the plate. The back side of the leading edge is canted so that at most speeds the shock wave is attached to that side of the plate (not affecting the flow over the sensing element of the transducer). Also, buried transducers (in blind holes) verify the premise that no vibratory motion is contributing to the measured data. In the second case, the flow characteristics are modified by the presence of the calibration body (a hemisphere facing the flow with the transducer at the stagnation point) but in a predetermined and calculable manner (see Figure 9). For the Saturn wind tunnel test, one of each of these types was constructed and tested. Each was superior in certain frequency ranges and certain Mach regions. The resultant calibration is plotted in Figure 10 with typical spectra in Figures 11 to 18. Substantial

energy is present in the 5000-10,000 cps range of frequencies. Other measurements in the tunnel verify the presence of this energy, but its exact origin is unknown at this time. An effective acoustical filter had been installed between the control valve and the test section at the inception of operation of this trisonic wind tunnel. Since the frequency of this extra energy does not appear dependent on Mach number (as would be the case if the control valve were the source and the acoustic filter was ineffective) the actual source of this energy is probably the boundary layers at the four perforated walls.

3.2.2 Transducers

The model ID80-M1 transducers were qualified for use in the test in three separate calibration procedures. Atlantic Research performed a linearity and sensitivity calibration of the transducers with their variable pressure or dead weight static pressure type calibrator. After delivery, the Douglas Company performed a low frequency acoustic calibration, using a Ling Altec model 12185, Microphone Calibrator, from 30 cps to 3000 cps. The Ling Temco Vought (L.T.V.) Research Center performed a high frequency acoustic calibration from 200 cps to 100,000 cps. This was a comparison type calibration using as a reference a Bruel & Kjaer 1/4" diameter microphone, model number 4136 (see Appendix A). The acoustic source for this calibration was a L.T.V. developed electro-static transducer, calibrated to 200,000 cps.

The validity of using an acoustic type of calibration to qualify the transducers for measuring the pressure fluctuations in a turbulent boundary layer lies in the fact that the transducer responds to pressure fluctuations at its surface independently of how these pressures are generated, whether by acoustic waves or by eddies convected by the flow. Bearing this in mind, it was determined that, with few exceptions, the ID80-M1 transducers could be considered as having a flat frequency response (within ± 2 db) from 200 cps to 80,000 cps, -- the latter being the upper frequency limit of interest.

The vibration sensitivity of the ID80-M1 transducers was evaluated by subjecting several transducers to vibration on a small calibrated vibration table through the range of 1 to 10 g rms at frequencies of 50, 100, 200, 400, 800, 1000, 2000, 4000, and 5000 cps. The transducers were vibrated in three mutually perpendicular directions. A typical response curve at 1 g rms normal to the sensing element is shown in Figure 19.

As the analysis of the vibration data could not be completed prior to the start of the test, and in order to safeguard the validity of the data taken during the test, each transducer and its associated cable was subjected to a 2 g rms vibration at 800 cps. These data were recorded and are tabulated in Figure 20. In all cases, it can be shown that the vibration-induced signals were not significant in comparison to the pressure-induced signals of the transducers during the test.

3.2.3 Amplifiers

The amplifiers and their input attenuators were individually calibrated through the expected range of frequencies, using standard techniques. Each of the thirty-foot extension probes was individually calibrated for attenuation characteristics.

3.2.4 Systems

With the probes installed in the model and connected to the amplifiers each channel was checked for continuity and attenuation by inserting a known voltage at the transducer end of the probe and checking the output of the terminated amplifier. This was done for several frequencies. In order to check each complete system from the transducer through its associated amplifier to the recorder amplifier once the model was installed in the tunnel, an airhorn producing a sound pressure level of approximately 130 db three inches from the horn, was placed at this distance away from each transducer in turn. Using one channel as a standard, the output of each of the other channels was compared to the standard. This ratio of outputs was checked against the respective transducer sensitivity data and amplifier calibration data. In this way, the relative sensitivity for each channel was confirmed.

3.2.5 Recorders

Each of the fourteen recording tracks of each of the tape recorders was individually calibrated. Tracks 1 and 2 of each recorder were FM recorded with a 54 kcps center frequency, for recording voice identification of runs, and tone bursts for the identification of stabilized data points. Tracks 3 through 14 of each recorder were direct record. Each of these tracks was calibrated from 100 cps to 100 kcps at 100 cps intervals and determined to have a flat response within ± 2 db. Checks during the test and a post test analysis confirmed that the ± 2 db calibration accuracy was maintained throughout the test. In addition, a 1000 cps reference signal was recorded on each track daily to verify the equipment reliability.

3.2.6 Data Reduction Equipment

The calibration of the data reduction equipment will be discussed in the section below on the techniques and equipment employed.

3.3 Precision of Measurements

The "probable error" of the transducers, based on measurements, is ± 2 db. The recording errors introduce an additional ± 2 db, while the auxiliary tape recorders' amplifiers and filters needed to reduce the data introduce another ± 3 db tolerance. The Sanborn equipment on which the data were transcribed introduces an additional ± 2 db. Finally, visual analysis of the printed Sanborn tapes involved an error of up to approximately ± 1 db.

If we assume the probability curve is applicable in this instance, we define the probable error of the data for 90% accuracy to be the square root of the sum of the squares of all the tolerances, or

$$\text{Probable error} = \pm \sqrt{4 + 4 + 9 + 4 + 1} = \pm \sqrt{22} = \pm 4.7 \text{ db}$$

Therefore, it is unlikely that a measurement error greater than ± 5 db would occur.

3.4 Data Reduction

The data, recorded on amplitude modulated tape recorder systems, were reduced in two ways. First, for a quick look at the quality of the data, oscillograms of the signal were produced. These showed the data to be of good quality throughout most of the testing and permitted preliminary estimates of overall magnitudes.

After the test was completed and the necessary equipment became available, "quasi"¹ rms octave band and overall levels for all the recorded data were needed. To fulfill this requirement, an Ampex FR600 tape recorder in conjunction with Allison octave band filters and Sanborn log audio pre-amplifiers and a Sanborn graphic level recorder were used. The "quasi" rms levels were then read and number values tabulated to facilitate data analysis. MSFC Aeroballistics Experimental Group is intending to perform power spectral density reduction on those items of particular interest. Each octave band filter was calibrated using a known white noise signal so that a filter correction could be included where necessary. These filter corrections (called track corrections in the data reduction) appear in tabular form in the data supplement, and account for deviations from the known 3 db per octave variation in octave band analysis of white noise.

¹ An averaging system calibrated to read rms values was utilized.

4.0 ANALYSIS

4.1 Spatial Distribution of Fluctuating Pressure Levels

Figures 21 through 48 indicate spatial distribution of the overall fluctuating pressure levels (OAFPL's) considered valid on those models tested. The levels which are suspect because of the apparent wind tunnel noise or instrumentation dropouts have been excluded. In addition, some have been excluded here because of their low level, but are discussed in a later section because of a persistent trend which suggests a possible reason for these low levels to have occurred.

The OAFPL's noted in the Figures, 21-48, are indicative of the expected levels on the surface of the three configurations tested of the Saturn I vehicle with an Apollo escape rocket attached in a 100-mile orbit trajectory. That is, the levels have had the following corrections incorporated:

1. Transducer calibration correction (see data supplement)
2. Attenuation setting (see data supplement)
3. Cable losses (compensation is made for the cable losses by modifying the transducer sensitivity value).
4. Data reduction filter corrections (see data supplement)
5. Dynamic pressure differences between the wind tunnel and in-flight environments (computed to be 7 db for all Mach numbers except $M = 1.6$ which was 6 db and $M = 0.8$ which was 4 db) resulting in the wind tunnel data being lowered to more nearly correspond to full scale values.
6. Averaging of the values for a particular transducer location when repeatability studies permitted it.

As cited, the above corrections include a modification of the measured rms pressure to include direct proportionality of the pressure magnitude on dynamic pressure ($1/2$ times the density of the air times the square of the free stream velocity). However, no correction for model scale to full scale Reynolds number differences was incorporated. The magnitude of the fluctuating pressures at the wall for a well-behaved turbulent

~~CONFIDENTIAL~~

boundary layer is known to have a weak dependence on Reynolds number through the skin friction coefficient. However, the pressure levels measured on the model were so much higher than flat wall wind tunnel experiments would predict (due to the influence of the abort tower), it is doubtful that this same dependency of the pressure magnitude on skin friction coefficient is present (see section 4.6 below). Also, since the measurements were taken at Reynolds numbers at least an order of magnitude below the full scale Reynolds numbers, linear extrapolation would be unrealistic.

No attempt has been made to incorporate finite transducer size corrections to determine the true mean pressure. The process of integration as suggested by Corcos, ref. 4, (based on an assumed space-time cross correlation at all points in the plane) would result in a correction on the order of 3.5 decibels to be added to the overall pressure level of that octave band whose full scale geometrical mean frequency is approximately 1,500 cps. When scaling from model to full scale, there is a possible slight frequency shift of the geometrical mean frequencies for each octave band depending on Mach number. This correction is also felt to be too detailed for the type of analysis performed here.

Some general trends can be observed in the data by examination of the overall fluctuating pressure quoted on the figures for zero angle of attack. For example, when a protrusion presents a minimal surface area to the flow and is aerodynamically faired, the fluctuating pressure levels are actually reduced near its leading edge. However, as in the case of the chill down duct, the levels to the side and rear of the leading edge are increased by the presence of the protrusion.

In contrast to this, protrusions which present large fairly blunt surfaces to the flow, such as a diameter change in the vehicle, produce large regions of separated flow in front of the disturbance in which high levels of fluctuating pressures exist. One difficulty in testing for these phenomena in a wind tunnel is the presence of reflected shock waves on the model body during transonic speeds. A recent full scale in-flight

~~CONFIDENTIAL~~

measurement suggested that the erratic and sometimes high levels measured at transonic speeds may be partially, if not entirely, due to these reflected shocks. If that is true, the somewhat peculiar variations measured during these speeds, may be attributed to this test limitation.

An attempt was made to determine if there was a roll angle dependency of pressure distribution around the vehicle by rolling the whole model at Mach 1.6. A comparison of the data shows that in all cases the levels were equal to or higher than those recorded before the roll. However, examination of the recorded tunnel characteristics for the roll run indicate that in addition to a 31.5° roll angle with the usual pitch directions of -8 to $+8$ degrees, there was a -17 degree yaw angle. In consequence, the levels recorded for this one special roll angle run are not indicative of the levels one might expect to record with a 0° yaw angle. It is felt that the -17 degree yaw angle influence was responsible for the maximum of 4 decibel increase in all the levels recorded. In the study of repeatability (next section), two of the three runs at Mach 0.8 for the A configuration had small yaw and roll angles other than 0° . The good repetitive quality of the data for these runs as well as for the rolled model run mentioned above suggests the independence of the levels on pitch, yaw, or roll except for a few particular model locations where such a dependence does exist (see Section 4.3 below). Actually, however, no valid conclusion can be drawn from the data of this test concerning the effects of a roll angle on the fluctuating pressures at the model's surface.

4.2 Repeatability

One of the prime concerns at the beginning of the test was whether the data were repeatable--that is, whether duplication of the results would be achieved during similar runs. To determine the extent of this, several runs were duplicated one or more times. The results are plotted on Figures 49 and 50. Two different configurations, A and B, are each examined for two different Mach numbers. It can be noted immediately from the figures that repeatability seems excellent except at the transonic speeds. Part of the difference between runs 12 and 15

~~CONFIDENTIAL~~

(configuration A) can be attributed to a considerable difference in wind tunnel total pressure between the two runs. If this correction is made in terms of a dynamic pressure or a correction, all the FPL's of run 15 are reduced by slightly over 3 decibels with respect to run 12. This would make the largest deviation from the arithmetic mean be approximately ± 3 decibels, which is acceptable. In the case of the B configuration at Mach 0.9, only one location has a really serious discrepancy. However, shadowgraphs of the tunnel flow indicate considerable difficulty with weak reflected shocks at the transonic speeds. The shock wave locations on the vehicle were not stable and thus it is to these effects that any variations are attributed.

Assuming the test results to be repeatable except perhaps at transonic speeds, it seems difficult to explain the difference in overall fluctuating pressure levels measured on the command module between the three configurations (an area unaffected by model changes) unless it is concluded that major modifications at the rear of the model can affect flow characteristics upstream or that the shock attachment position produces a very severe yet localized effect. Bearing in mind the earlier conclusion of very good repeatability, it would seem that one of these conjectures is a necessary corollary.

Four transducers were placed on fin plane IV (opposite four of the transducers on fin plane II) to investigate symmetry of the vehicle. These make it clear that the high fluctuating pressure levels on the command module are a localized condition due to the shock waves and perturbed flow behind the escape rocket. Figure 51 indicates the variation with configuration and Mach number of two transducer locations both at Station 1637 but 180° apart. Some differences occur between transducers on opposite sides of the model, but larger differences exist between the model configurations. For the most part, symmetrically placed transducers show similarities in magnitudes and agreement in angle of attack dependency (though reversed--the minus angles for one are equivalent to the positive angles for the other 180° away).

4.3 Angle of Attack Dependence

One of the most interesting aspects of the boundary-layer-induced fluctuating pressure test is the dependence of overall level for any one transducer location on angle of attack. When the data are examined closely the following conclusions for the Saturn vehicle become obvious. First, for most positions, very little change occurs with a pitch angle of attack variation from -8° to $+8^\circ$. Secondly, where a marked angle of attack dependency does exist, it invariably is associated with a region of the surface being affected either by (1) a shock wave attached to the body and located over the sensing element, or (2) "cavity resonance" effects within separated flow regions. To elaborate further, when a sensing element is directly below a shock wave attached to the body, a pitching of the model will alter the shock attachment location (see Figures 52-55) and thus might vary the levels of the recorded signal by 0-25 db.¹ The largest variation recorded in this test was on the order of 20 db. Most of the energy was between 20-100 cps full scale (700-3400 cps model scale) when the sensing element was directly beneath a shock that was somewhat detached from the surface but affecting the boundary layer in a localized region (leeward side of pitched model). By contrast, when the transducer was just in front of or just behind the attached shock (windward side) the octave band spectrum energy was well distributed throughout most of the frequencies (10-1500 cps full scale or 300-70,000 cps model scale). Figures 56 to 63 illustrate this point.

The second association mentioned above is the most surprising. Within separated flow regions (between the oblique shock at the point of separation or a protrusion such as the ullage rocket and the end of the separated flow volume) whistle or organ pipe-like resonances seem to occur. The sawtooth distribution of pressure levels within these resonator volumes is observable at all speeds tested. Figures 64 to 66 clearly show the sawtooth pressure distribution, as a function of Mach number,

¹ Based on experimentation in the Douglas 1 ft x 1 ft wind tunnel - data conveyed verbally to the writer.

which telescopes to remain within a "confined" region of separated flow for each of the models at 0° angle of attack. The phenomenon is greatly reduced for the B configuration on Fin plane II where the I-beam wedge minimizes the "parallel wall" cavity. The shadowgraphs in Figures 67 to 69 show the change in character with angle of attack of the separated flow region between an ullage rocket and the S-IV to S-I juncture. When the model is pitched down, multiple shocks (due to the chillover duct) appear to be affecting the region in addition to the turbulence. As the model pitches up, this region becomes a leeward pocket such that the flow no longer blows across its opening to generate acoustic-type resonances. This appears to be the explanation for the dependence on angle of attack of the spectrum shape for the affected transducer locations.

Another experimenter² has recently measured a similar type of phenomenon within the separated flow region, and concurs that an adequate explanation for the results does not exist at this time.

Another factor to be considered is the angle of attack influence on the octave band spectrum. Figures 70 to 75 are typical examples of those measurements within a separated flow region which showed a marked dependence on the angle of attack. As stated earlier, the transducers so affected (providing a variation in overall level greater than or equal to 8 db within the -8° to $+8^\circ$ regime) were, in all instances, located in the very near vicinity of a shock wave, or near what appears to be nodal positions in a separated flow region of the model.

² A. Kistler verbally presented results in the Brussels Symposium on "The Mechanisms of Noise Generated by Turbulent Flows" during the spring of 1963 that indicate he measured just such a surprising result. The title of his paper was "Surface Pressure Fluctuations Produced by Attached and Separated Supersonic Boundary Layers".

4.4 Spectra*

No clear-cut distinction was apparent between the mechanisms which produced differently shaped spectra. When the mass of data is examined, a particular spectrum shape can usually be found associated with any kind of flow for any Mach number. This is not to say that general trends do not appear, but rather that the categorizing of spectra is not invariant.

With this in mind, the following major octave band spectrum shapes were identified, and these were associated with the flow characteristics which produced such a shape the majority of the time on the Saturn I model.

1. Smooth body turbulent boundary layer (influenced by the abort tower at all Mach numbers tested) often produced a spectrum in which the peak was located in the low frequencies (10-100 cps full scale frequencies)
2. A separated region of turbulent flow at subsonic or transonic speeds often indicated a double peak spectrum. One of the peaks would usually occur in the low frequencies (10-100 cps full scale) with an additional peak often occurring simultaneously in the mid-frequencies (300-1600 cps full scale)
3. At supersonic speeds in the separated regions, the low frequency peak disappeared leaving only a mid-frequency peak (300-1600 cps full scale)
4. In flow regions other than separated at the supersonic speeds, the octave band spectra often became quite broad and flat throughout the frequency range tested.
5. In rare instances, at transonic speeds only, the separated flow conditions combined with shock wave interaction to produce a few spectra which had a rather sharp peak between 100-300 cps.

The above are general trends which are commonplace, but which are transcended in many instances. It had been hoped that more definitive patterns would evolve. However, the abort tower-escape rocket combination seems

*Note: The word "spectra" will be used herein to denote the shapes of the octave band fluctuating pressure levels over the frequencies measured during this test (300-78,000 cps model scale).

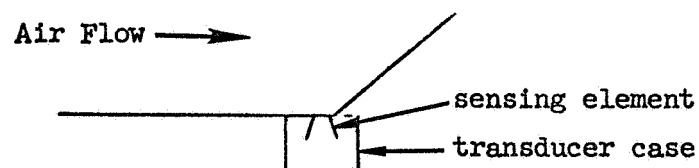
~~CONFIDENTIAL~~

to be markedly influencing the fluctuating pressure characteristics over the entire vehicle.

4.5 Explanation of the Low FPL's

There were many overall fluctuating pressure levels measured on the models which were considerably below the apparent wind tunnel noise. Figure 76 indicates the percentage of measurements which were above the apparent wind tunnel noise levels, and thus, also shows the percent falling below (about 20% of the total). Some of these low levels were attributed to dropouts of response of the transducers. (Due to the tight scheduling, the new transducer design, and difficulties in manufacture and calibration of the transducers, some instrumentation was used which proved to be of intermittent behavior.) The number of transducers with this problem was, however, relatively small. In addition to these few measurements attributed to faulty electronics, there were still many data points which registered levels below the apparent noise levels of the tunnel.

Section 4.3 indicated one phenomenon which allowed such low levels to occur--i.e., organ pipe-like resonance nodes. Another instance of especially low levels, showing remarkable consistency of behavior, occurred when the sensing element was located in a corner. The sketch directly below indicates the situation.



For the C configuration, the addition of a 20° fairing produced such a condition for a whole row of transducers. These were uniformly low. At other times, sensing elements a little further away on either side of a corner also exhibited such a low level, but this result was erratic and usually occurred at some angle of attack other than zero. In addition, when a transducer was located near one of the nodal positions for the

acoustic-type resonance within the separated region, low level data were observed. If the apparent wind tunnel noise is sufficiently scattered and diffracted by the flow, then such a low level condition could exist. Static pressure measurements in such notches and separated flow regions did not indicate a reduced gas pressure which might otherwise account for such a low level.

One striking uniformity does exist between the low level measurements. They are, without any exceptions, contained within separated flow regional boundaries (including those transducers located on the antenna panel on the booster stage). It can generally be concluded that the highest and the lowest levels are equally prevalent within these separated regions, and further studies are necessary to understand completely the unusual variations which occur. Tentative explanations have been propounded, but only a test program designed explicitly to define the true spatial distribution of fluctuating pressures within such a separated region could verify any theoretical considerations.

4.6 Comparison With Other Measurements

Few other measurements are available which can directly be compared to the wind tunnel studies discussed herein. Laboratory studies of the boundary layer at the wall of the wind tunnel by Willmarth (for subsonic speeds) reference 5, have been compared with some of the clean body measurements for transducers located in the middle of cylindrical sections in somewhat well-behaved model flow (Apollo tower attached). Figures 77 to 82 show the results of the Saturn wind tunnel study for five such locations plotted in terms of the dimension-less variables utilized by Willmarth.

To compute the boundary layer thickness, the leading edge was assumed to be that of the escape rocket. An average curve for Willmarth's wind tunnel wall studies has also been included. Experiments by Von Gierke, Mull, and Algranti, and Williams, references 6, 7, and 8, seem to verify Willmarth's values within experimental error limits.

A recent document by Kistler and Chen (ref. 9) presents data for a well-behaved turbulent boundary layer on a flat surface in a supersonic wind tunnel. Unfortunately, the frequency region of greatest interest in terms of the vehicle ($\omega \delta^*/U_{\infty} < 1$) shows considerable scatter, and as plotted (on a linear scale) presents that information too close to the origin to be accurately used in comparisons. In addition, no actual values of mean square pressure have been quoted, so the magnitude of the results from Kistler and Chen is not readily available. However, the data being of such interest, the following procedures were used to manage a rough comparison of supersonic and subsonic test results.

1. Assume a correction for the variation in mean skin friction at the wall with Mach number based on the best available test information on drag.
2. Calculate the ratio of mean square pressure to mean skin friction of Willmarth's data to that of Kistler and Chen.
3. Utilize the factor in 2 to denormalize the results quoted in Figure 8 of ref. 9 based on the mean square pressure measurements of Willmarth, and the integrated areas under the curves.

If this denormalization was successful (the data hopefully resembling that which was measured) then comparison of both experiments indicates a considerable difference in spectrum shape (see Figure 77) between flat plate subsonic and supersonic measurements. Comparing both of these experimenters' work with the Saturn wind tunnel data, results in unsatisfactory conclusions. For some locations, the general spectrum shape resembles that of Willmarth except for high levels in the very low frequencies. For other locations, the spectrum shape resembles the Kistler and Chen data at least for low frequencies. The wide scatter in the Saturn wind tunnel data is due in part to the calculation of the boundary layer displacement thickness δ^* . The Saturn configurations make it impossible to accurately calculate δ^* , so it is assumed that the escape rocket nose is the leading edge of a smooth vehicle shape (this being a necessary but poor assumption). It is therefore obvious that no valuable conclusions can be reached regarding flat wall wind tunnel data as compared to the Saturn model data.

~~CONFIDENTIAL~~

It is evident that the full scale Saturn levels are considerably higher than the levels measured by Willmarth or Kistler and Chen. (Up to 34 db at transonic speeds which is 50 times the original pressure and up to 29 db at supersonic speeds which is 28 times the original pressure -- $\sqrt{\frac{p^2}{p}} = 0.3q$ and $0.168q$ respectively.)

Preliminary comparison of this study's data with a similar test performed on a larger model at North American showed good agreement. An in-flight measurement taken on a Saturn vehicle with dummy upper stages was compared where possible with the wind tunnel information. Such a comparison is indicated in Figure 83. It should be noted that the model scale transducer location used for comparison was somewhat comparable to the full scale L65-20 measurement for subsonic speeds (through Mach 1.2) and for higher Mach numbers, the model scale transducer location was approximately 45° away from the first location. This change resulted from model instrumentation problems, and means that for supersonic speeds, the model scale information is not being influenced by the near proximity of a hydrogen chill-down duct. The loss of agreement in the overall pressure fluctuation levels for Mach numbers above maximum q might possibly be due to the above described variations for maximum q and for a higher Mach number (corresponding to the peak full scale measured levels). Once again, the loss of the influence of the hydrogen chill-down duct on the model scale measurement (as well as strong cross winds affecting the full scale vehicle during this portion of the flight) might conceivably have produced the spectra differences at the higher Mach numbers. More detailed comparison of the model scale and full scale data is currently being performed, and will be presented in another DAC report.

There have been many wind tunnel studies on models similar to, or geometrically like, the Saturn vehicle. However, prior to these Saturn tests, no attempt had been made to extend the "full scale" frequency range beyond 100 cps. Thus, no attempt can be made to compare the low frequency data of these other tests with the wide frequency range data of this test.

~~CONFIDENTIAL~~

4.7 Static Pressure Data

During the test, a limited examination of static pressures on the model was performed concurrently with the FPL investigation. Only 13 static taps on the model could be recorded during any one run. Some of these are in fin plane II of the vehicle (the pitch plane) and pressure coefficients from these taps are plotted versus vehicle position in Figures 87 through 91. Two configurations are covered by this series of graphs, and on Figure 87 is shown a comparison of the DAC static pressure data with that interpolated from a 0.778% model measured at Marshall Space Flight Center. Figures 88-91 show a comparison between the DAC measured data and a Langley pressure-force test (ref. 10). In addition, a comparison between the DAC model data with that taken during flight on the SA-3 full scale vehicle indicates excellent correlation in all but one measurement. The following table exemplifies this. A vehicle pitch of 4° has been included in the model data to correspond with the in-flight information.

Model Scale Station (in)	Model Scale Cp	Full Scale Cp	Full Scale Station (in)	Mach No.
Leeward Measurements				
985	0.42	0.48	989.3	1.2
963	0.44	0.48	1019.3	1.2
985*	0.39			1.2
985	0.32	0.32	989.3	1.6
963	0.33	0.29	1019.3	1.6
985*	0.30			1.6
Windward Measurements				
985	0.52	0.61	989.3	1.2
963	0.57	0.54	1019.3	1.2
985*	0.50			1.2
985	0.39	0.34	989.3	1.6
963	0.45	0.017	1019.3	1.6
985*	0.36			1.6

* 45° away from the fin plane under examination

~~CONFIDENTIAL~~

No correlation between sharp static pressure gradients over the surface with particularly high fluctuating pressure levels can be discerned. In addition, no unusually low static pressures are observable in the locality of the extremely low fluctuating pressure levels measured directly in front of a fairing. In every respect, the static pressures measured during this test were in agreement with the expected ones.

~~CONFIDENTIAL~~

5.0 CONCLUSIONS

An extensive wind tunnel study to investigate the fluctuating pressures at the surface of the Saturn vehicle has been described in this report. The results have indicated a considerable success in this rather difficult undertaking.

The test has shown some interesting trends pertaining to the turbulent boundary-layer-induced fluctuating pressures at the surface of the Saturn model in particular, and to turbulent boundary layer studies in general.

They are:

1. Fluctuating pressure levels are increased to the side and rear of large protrusions (whether faired or not).
2. Abrupt broad-front high protuberances (such as a major vehicle diameter change) produce large regions of separated flow in which an unusual pressure distribution is observed.
3. Octave band spectra of the fluctuating pressures in disturbed flow have various shapes which are sometimes quite unlike wind tunnel flat wall spectra (produced by a well-behaved slowly growing turbulent boundary layer). The various shapes can be generally associated with particular flow characteristics, but erratic overlapping of these general categories exists at all times--perhaps attributable to the Apollo escape rocket and tower assembly.
4. Fluctuating pressure level dependence on pitch angle was negligible except in isolated cases where the measurement was affected by a shock wave or was near what appears to be a nodal point in the separated regions.
5. Depressed edges usually result in very low levels.
6. Repeatability of the data was very good.
7. The data compare favorably with other available model scale and full scale test information.

The above results indicate that the purpose of the test was achieved.

Prediction of increased fluctuating pressures at the vehicle surface due

~~CONFIDENTIAL~~

to the protuberances (up to a maximum of 35 and 30 db for transonic and low supersonic flight speeds, respectively) was verified. The resultant effects of these increased loads on the structure is beyond the scope of this report. In addition, even though the relative increases are no doubt valid and preliminary comparisons with full scale data appears promising, the actual order of magnitude and frequency scaling of the model scale data to predict full scale results must be further verified.

Finally, additional studies are certainly warranted to investigate the flow condition described above which contains some of the highest as well as the lowest levels recorded on the model. A complete description of the excitation including spatial pressure distribution as it varies with the several parameters involved, and space time correlation, is necessary before an intelligent evaluation can be made of the resultant influence on the vehicle.

~~CONFIDENTIAL~~

REFERENCES

1. Aldrich, J. F. L., Trisonic Four Foot Wind Tunnel Description of the Facility and Provisions for Testing, DAC Report LB-30761, December 29, 1961.
2. Mahr, H. N. and Shaw, W. J., Investigation of Surface Pressure Distribution of the Saturn SA-5 Pressure Model, SVM-14, at Mach 0.8 to 5.0, Volume 1 - Test Report, DAC SM-43053.
3. Bonin, L. J., Saturn SA-5 Pressure Test Model No. DSV-4, DAC Report SM-42455, October, 1962.
4. Corcos, G. M., "Resolution of Pressure in Turbulence," J. of Acoust. Soc. of Am. 35, 192-199 (February 1963).
5. Willmarth, W. W., Space-Time Correlations and Spectra of Wall Pressure in a Turbulent Boundary Layer, NASA Memo 3-17-59W (March 1959)
6. Von Gierke, H. E., "Types of Pressure Fields of Interest in Acoustical Fatigue Problems" WADC TR 59-676 pp 57-84, March, 1961.
7. Mull, H. R. and Algranti, J. S., Flight Measurement of Wall Pressure Fluctuations and Boundary Layer Turbulence, NASA TN D-280, October, 1960.
8. Williams, D. J. M., Measurement of the Surface Pressure Fluctuations in a Turbulent Boundary Layer in Air at Supersonic Speeds, University of Southampton, AASU Report 162, December, 1960.
9. Kistler, A. L., and Chen, W. S. The Fluctuating Pressure Field in a Supersonic Turbulent Boundary Layer, TR 32-277, Jet Propulsion Laboratory, August 15, 1962.
10. Pearson, Albin O., Wind Tunnel Investigation of Transonic Speeds of the Static Aerodynamic Characteristics and Pressure Distributions of a Three-Stage Saturn Launch Vehicle, NASA TM X-738, January, 1963.
11. Van Houten, J. J., "Electrostatic Transducers for Ultrasonics", Audio Engineering Society Preprint No. 262, October, 1962
12. "Method for Measuring and Calibrating the Diffraction Coefficient of Microphones," Acoustica, Vol. 5, No. 3, February, 1960.

~~CONFIDENTIAL~~

APPENDIX A

Quoted from a LTV RESEARCH CENTER, Western Division Note

Ling-Temco-Vought, Inc.
Anaheim, California

CALIBRATION OF THE ATLANTIC RESEARCH PRESSURE TRANSDUCER, LD 80-M1

For

Douglas Aircraft Company
Missile & Space Systems Division
Santa Monica, California

SUMMARY

A comparison calibration of the Atlantic Research Pressure Transducer, LD 80-M1, has been performed. The pressure sensitivity of the transducer was compared to a B & K 1/4-inch microphone at frequencies up to 100 kcps. Sinusoidal signals were generated by the electrostatic transmitter as an ultrasonic source for making this comparison. Diffraction corrections were calculated taking the active membrane and housing size of the microphone into account.

INTRODUCTION

The measurement of boundary layer noise with a flush-mounted transducer requires pressure calibration of the transducer. This calibration is performed at frequencies up to 100 kcps in order to cover the frequency range of interest during model studies. To cover this frequency range, electrostatic transmitters are used because of the uniform response achieved by these devices, Reference 11. With the electrostatic transmitter as a common sound source, a comparison of the free field transducer sensitivity to that of a laboratory standard is made. Corrections which account for the physical size of the device are applied to the free field sensitivity measured in order to obtain true pressure response.

~~CONFIDENTIAL~~

CALIBRATION TECHNIQUE

Due to the extremely low sensitivity of the Atlantic Research Pressure Transducer, the electrostatic transmitter was placed approximately 6 inches from the active element. With this close spacing, standing waves between sensing element and transmitter were possible, therefore, a warble tone signal was used to perform the calibration. A B & K 1/4-inch Condenser Microphone was used as the laboratory standard and a point-by-point comparison of sensitivity at frequencies from 1600 cps to 100 kcps was made. Also, a response recording of each transducer and the laboratory standard was made covering the range from 15 kcps to 100 kcps.

The pressure sensitivity of the microphone was obtained by subtracting a calculated diffraction coefficient from the measured free-field response. A typical calibration is shown in Figure 92.

Frequency response recordings of a group of transducers show a smooth response and do not justify the peak at 70 kcps. Combined with the information supplied by the customer that the resonance frequency of the ceramic element is at about 400 kcps, it becomes apparent that the actual diffraction differs from that calculated. The actual diffraction coefficient was determined by averaging the free field response of a number of transducers with uniform response and assuming that their pressure response is flat up to 100 kcps. This actual diffraction coefficient is shown in Figure 93 (bottom curve). A pressure response obtained by applying the actual diffraction coefficient is shown by the solid line in Figure 92.

CALCULATIONS AND DIFFRACTION COEFFICIENTS

Diffraction coefficients were calculated by procedures described in Reference 12. The active membrane diameter used was .1 inch with an outer housing diameter of .375-inches. The calculated diffraction coefficient is shown in Figure 93 (top curve). Also shown in Figure 93 is the diffraction coefficient derived by assuming the average Atlantic Research Microphone has a flat response. The calculated values established below 40 KC are used with confidence since only first order diffraction effects exist at these frequencies. At

~~CONFIDENTIAL~~

higher frequencies, the theory applied breaks down as a result of inadequacies of the assumption in its derivation and would be expected to give an unreliable result.

CONCLUSION

The method for obtaining a pressure calibration for the Atlantic Research Microphone has been reported. The calibration is accurate with ± 1 db up to 20 kcps and ± 2 db above this frequency.

~~CONFIDENTIAL~~

A RIGID 2.75% SATURN I MODEL WITHOUT PROTUBERANCES

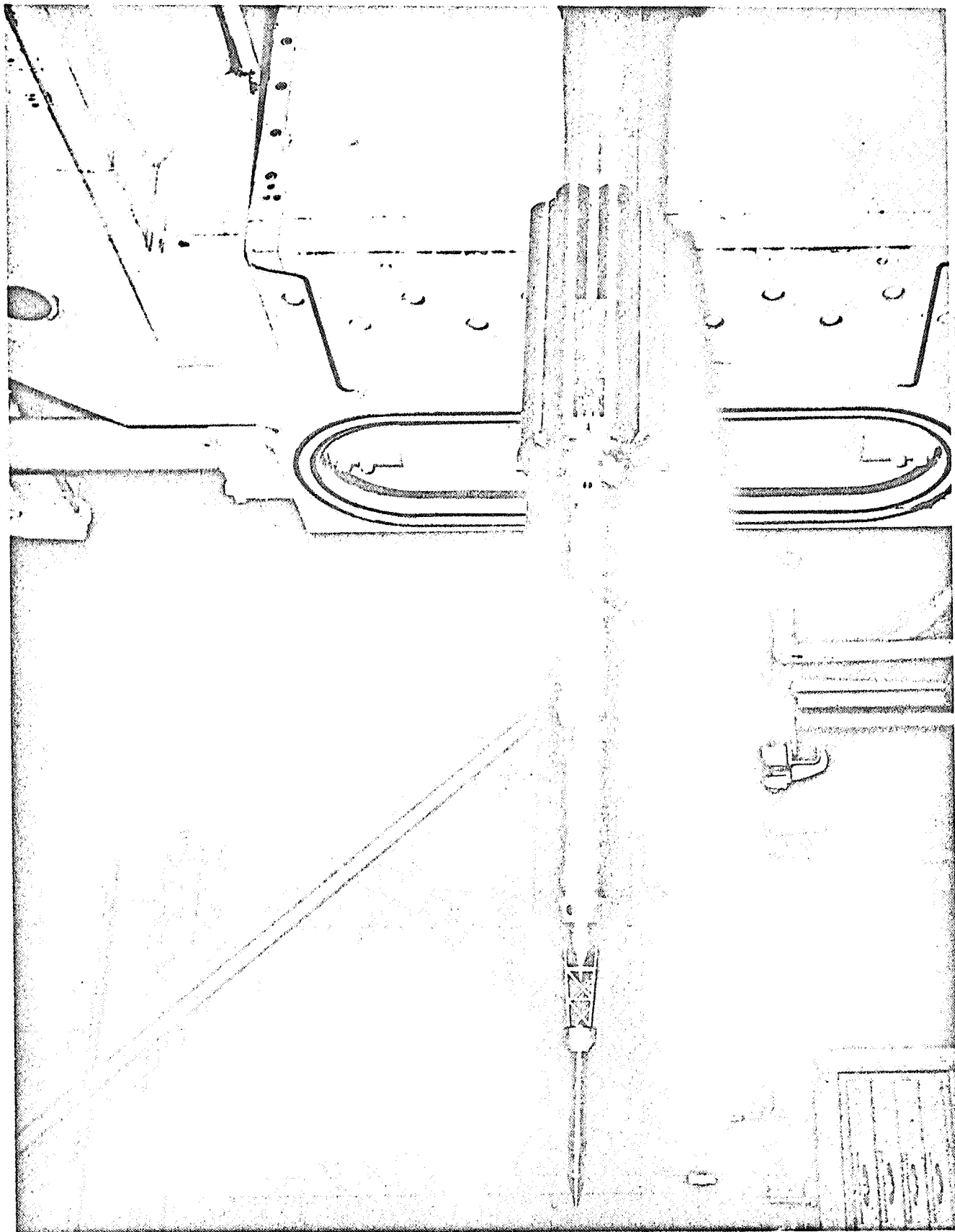


FIGURE 1

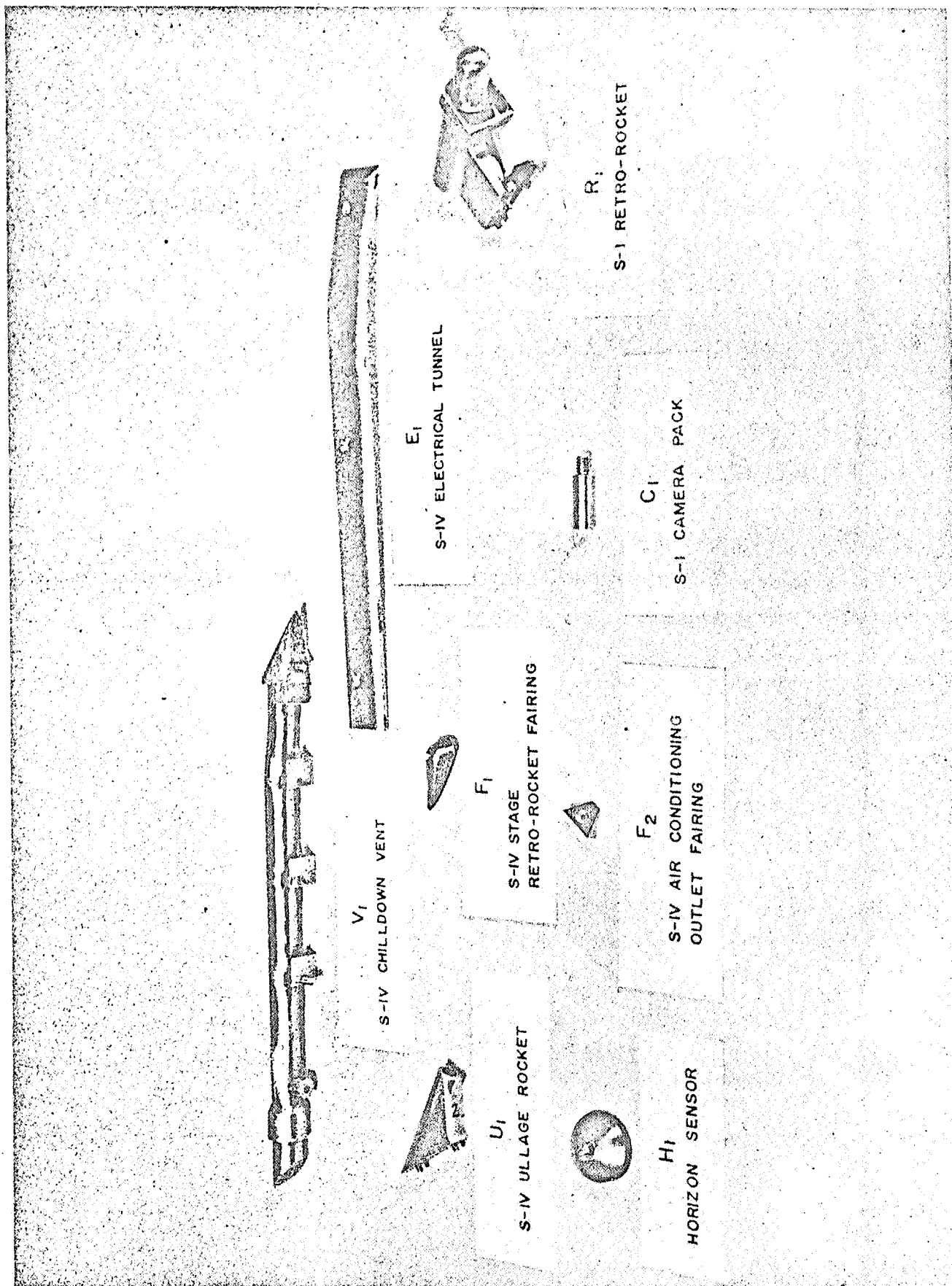
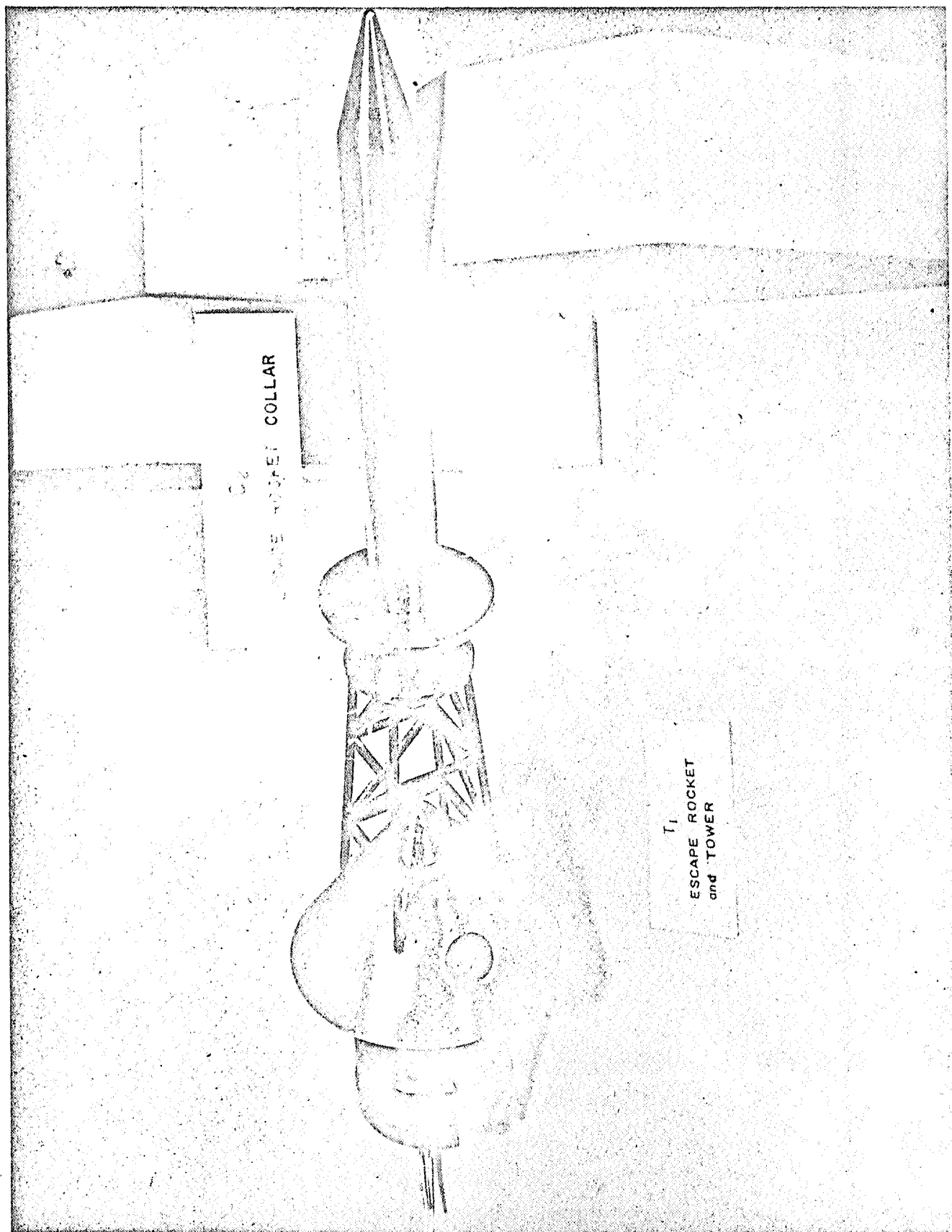


FIGURE 2

DETACHABLE PROTRUSIONS FOR THE SATURN MODEL

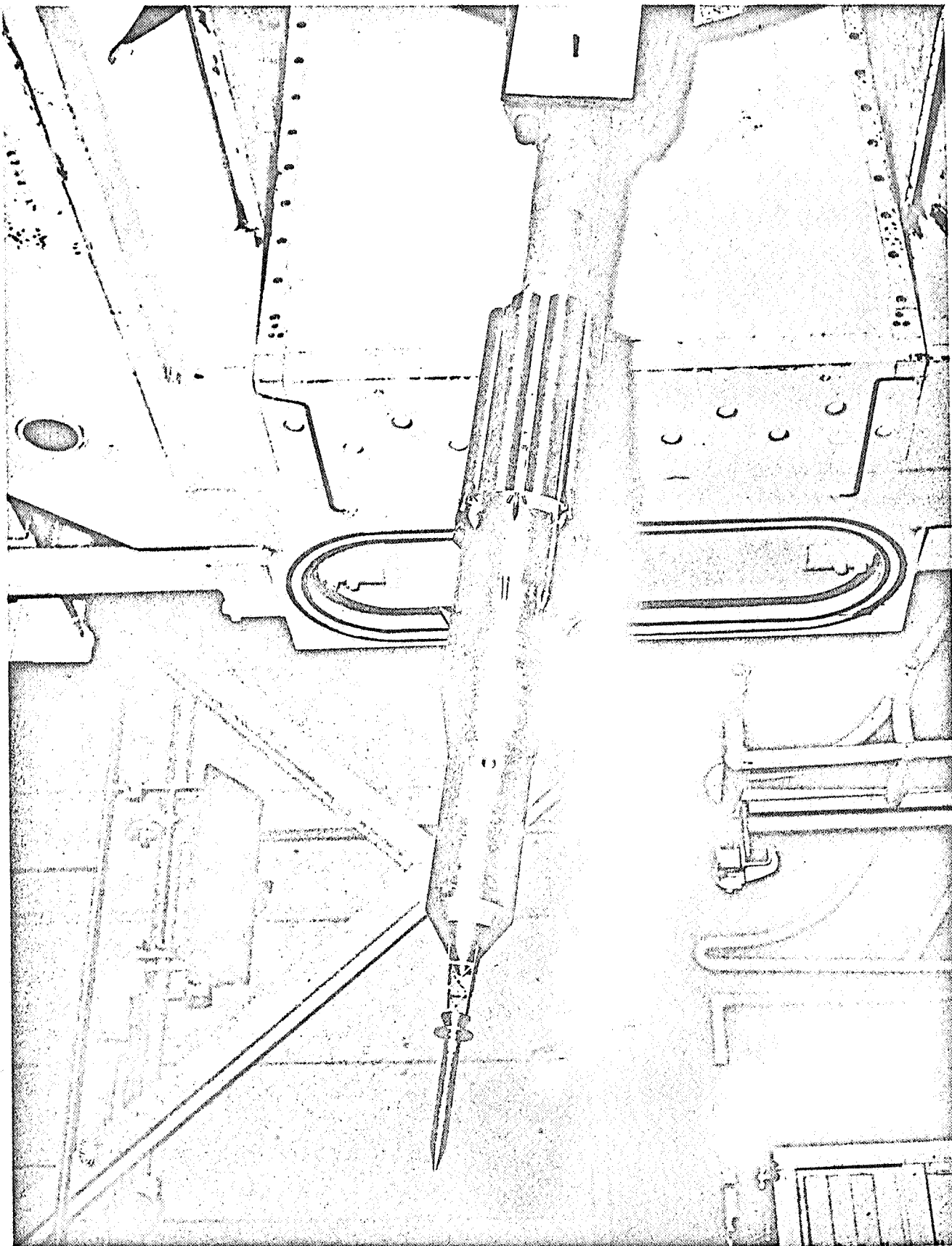


DETACHABLE APOLLO ABORT TOWER AND ESCAPE ROCKET MODEL

FIGURE 3

~~CONFIDENTIAL~~

CONFIDENTIAL



COMPLETE MODEL OF THE SATURN I VEHICLE (2.75%)

FIGURE 4

CONFIDENTIAL

THE FLIGHT VEHICLE MODEL MODIFIED BY A 20° FAIRING AT THE SI-SIV JUNCTURE

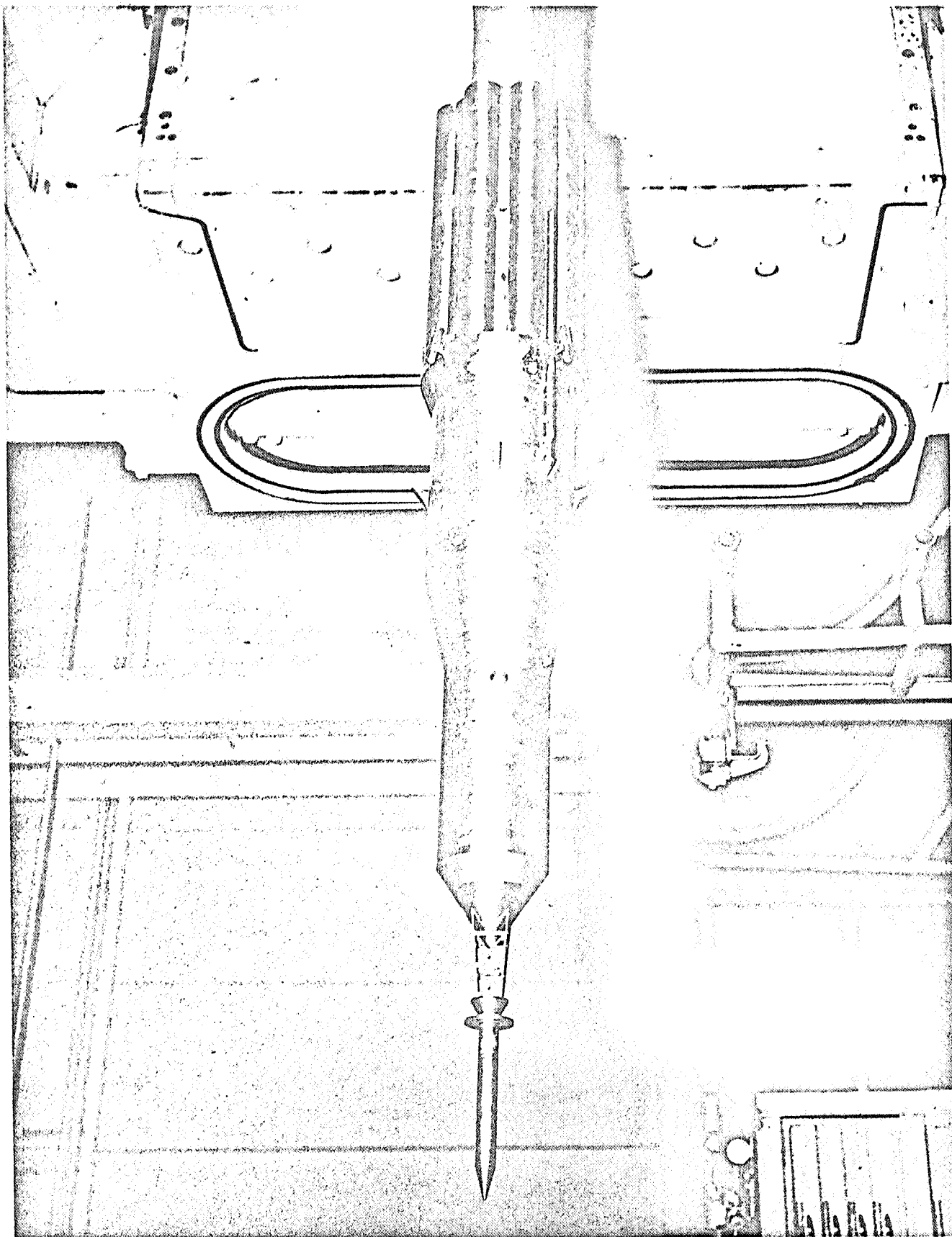
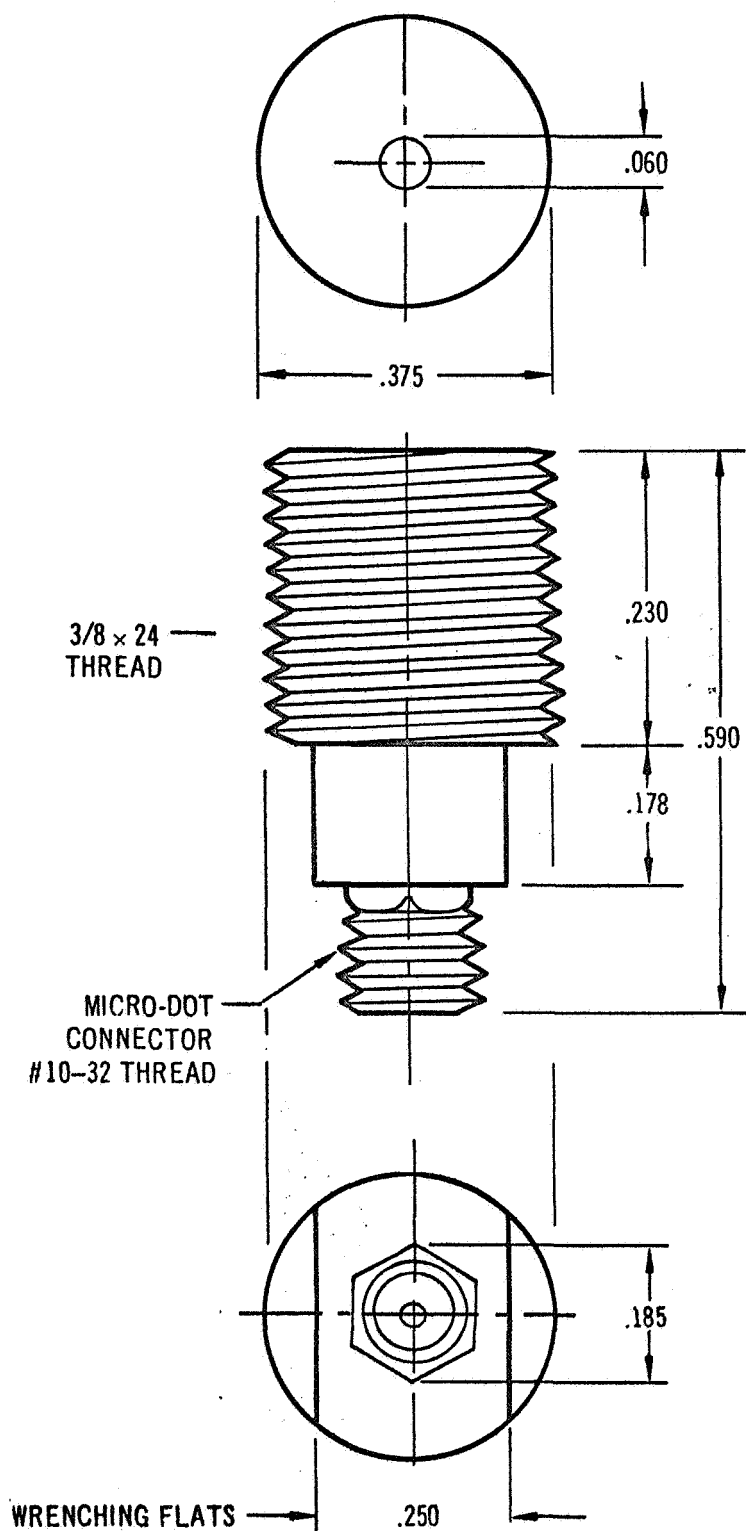


FIGURE 5

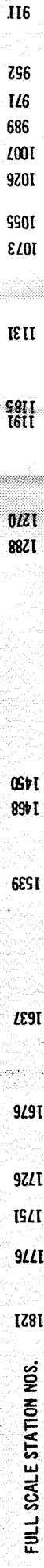
GEOMETRY OF THE ATLANTIC RESEARCH MODEL LD 80-MI TRANSDUCER



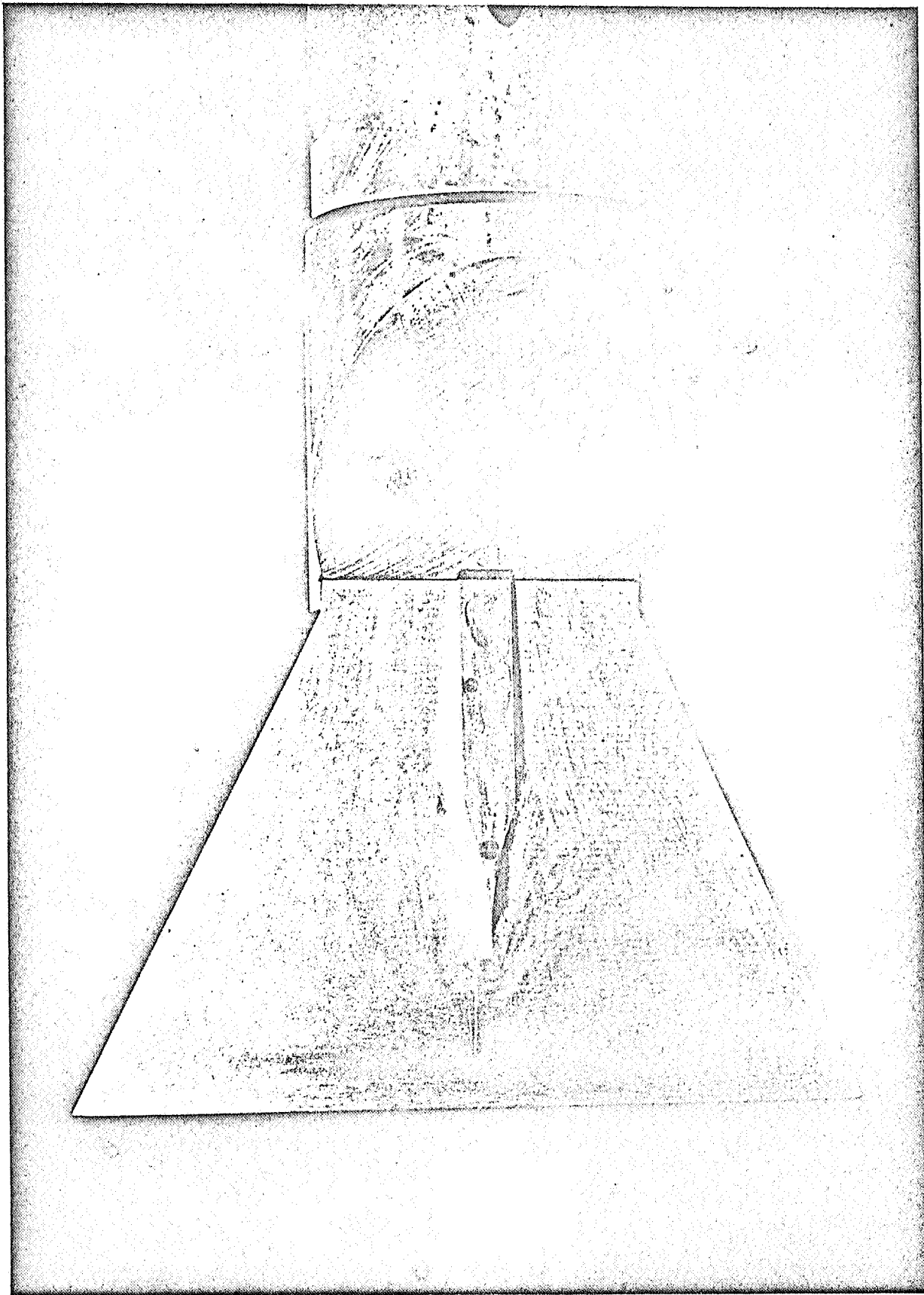
(DIMENSIONS IN INCHES)

FIGURE 6

A	0°	1, 2, 3, 4, 5, 6, 7, 8, 9, 10, 11, 12, 13, 14, 15, 16, 17, 18, 19, 20, 21, 22, 23, 24, 25, 26, 27, 28, 29, 30, 31, 32, 33, 34, 35, 36, 37, 38, 39, 40, 41, 42, 43, 44, 45, 46, 47, 48, 49, 50, 51, 52, 53, 54, 55, 56, 57, 58, 59, 60, 61, 62, 63, 64, 65, 66, 67, 68, 69, 70, 71, 72, 73, 74, 75, 76, 77, 78, 79, 80, 81, 82, 83, 84, 85, 86, 87, 88, 89, 90, 91, 92, 93, 94, 95, 96, 97, 98, 99, 100, 101, 102, 103, 104, 105, 106, 107, 108, 109, 110, 111, 112, 113, 114, 115, 116, 117, 118, 119, 120, 121, 122, 123, 124, 125, 126, 127, 128, 129, 130, 131, 132, 133, 134, 135, 136, 137, 138, 139, 140, 141, 142, 143, 144, 145, 146, 147, 148, 149, 150, 151, 152, 153, 154, 155, 156, 157, 158, 159, 160, 161, 162, 163, 164, 165, 166, 167, 168, 169, 170, 171, 172, 173, 174, 175, 176, 177, 178, 179, 180, 181, 182, 183, 184, 185, 186, 187, 188, 189, 190, 191, 192, 193, 194, 195, 196, 197, 198, 199, 200, 201, 202, 203, 204, 205, 206, 207, 208, 209, 210, 211, 212, 213, 214, 215, 216, 217, 218, 219, 220, 221, 222, 223, 224, 225, 226, 227, 228, 229, 230, 231, 232, 233, 234, 235, 236, 237, 238, 239, 240, 241, 242, 243, 244, 245, 246, 247, 248, 249, 250, 251, 252, 253, 254, 255, 256, 257, 258, 259, 260, 261, 262, 263, 264, 265, 266, 267, 268, 269, 270, 271, 272, 273, 274, 275, 276, 277, 278, 279, 280, 281, 282, 283, 284, 285, 286, 287, 288, 289, 290, 291, 292, 293, 294, 295, 296, 297, 298, 299, 300, 301, 302, 303, 304, 305, 306, 307, 308, 309, 310, 311, 312, 313, 314, 315, 316, 317, 318, 319, 320, 321, 322, 323, 324, 325, 326, 327, 328, 329, 330, 331, 332, 333, 334, 335, 336, 337, 338, 339, 340, 341, 342, 343, 344, 345, 346, 347, 348, 349, 350, 351, 352, 353, 354, 355, 356, 357, 358, 359, 360, 361, 362, 363, 364, 365, 366, 367, 368, 369, 370, 371, 372, 373, 374, 375, 376, 377, 378, 379, 380, 381, 382, 383, 384, 385, 386, 387, 388, 389, 390, 391, 392, 393, 394, 395, 396, 397, 398, 399, 400, 401, 402, 403, 404, 405, 406, 407, 408, 409, 410, 411, 412, 413, 414, 415, 416, 417, 418, 419, 420, 421, 422, 423, 424, 425, 426, 427, 428, 429, 430, 431, 432, 433, 434, 435, 436, 437, 438, 439, 440, 441, 442, 443, 444, 445, 446, 447, 448, 449, 450, 451, 452, 453, 454, 455, 456, 457, 458, 459, 460, 461, 462, 463, 464, 465, 466, 467, 468, 469, 470, 471, 472, 473, 474, 475, 476, 477, 478, 479, 480, 481, 482, 483, 484, 485, 486, 487, 488, 489, 490, 491, 492, 493, 494, 495, 496, 497, 498, 499, 500, 501, 502, 503, 504, 505, 506, 507, 508, 509, 510, 511, 512, 513, 514, 515, 516, 517, 518, 519, 520, 521, 522, 523, 524, 525, 526, 527, 528, 529, 530, 531, 532, 533, 534, 535, 536, 537, 538, 539, 540, 541, 542, 543, 544, 545, 546, 547, 548, 549, 550, 551, 552, 553, 554, 555, 556, 557, 558, 559, 560, 561, 562, 563, 564, 565, 566, 567, 568, 569, 570, 571, 572, 573, 574, 575, 576, 577, 578, 579, 580, 581, 582, 583, 584, 585, 586, 587, 588, 589, 590, 591, 592, 593, 594, 595, 596, 597, 598, 599, 600, 601, 602, 603, 604, 605, 606, 607, 608, 609, 610, 611, 612, 613, 614, 615, 616, 617, 618, 619, 620, 621, 622, 623, 624, 625, 626, 627, 628, 629, 630, 631, 632, 633, 634, 635, 636, 637, 638, 639, 640, 641, 642, 643, 644, 645, 646, 647, 648, 649, 650, 651, 652, 653, 654, 655, 656, 657, 658, 659, 660, 661, 662, 663, 664, 665, 666, 667, 668, 669, 670, 671, 672, 673, 674, 675, 676, 677, 678, 679, 680, 681, 682, 683, 684, 685, 686, 687, 688, 689, 690, 691, 692, 693, 694, 695, 696, 697, 698, 699, 700, 701, 702, 703, 704, 705, 706, 707, 708, 709, 710, 711, 712, 713, 714, 715, 716, 717, 718, 719, 720, 721, 722, 723, 724, 725, 726, 727, 728, 729, 730, 731, 732, 733, 734, 735, 736, 737, 738, 739, 740, 741, 742, 743, 744, 745, 746, 747, 748, 749, 750, 751, 752, 753, 754, 755, 756, 757, 758, 759, 760, 761, 762, 763, 764, 765, 766, 767, 768, 769, 770, 771, 772, 773, 774, 775, 776, 777, 778, 779, 780, 781, 782, 783, 784, 785, 786, 787, 788, 789, 790, 791, 792, 793, 794, 795, 796, 797, 798, 799, 800, 801, 802, 803, 804, 805, 806, 807, 808, 809, 810, 811, 812, 813, 814, 815, 816, 817, 818, 819, 820, 821, 822, 823, 824, 825, 826, 827, 828, 829, 830, 831, 832, 833, 834, 835, 8
---	----	--



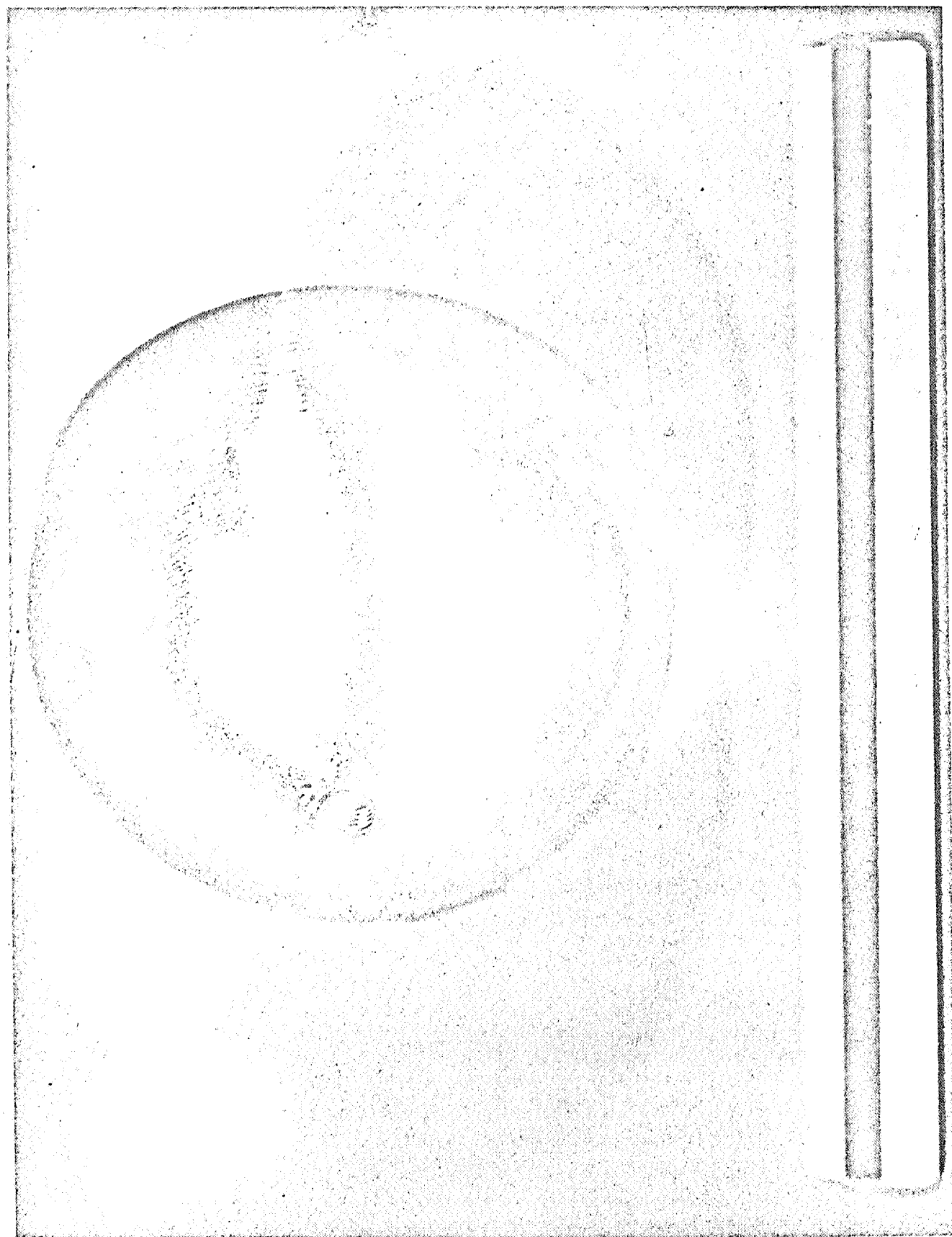
CONFIDENTIAL



REAR VIEW OF THE FLAT PLATE SHOWING THE FAIRING
OVER THE TRANSDUCER CASE AND LEAD
(SENSING ELEMENT FLUSH IN OPPOSITE SIDE)

FIGURE 8

CONFIDENTIAL



HEMISPHERE USED TO CALIBRATE THE WIND TUNNEL

FIGURE 9

APPARENT NOISE LEVELS IN THE CENTER OF THE
DOUGLAS AEROPHYSICS LAB. 4' x 4' TRISONIC TUNNEL

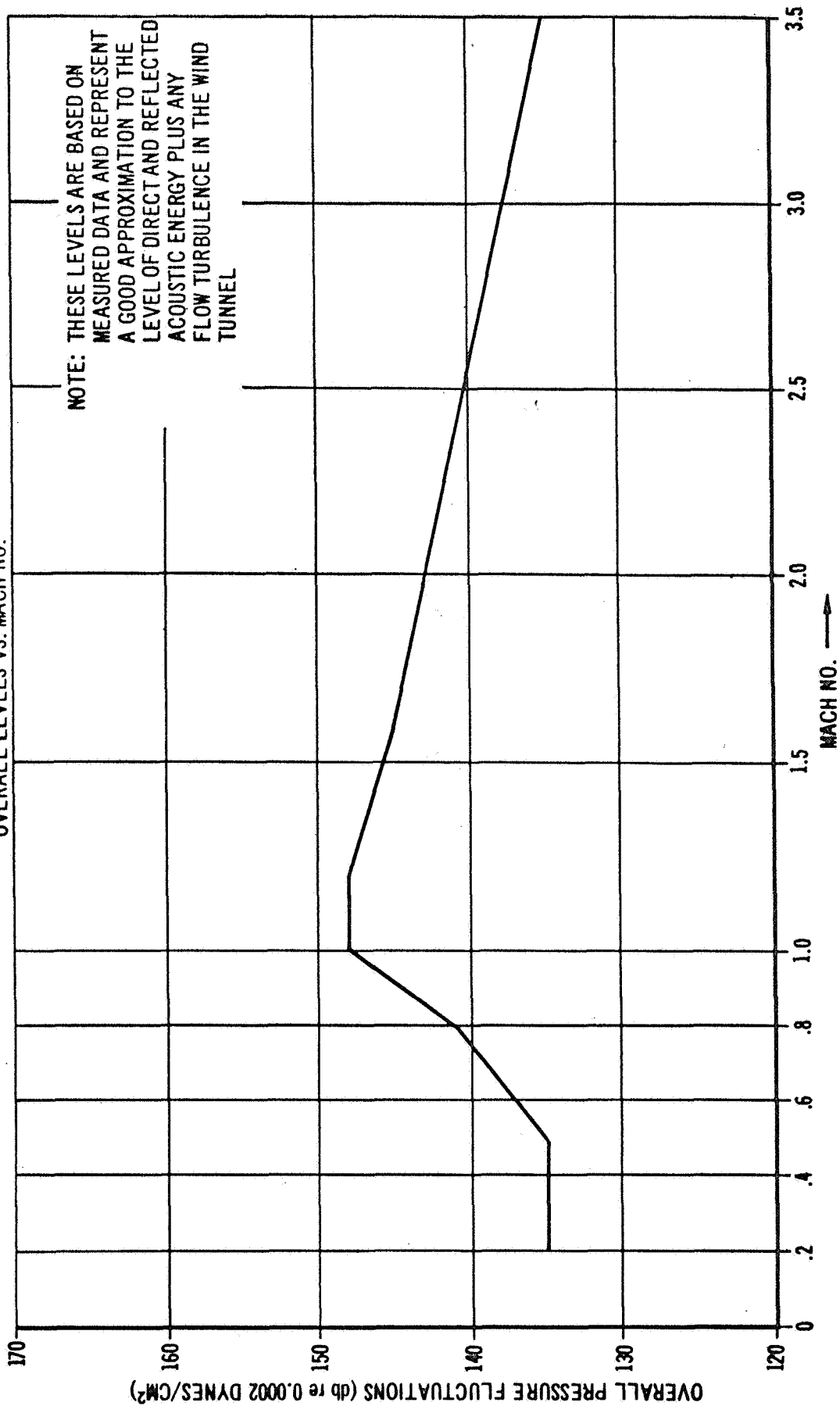


FIGURE 10

APPARENT WIND TUNNEL NOISE SPECTRUM SHAPE
AT MACH 0.8 MEASURED ON THE FLAT PLATE

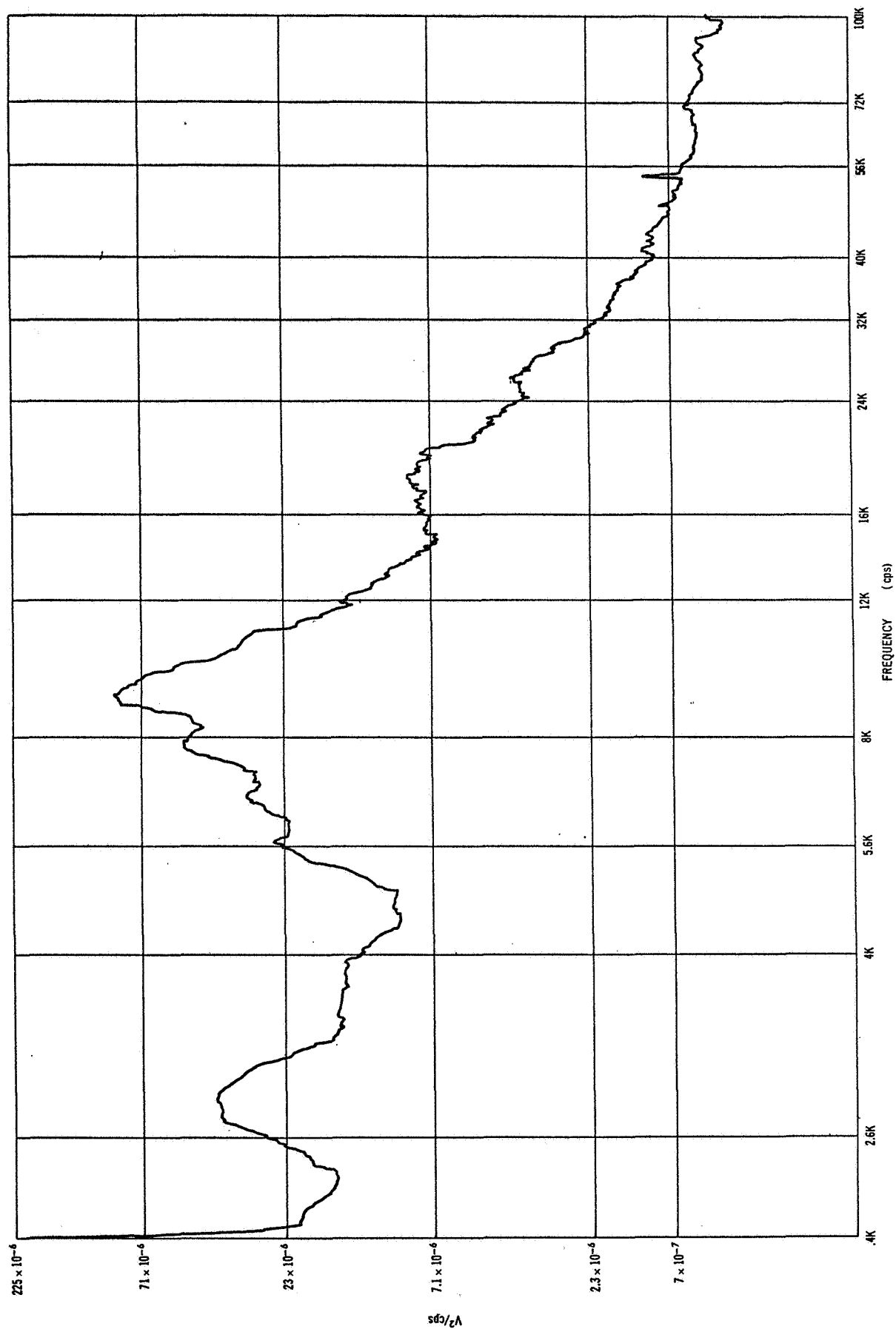


FIGURE 11

APPARENT WIND TUNNEL NOISE SPECTRUM SHAPE
AT MACH 0.8 MEASURED ON THE HEMISPHERE

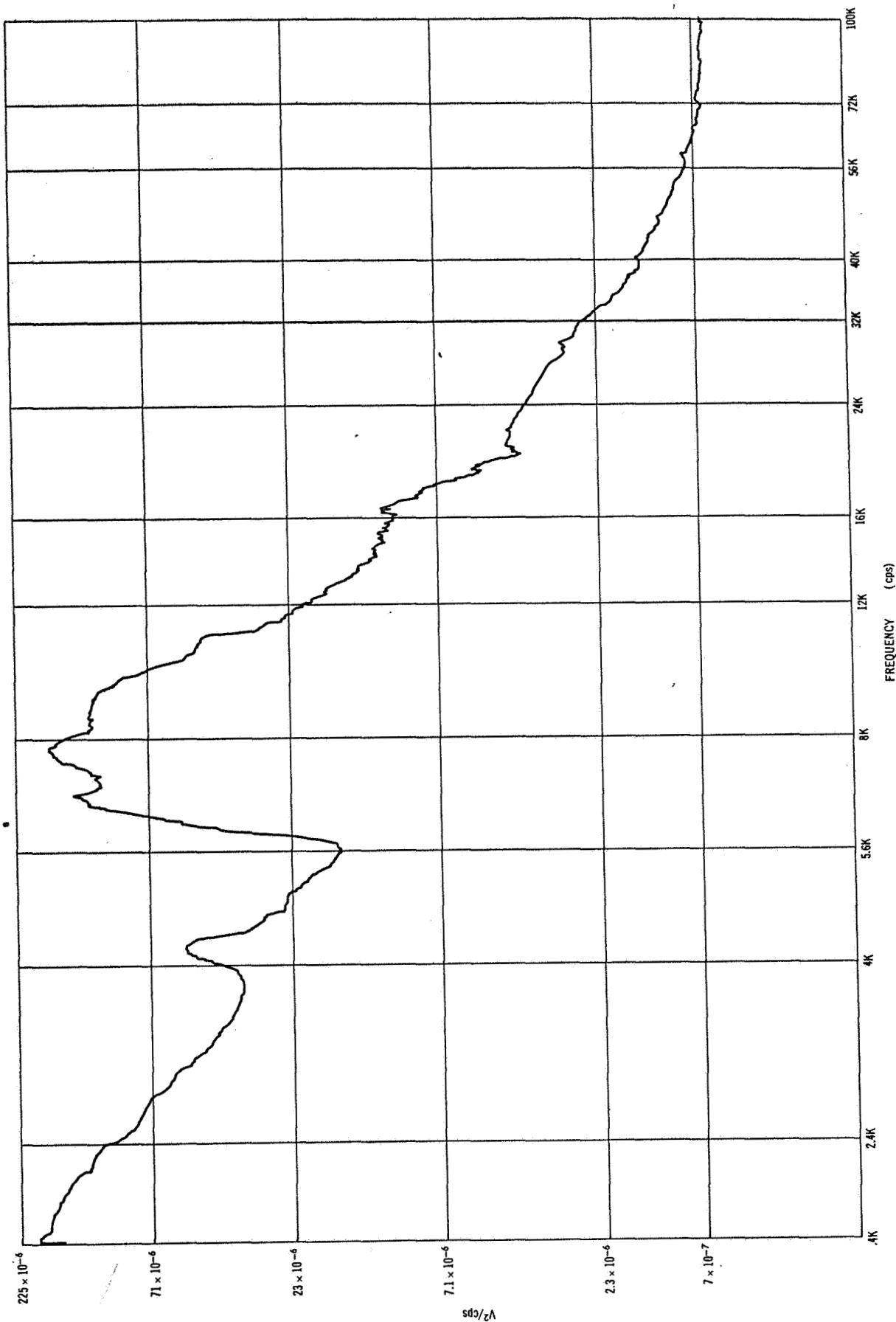


FIGURE 12

CONFIDENTIAL

APPARENT WIND TUNNEL NOISE SPECTRUM SHAPE
AT MACH 1.0 MEASURED ON THE FLAT PLATE

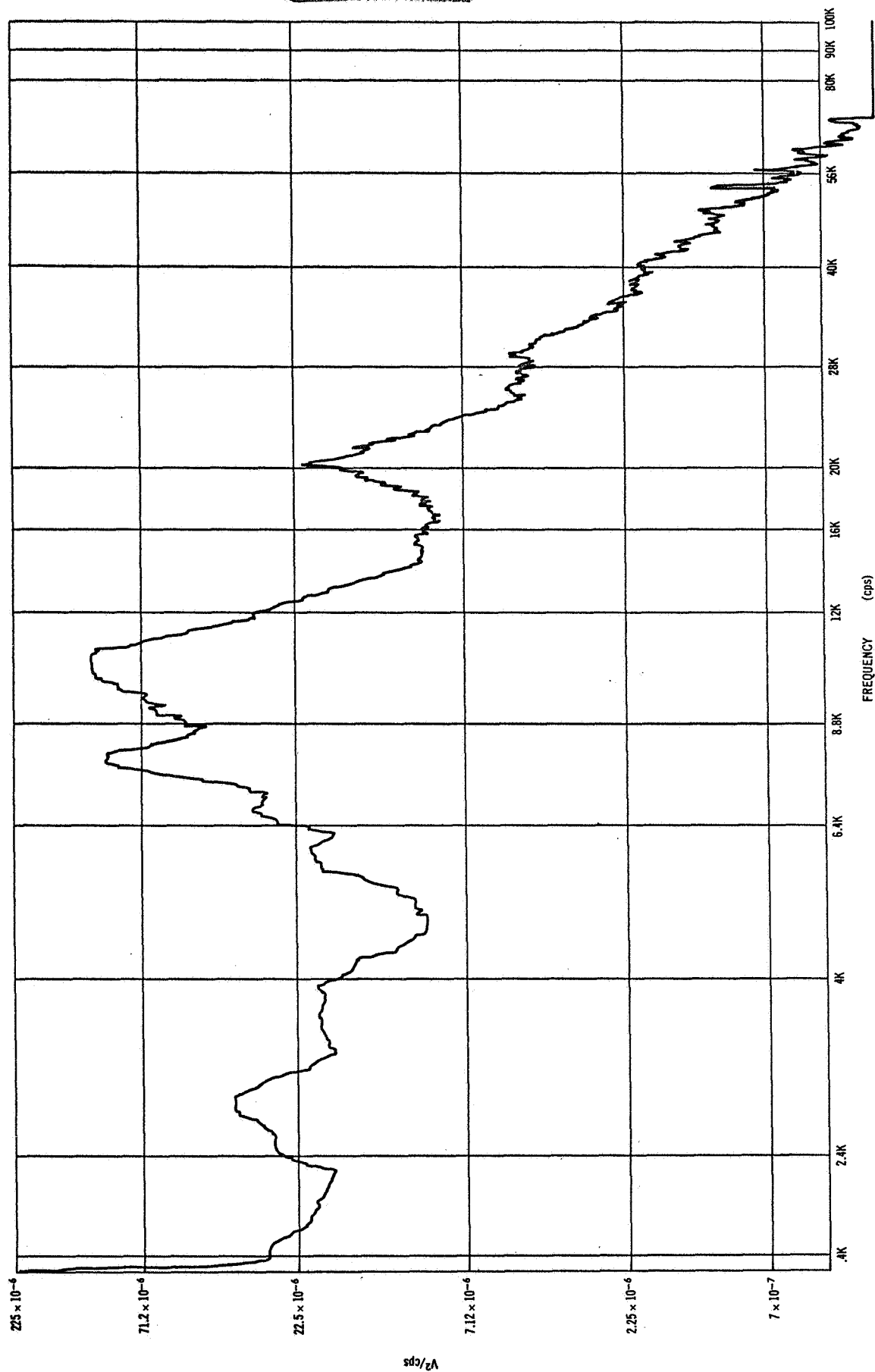


FIGURE 13

CONFIDENTIAL

CONFIDENTIAL

APPARENT WIND TUNNEL NOISE SPECTRUM SHAPE
AT MACH 1.0 MEASURED ON THE HEMISPHERE

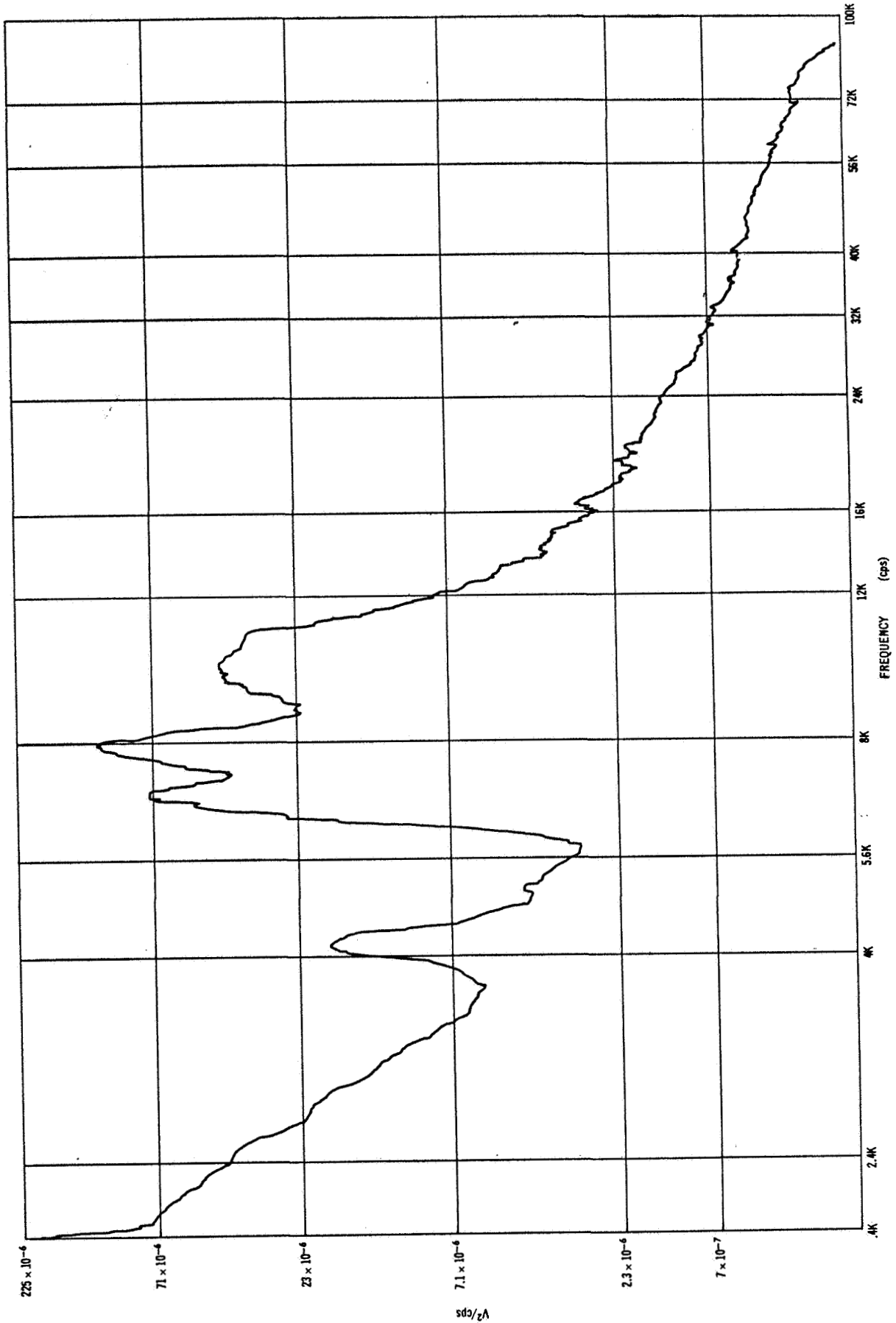


FIGURE 14

CONFIDENTIAL

APPARENT WIND TUNNEL NOISE SPECTRUM SHAPE
AT MACH 1.6 MEASURED ON THE FLAT PLATE

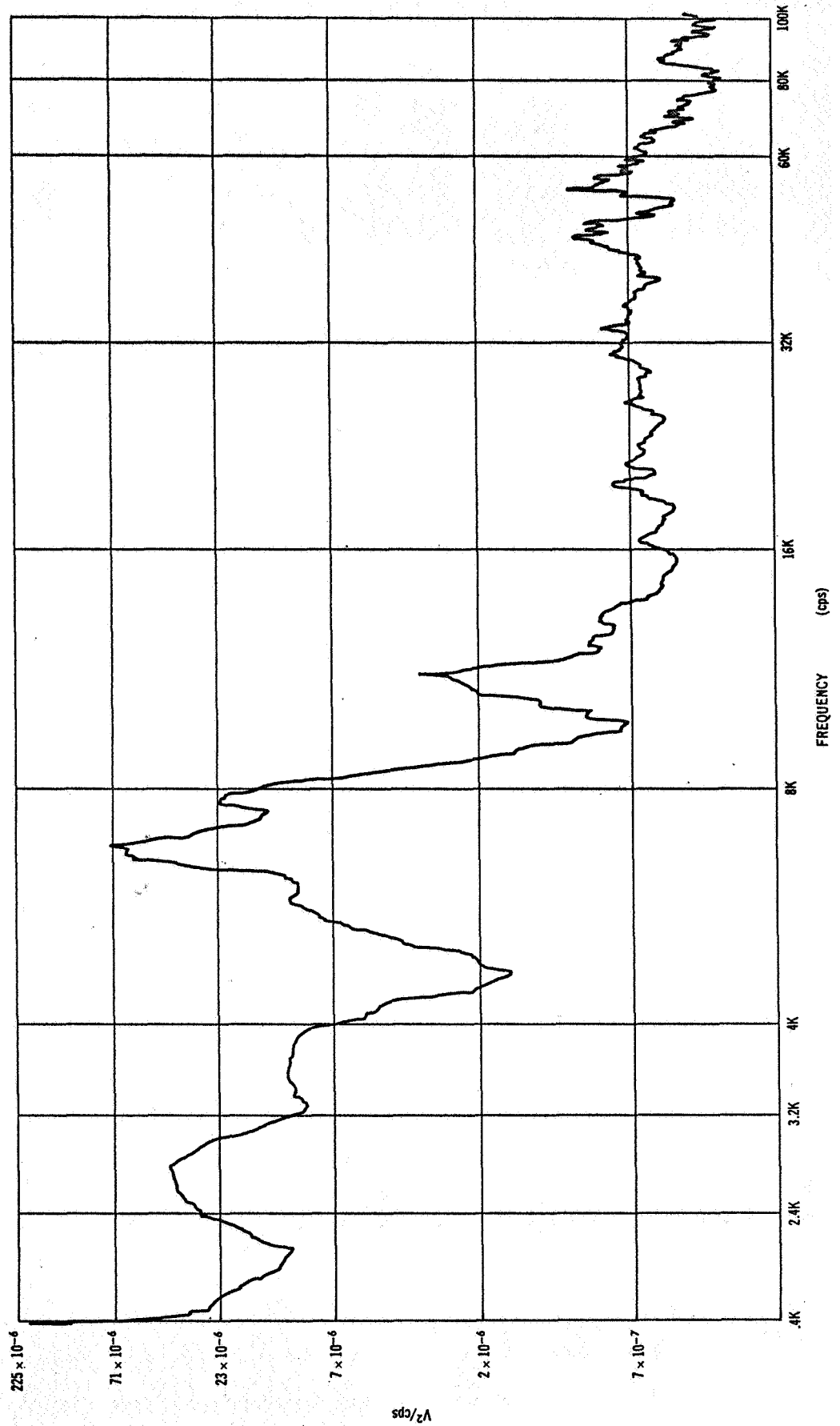


FIGURE 15

CONFIDENTIAL

CONFIDENTIAL

APPARENT WIND TUNNEL NOISE SPECTRUM SHAPE
AT MACH 1.6 MEASURED ON THE HEMISPHERE

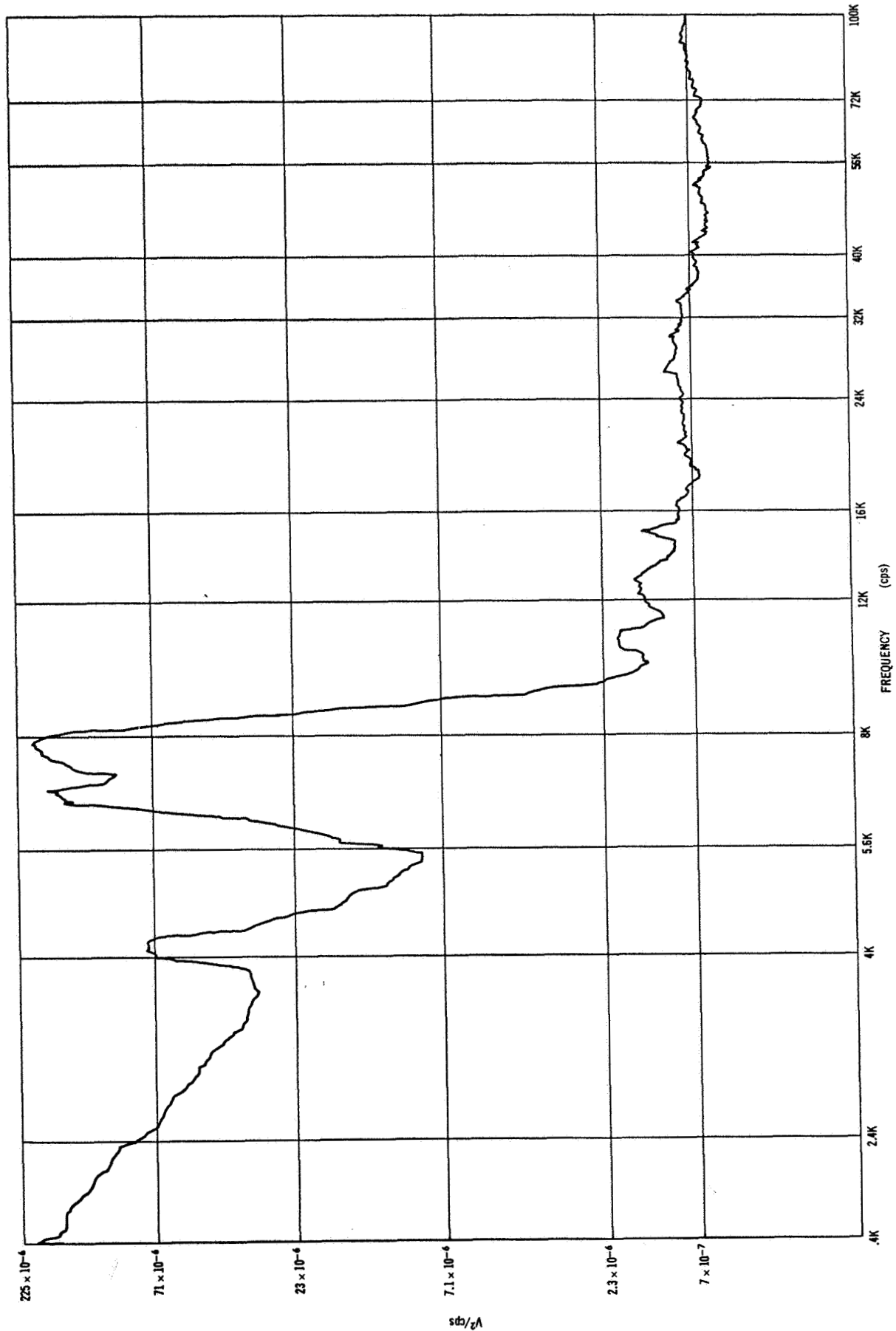


FIGURE 16

CONFIDENTIAL

CONFIDENTIAL

APPARENT WIND TUNNEL NOISE SPECTRUM SHAPE
AT MACH 3.5 MEASURED ON THE FLAT PLATE

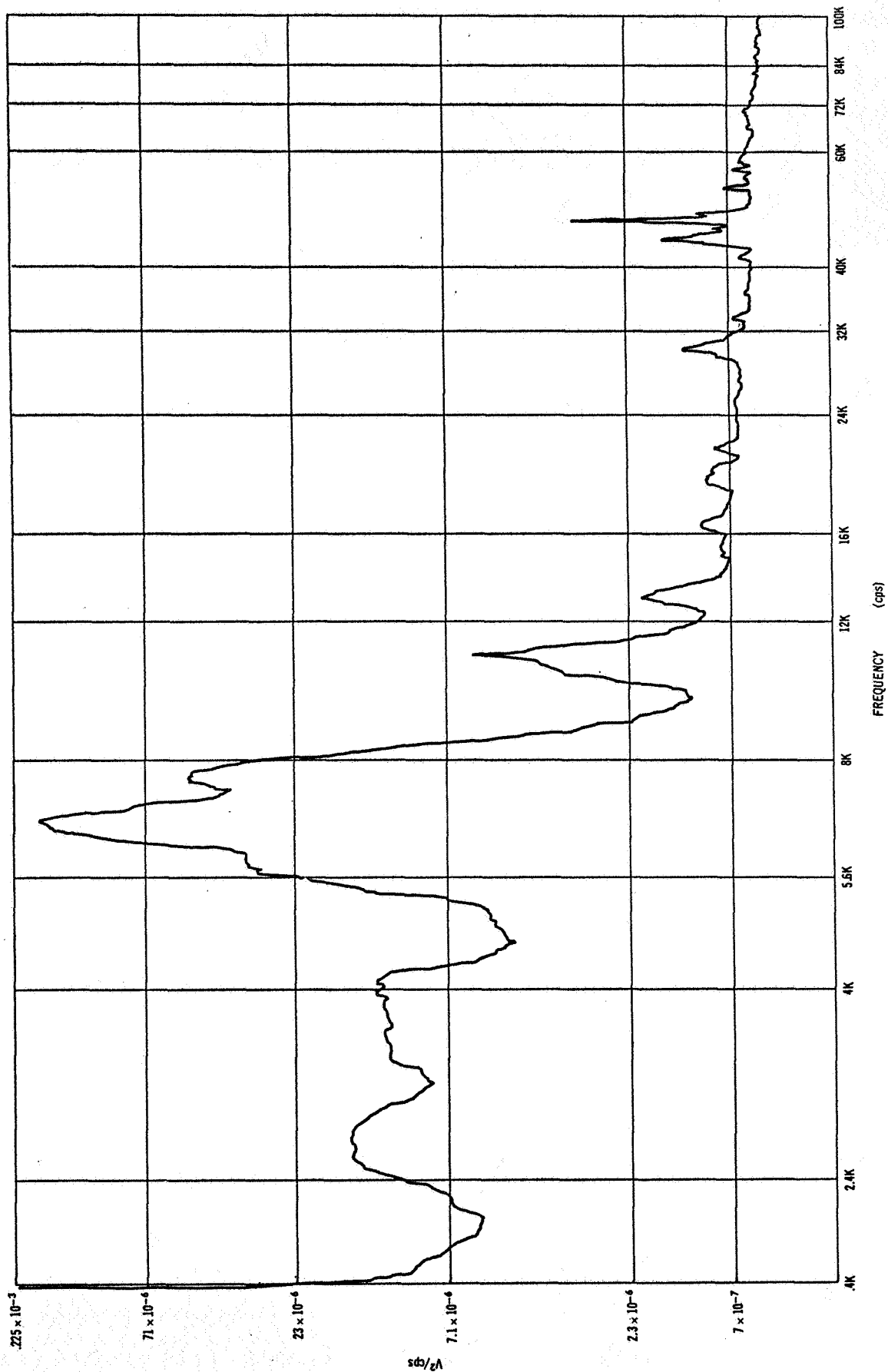


FIGURE 17

CONFIDENTIAL

APPARENT WIND TUNNEL NOISE SPECTRUM SHAPE
AT MACH 3.5 MEASURED ON THE HEMISPHERE

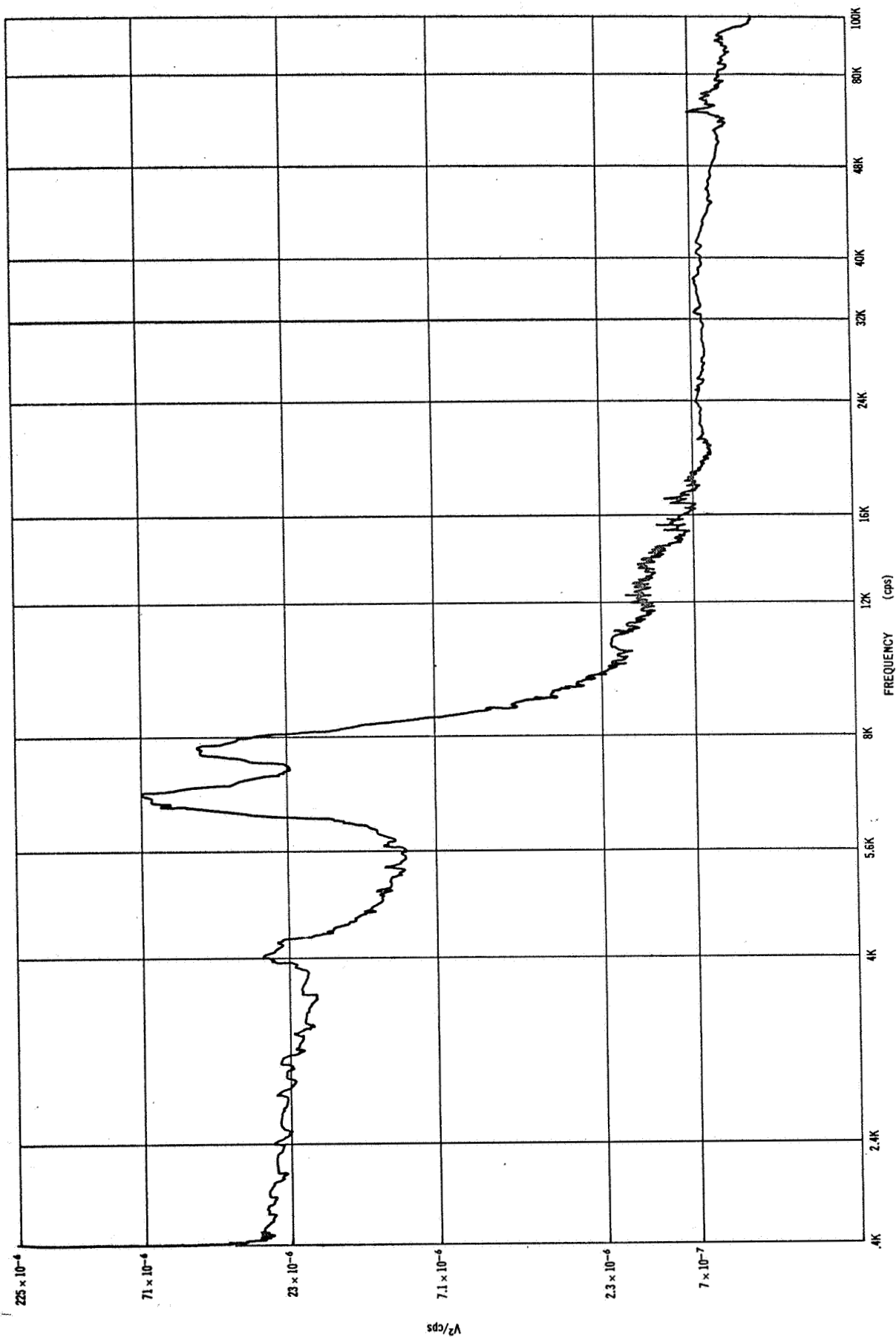


FIGURE 18

TYPICAL LD80-M1 VIBRATION RESPONSE
AT 1G R.M.S. SINE WAVE INPUT

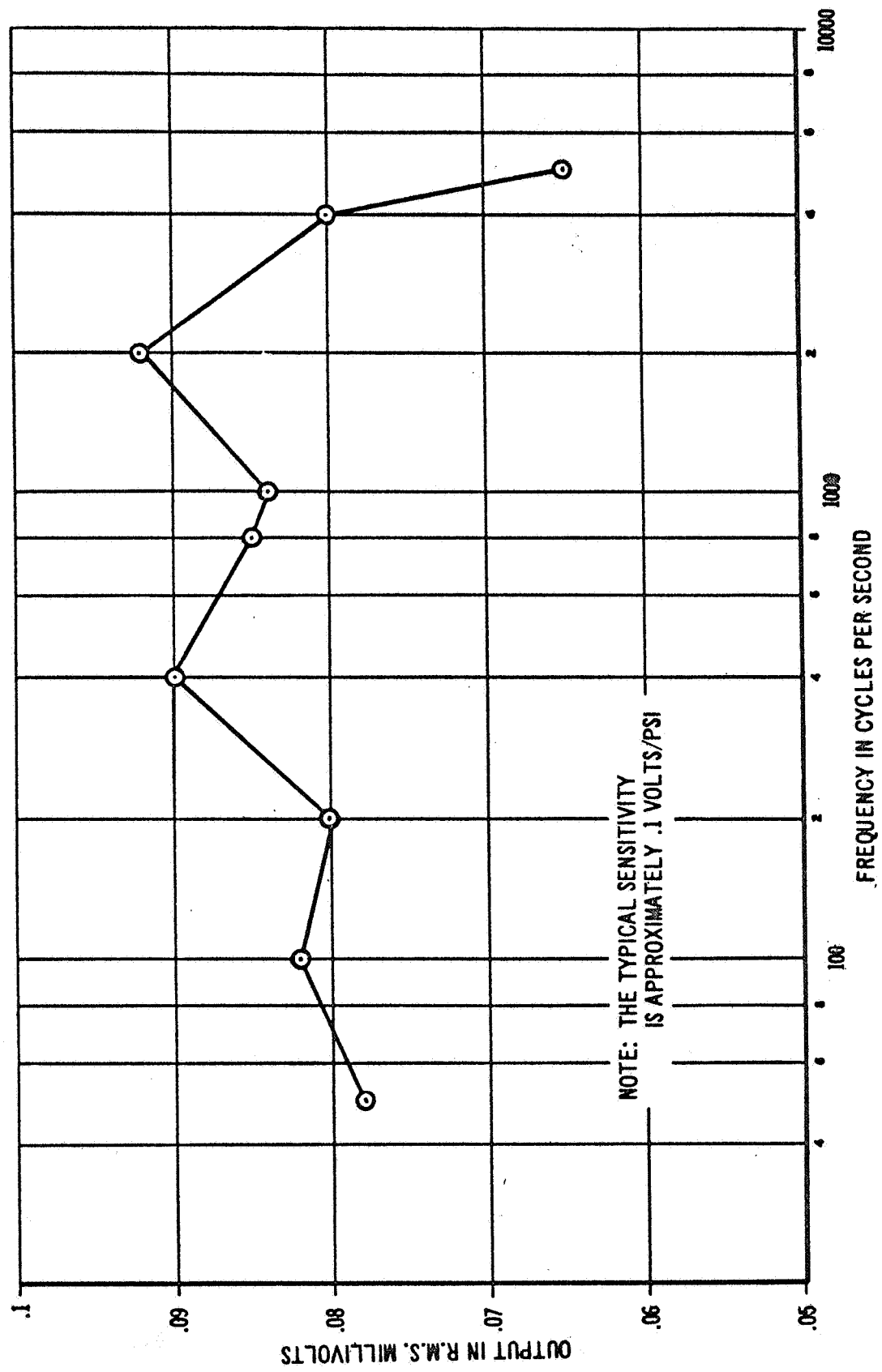


FIGURE 19

**VIBRATION SENSITIVITY OF THE
LD 80-MI'S TO A 2G SINE WAVE INPUT AT 800 CPS**

TRANSDUCER SERIAL NO.	OUTPUT IN RMS MILLIVOLTS	TRANSDUCER SERIAL NO.	OUTPUT IN RMS MILLIVOLTS
0	.17	31	.33
2	.23	32	.20
3	.27	33	.37
5	.19	34	.15
6	.12	35	.13
7	.19	36	1.90
10	.20	39	.29
11	.52	42	.31
12	.76	43	.46
13	.41	44	.77
14	.20	45	.62
15	.28	47	.61
20	.34	48	2.80
21	.17	49	.68
22	.26	50	.65
24	.15	52	3.70
27	.22	54	3.90
28	.22	55	1.12
29	.35	59	.90
30	.35	60	.44

FIGURE 20

CONFIDENTIAL

OVERALL FLUCTUATING PRESSURE LEVEL DISTRIBUTION
OVER THE 2.75% SATURN MODEL

MACH NO. 0.8
ANGLE OF ATTACK 0°
CONFIGURATION B

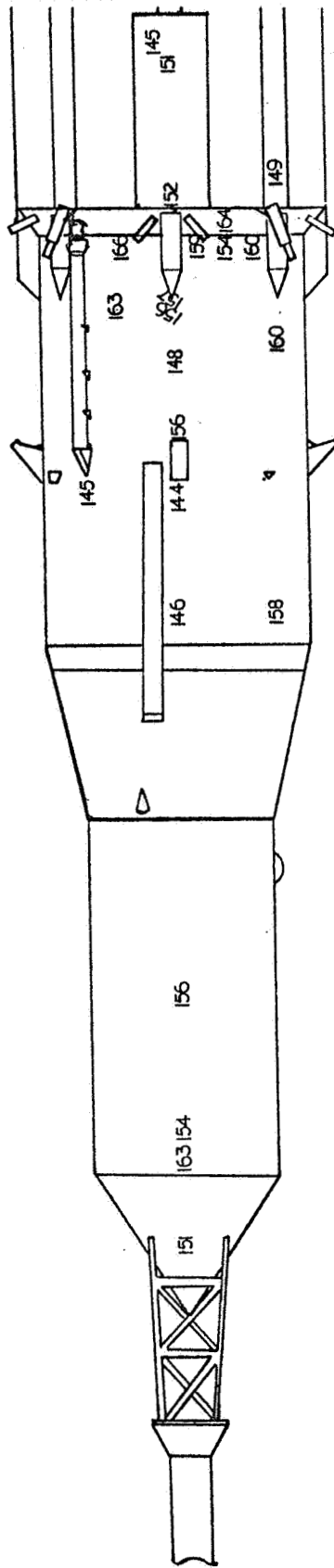


FIGURE 21

CONFIDENTIAL

OVERALL FLUCTUATING PRESSURE LEVEL DISTRIBUTION
OVER THE 2.75% SATURN MODEL

MACH NO. 0.9
ANGLE OF ATTACK 0°
CONFIGURATION B

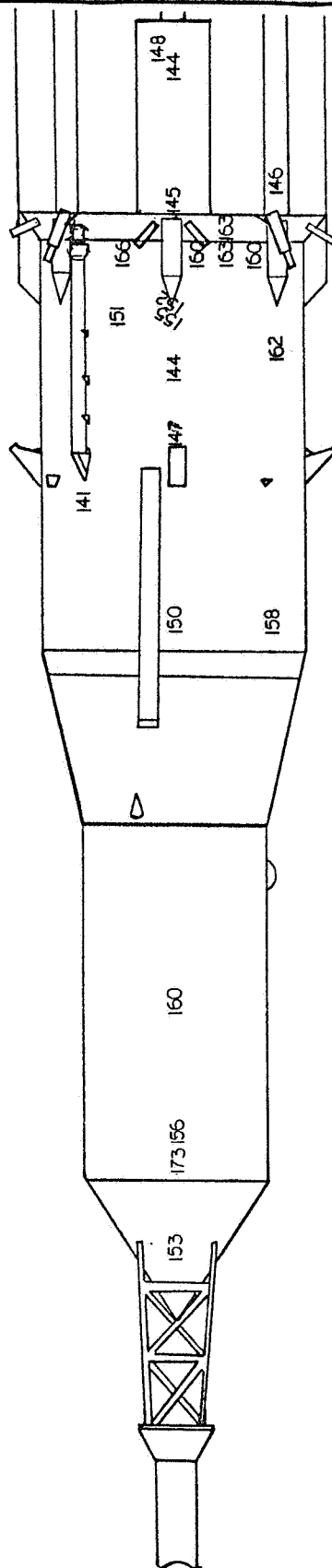


FIGURE 22

CONFIDENTIAL

OVERALL FLUCTUATING PRESSURE LEVEL DISTRIBUTION OVER THE 2.75% SATURN MODEL

MACH NO. 0.95
ANGLE OF ATTACK 0°
CONFIGURATION 8

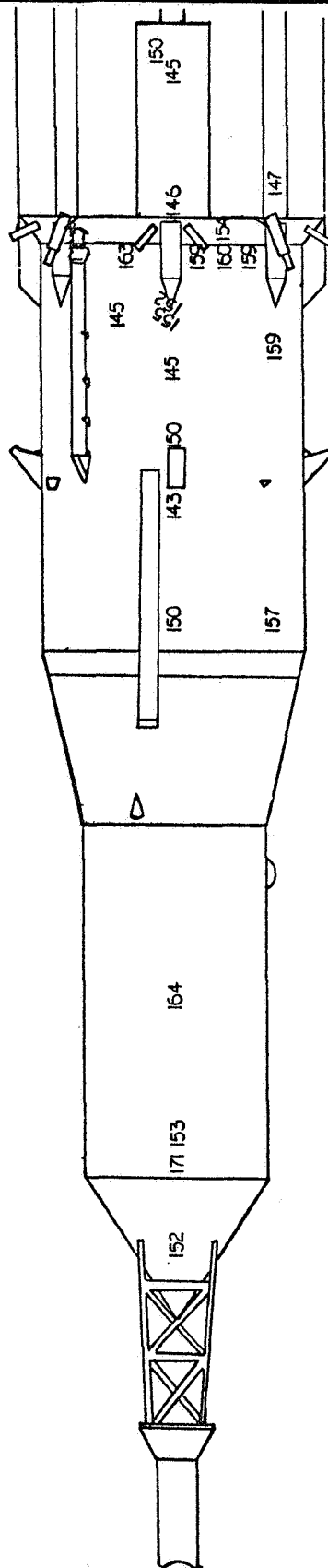
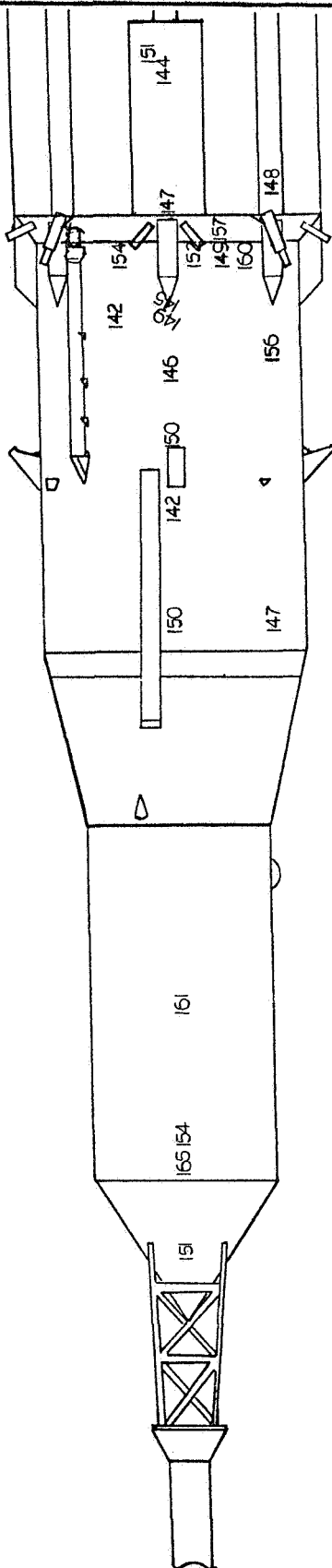


FIGURE 23

CONFIDENTIAL

OVERALL FLUCTUATING PRESSURE LEVEL DISTRIBUTION OVER THE 2.75% SATURN MODEL

MACH NO. 1.0
ANGLE OF ATTACK 0°
CONFIGURATION B

**FIGURE 24**

57

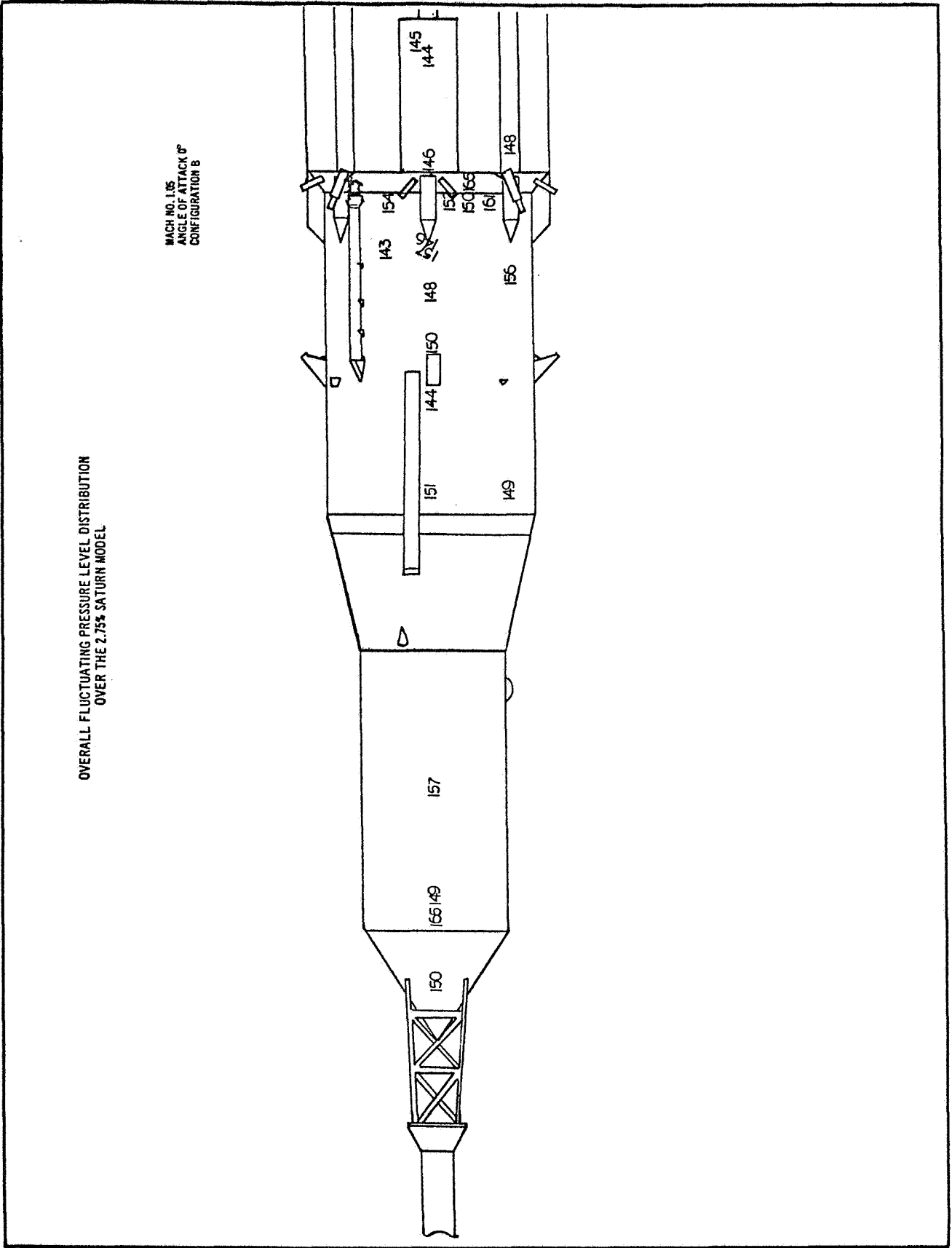


FIGURE 25

CONFIDENTIAL

OVERALL FLUCTUATING PRESSURE LEVEL DISTRIBUTION
OVER THE 2.75% SATURN MODEL

MACH NO. 1.2
ANGLE OF ATTACK 0°
CONFIGURATION B

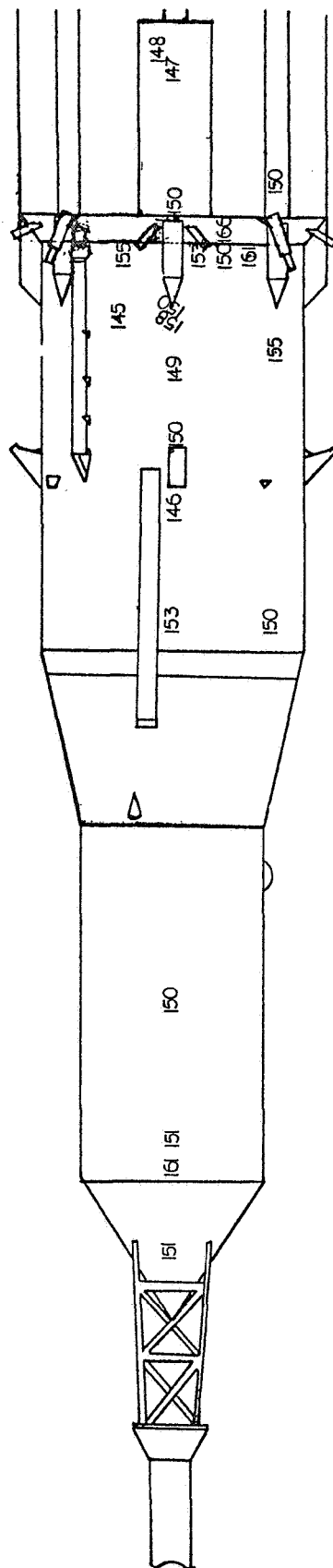


FIGURE 26

CONFIDENTIAL

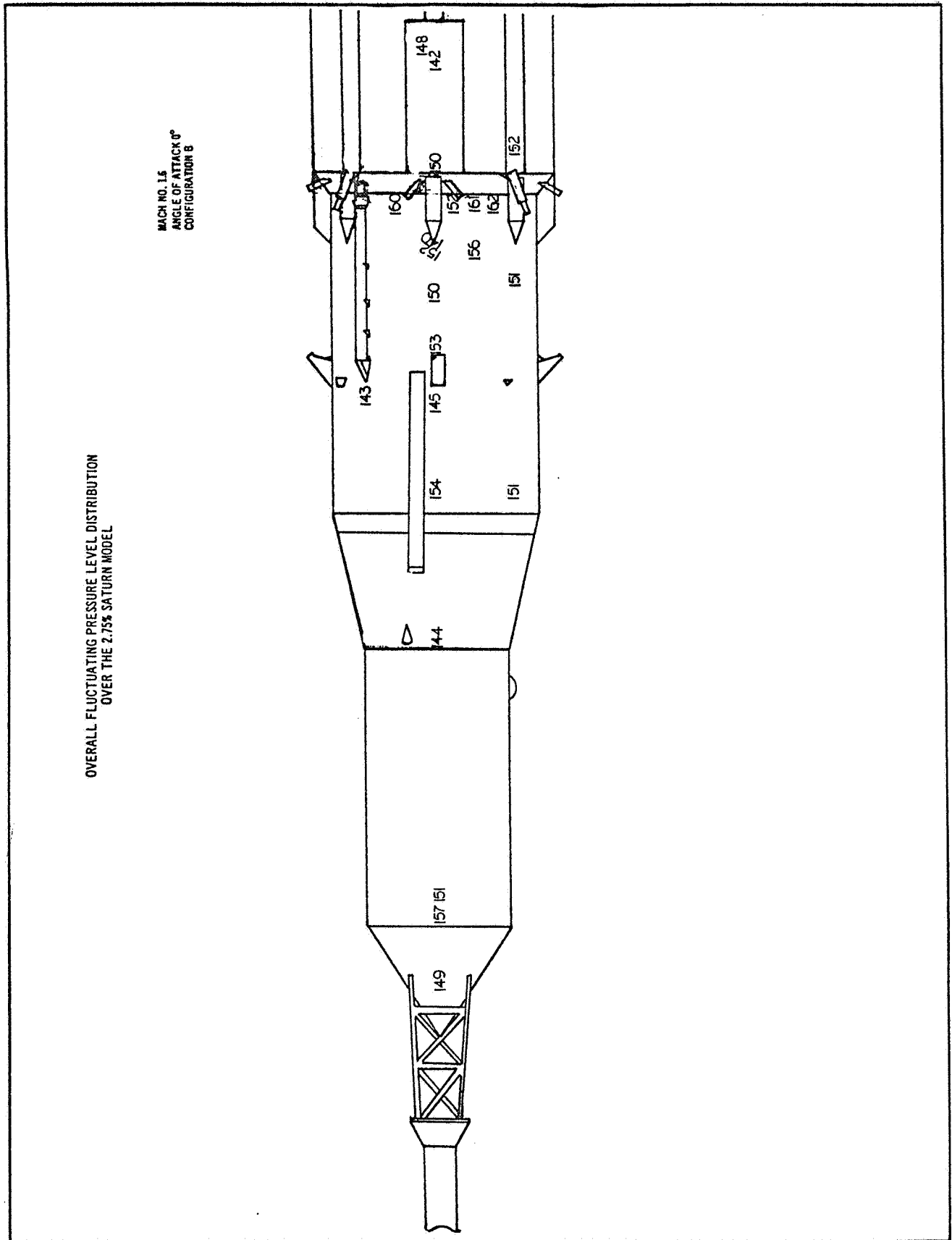


FIGURE 27

CONFIDENTIAL

OVERALL FLUCTUATING PRESSURE LEVEL DISTRIBUTION
OVER THE 2.75% SATURN MODEL

MACH NO. 1.8
ANGLE OF ATTACK 0°
CONFIGURATION B

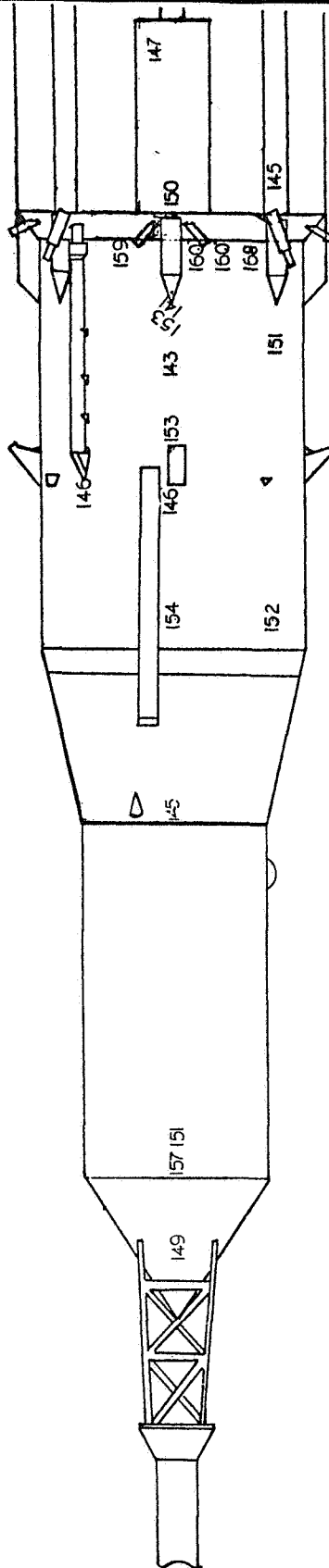


FIGURE 28

CONFIDENTIAL

CONFIDENTIAL

OVERALL FLUCTUATING PRESSURE LEVEL DISTRIBUTION OVER THE 2.75% SATURN MODEL

MACH NO. 2.0
ANGLE OF ATTACK 0°
CONFIGURATION 8

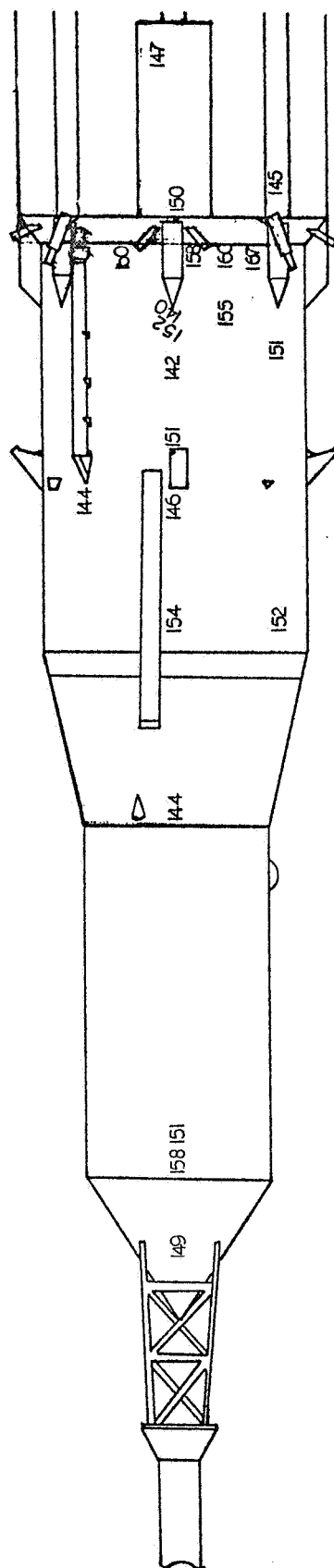


FIGURE 29

~~CONFIDENTIAL~~

OVERALL FLUCTUATING PRESSURE LEVEL DISTRIBUTION
OVER THE 2.75% SATURN MODEL

MACH NO. 3.5
ANGLE OF ATTACK 0°
CONFIGURATION B

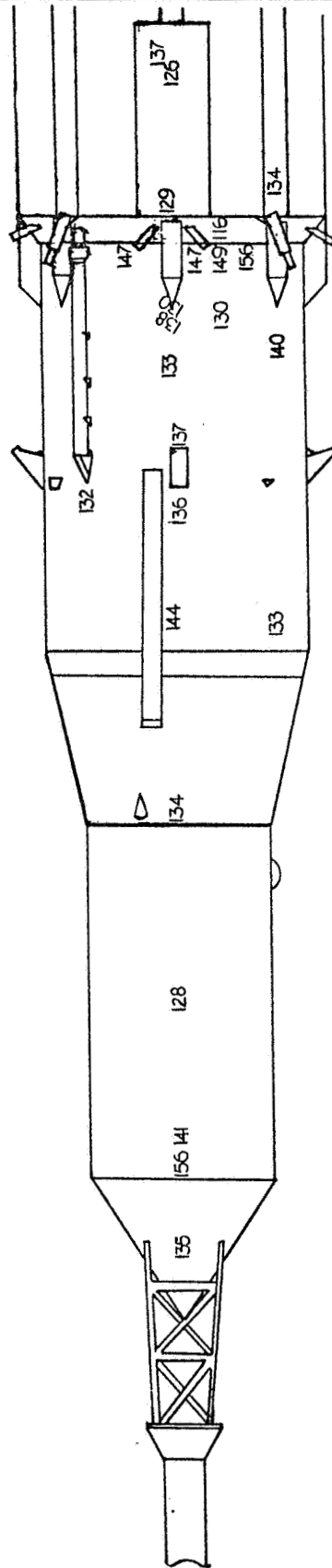


FIGURE 30

CONFIDENTIAL

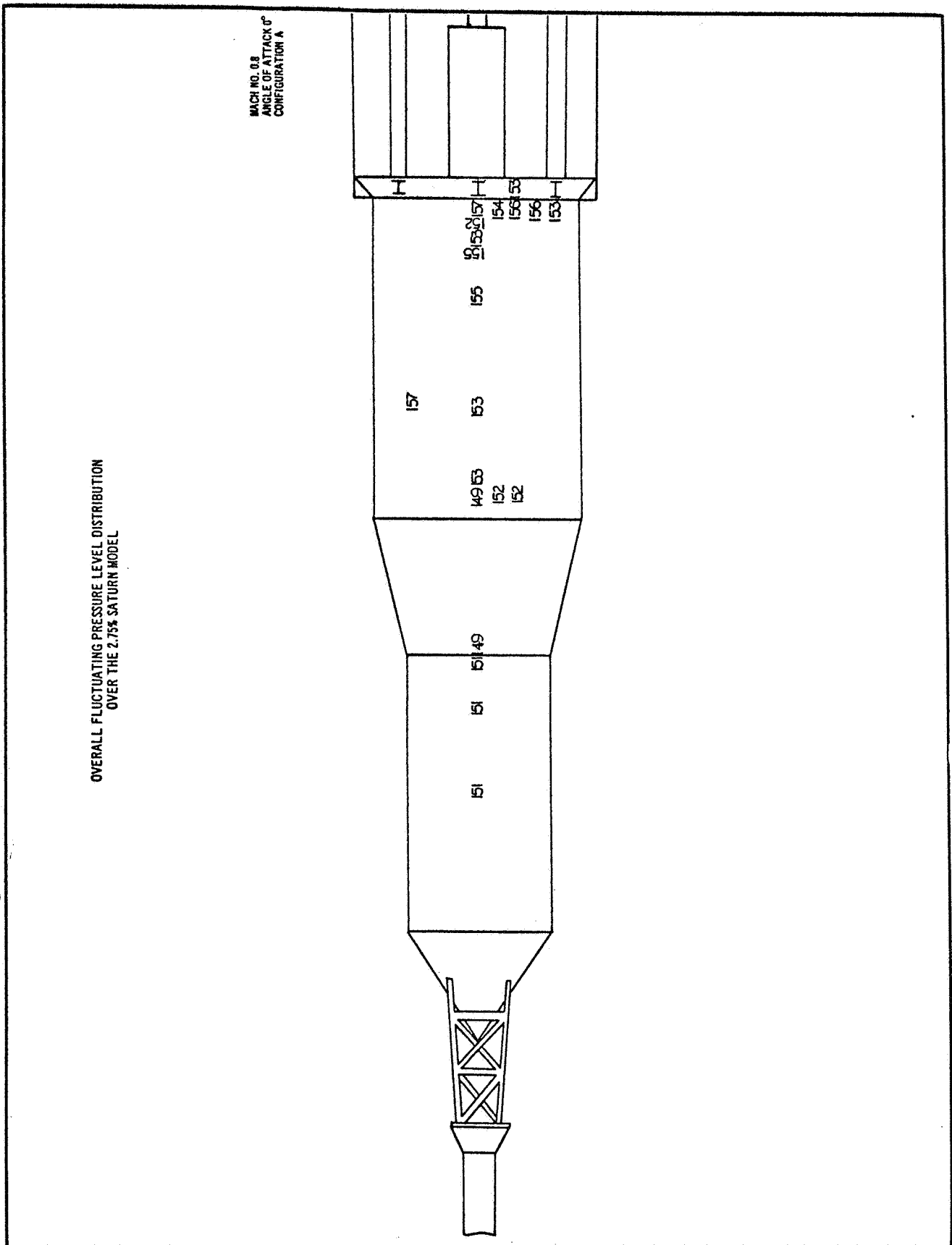


FIGURE 31

CONFIDENTIAL

CONFIDENTIAL

OVERALL FLUCTUATING PRESSURE LEVEL DISTRIBUTION
OVER THE 2.75% SATURN MODEL

MACH NO. 9
ANGLE OF ATTACK 0°
CONFIGURATION A

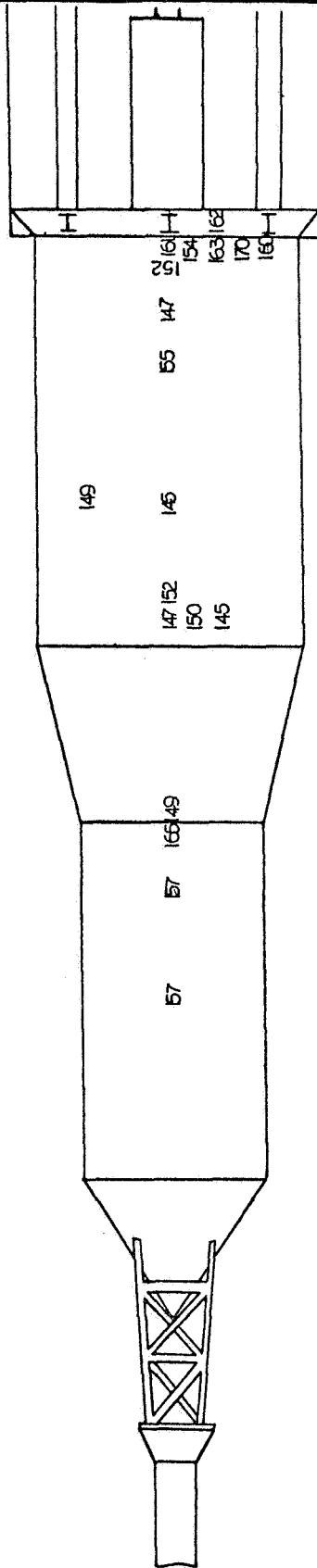


FIGURE 32

CONFIDENTIAL

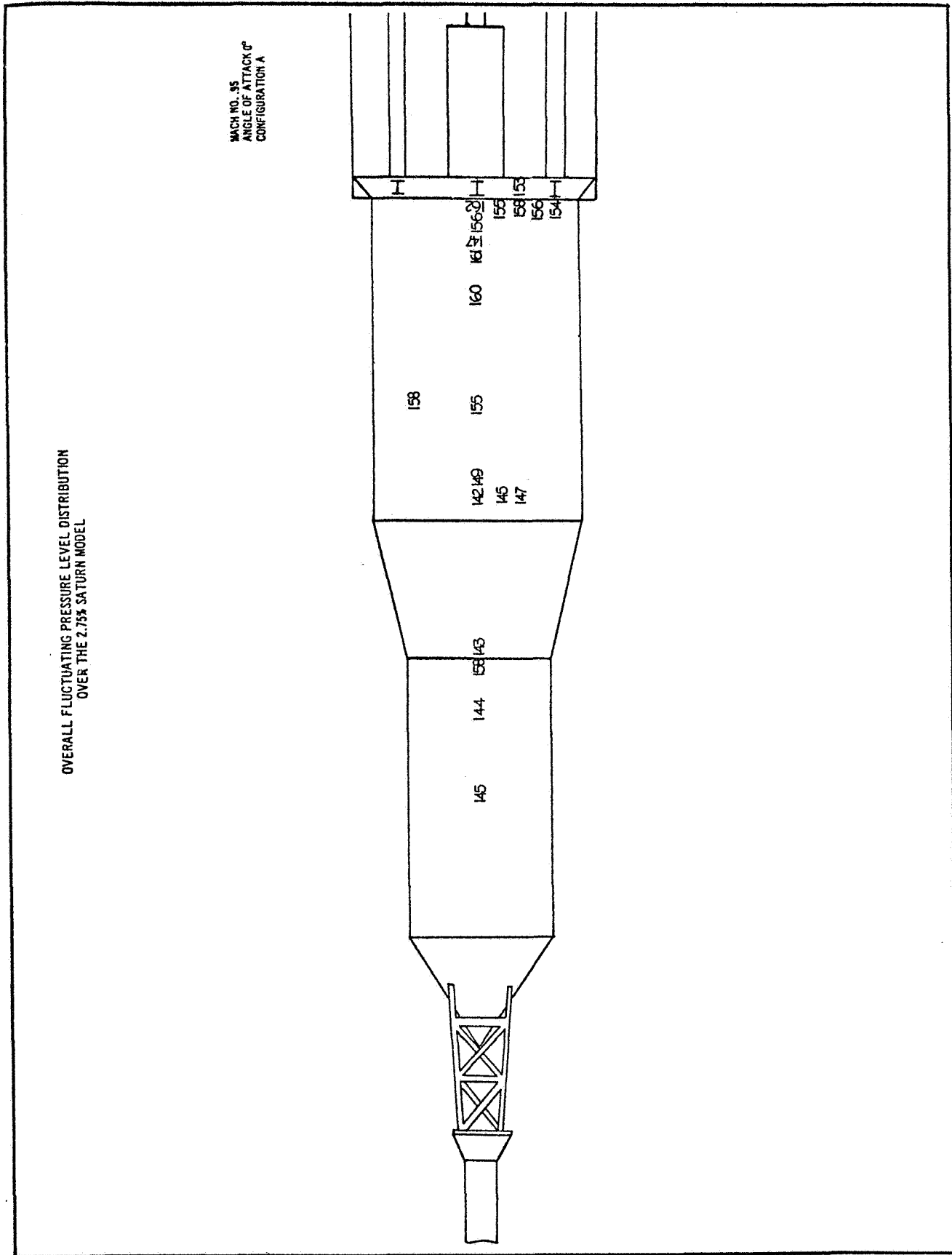


FIGURE 33

OVERALL FLUCTUATING PRESSURE LEVEL DISTRIBUTION
OVER THE 2.75% SATURN MODEL

MACH NO. 1.0
ANGLE OF ATTACK 0°
CONFIGURATION A

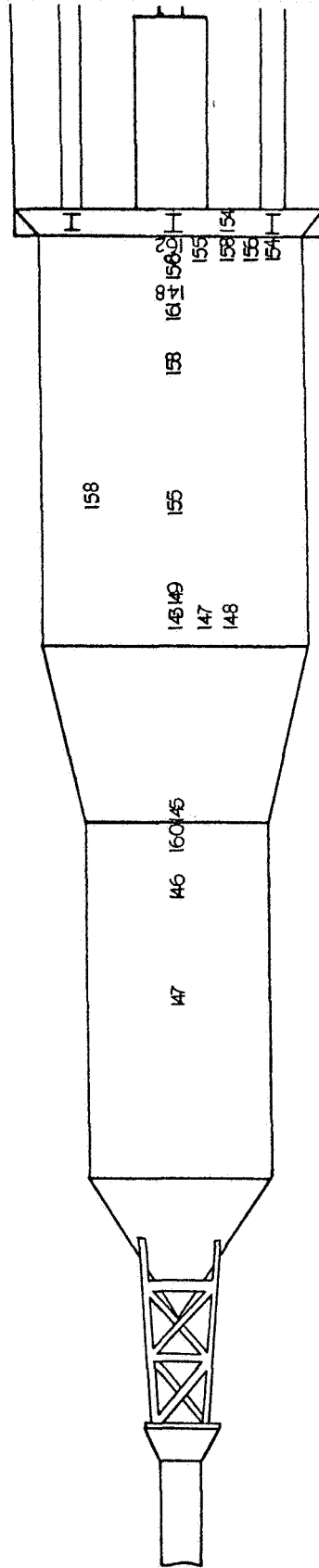


FIGURE 34

CONFIDENTIAL

CONFIDENTIAL

OVERALL FLUCTUATING PRESSURE LEVEL DISTRIBUTION
OVER THE 2.75% SATURN MODEL

MACH NO. 1.05
ANGLE OF ATTACK 0°
CONFIGURATION A

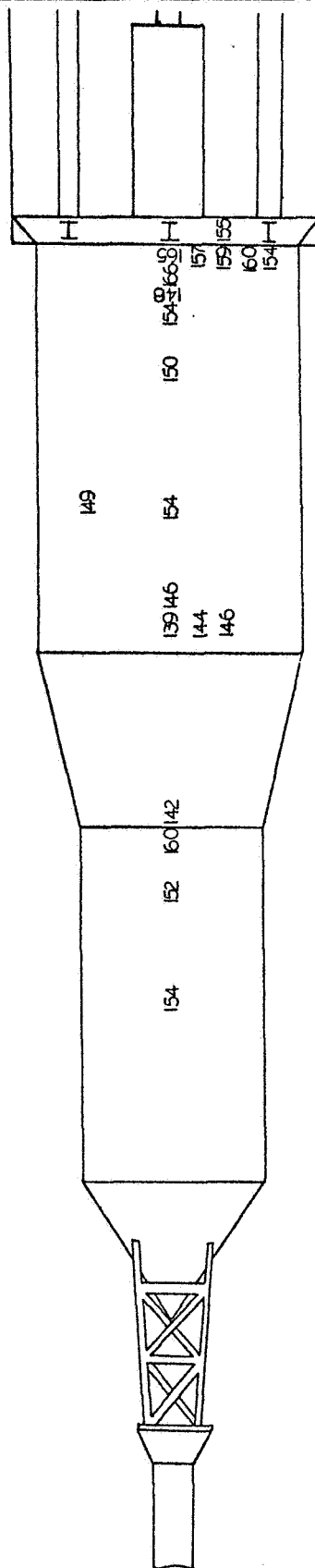


FIGURE 35

CONFIDENTIAL

OVERALL FLUCTUATING PRESSURE LEVEL DISTRIBUTION
OVER THE 2.75% SATURN MODEL

MACH NO. 1.2
ANGLE OF ATTACK 0°
CONFIGURATION A

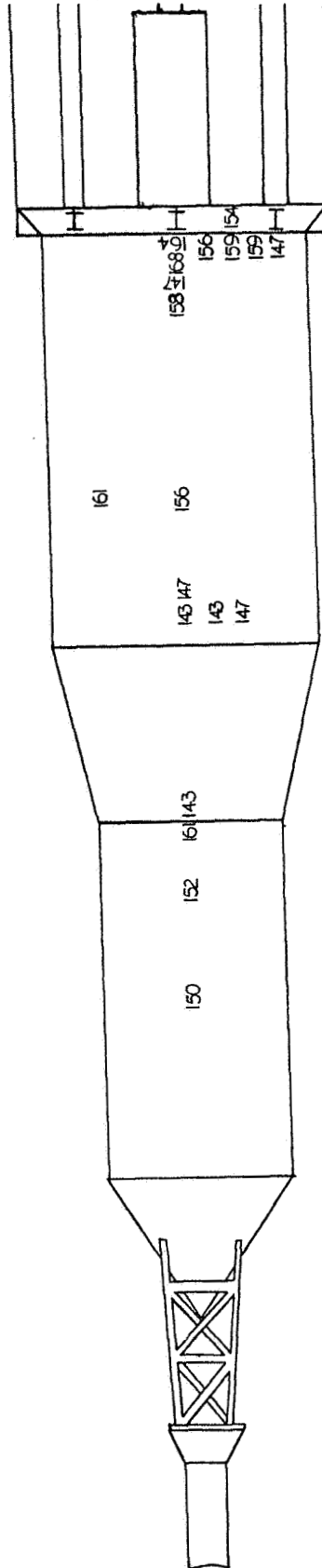


FIGURE 36

OVERALL FLUCTUATING PRESSURE LEVEL DISTRIBUTION
OVER THE 2.75% SATURN MODEL

MACH NO. 1.6
ANGLE OF ATTACK 0°
CONFIGURATION A

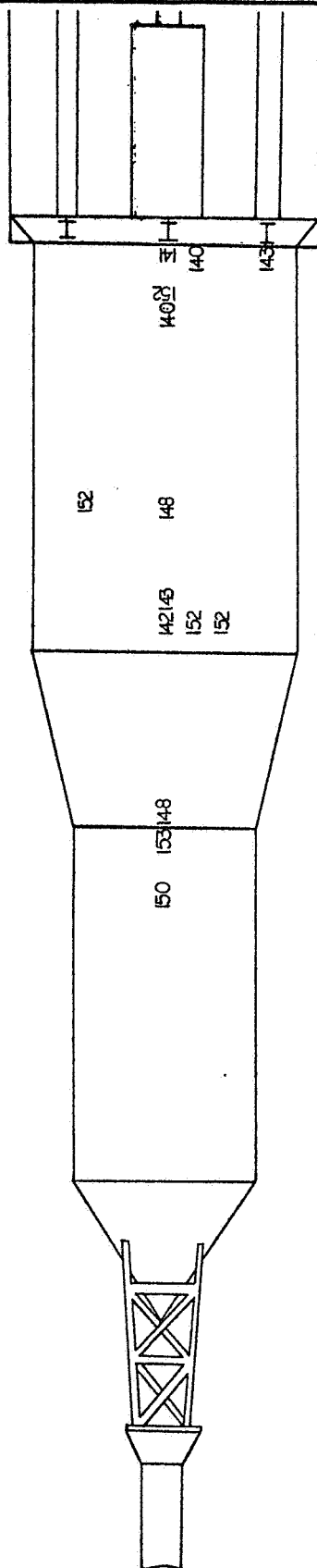


FIGURE 37

CONFIDENTIAL

OVERALL FLUCTUATING PRESSURE LEVEL DISTRIBUTION
OVER THE 2.75% SATURN MODEL

MACH NO. 1.8
ANGLE OF ATTACK 0°
CONFIGURATION A

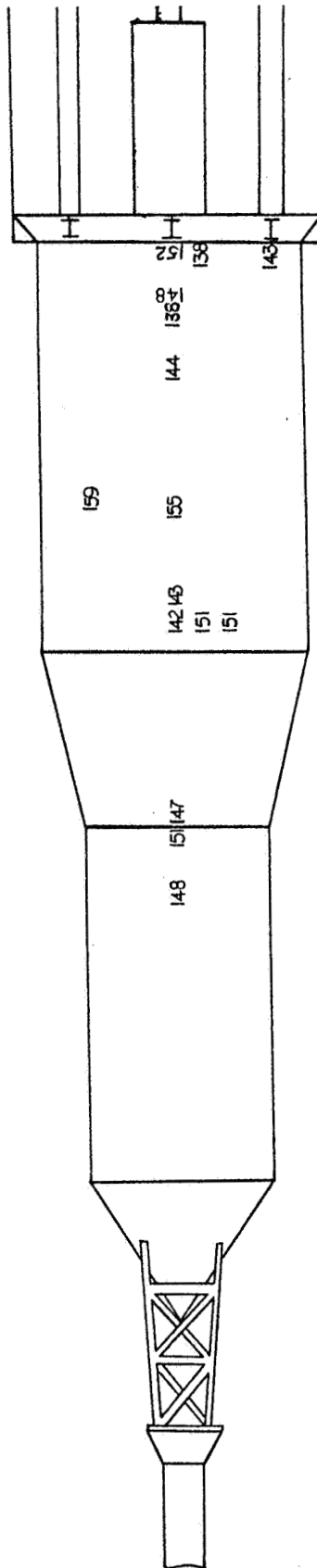


FIGURE 38

CONFIDENTIAL

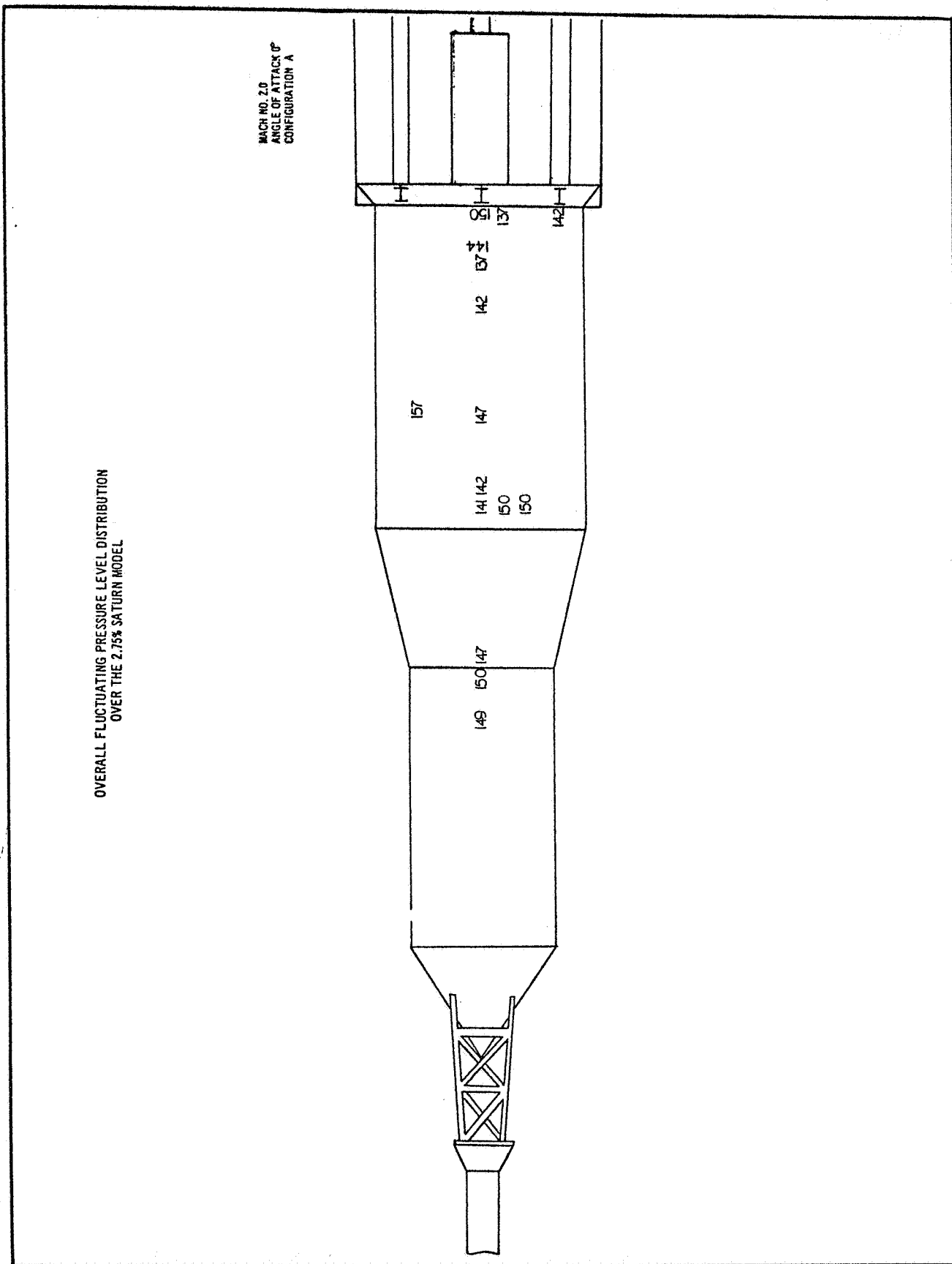


FIGURE 39

~~CONFIDENTIAL~~

OVERALL FLUCTUATING PRESSURE LEVEL DISTRIBUTION
OVER THE 2.75% SATURN MODEL

MACH NO. 0.8
ANGLE OF ATTACK 0°
CONFIGURATION C

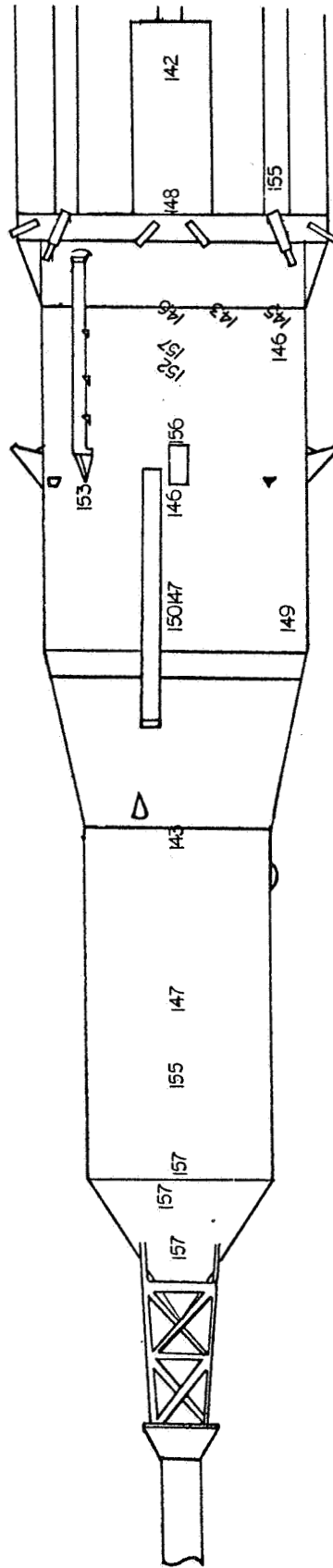


FIGURE 40

~~CONFIDENTIAL~~

OVERALL FLUCTUATING PRESSURE LEVEL DISTRIBUTION
OVER THE 2.75% SATURN MODEL

MACH NO. 0.9
ANGLE OF ATTACK 0°
CONFIGURATION C

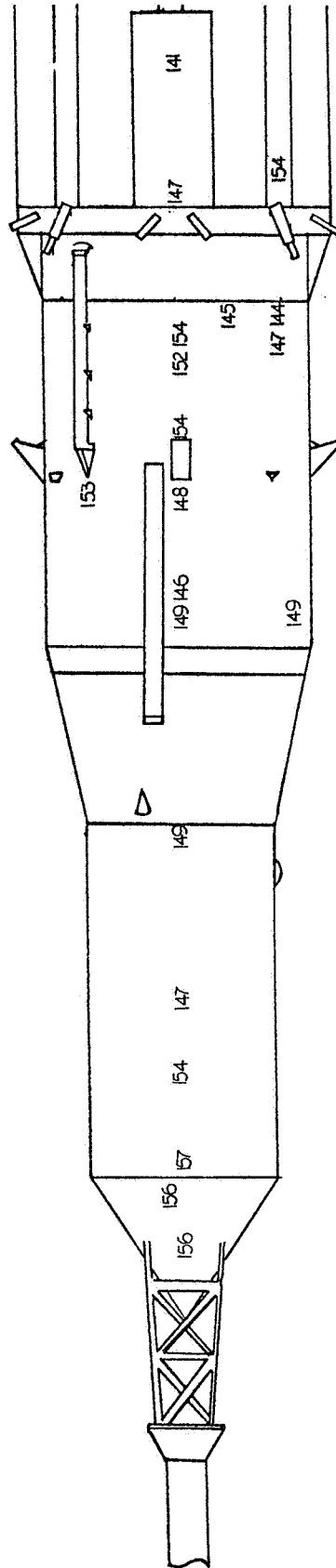


FIGURE 41

CONFIDENTIAL

OVERALL FLUCTUATING PRESSURE LEVEL DISTRIBUTION
OVER THE 2.75% SATURN MODEL

MACH NO. 0.95
ANGLE OF ATTACK OF
CONFIGURATION C

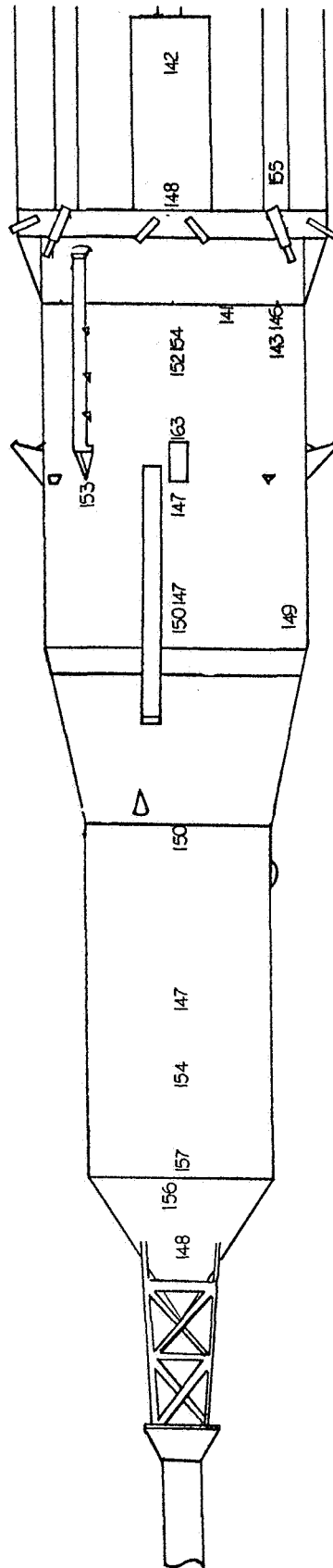


FIGURE 42

CONFIDENTIAL

OVERALL FLUCTUATING PRESSURE LEVEL DISTRIBUTION
OVER THE 2.75% SATURN MODEL

MACH NO. 1.00
ANGLE OF ATTACK 0°
CONFIGURATION C

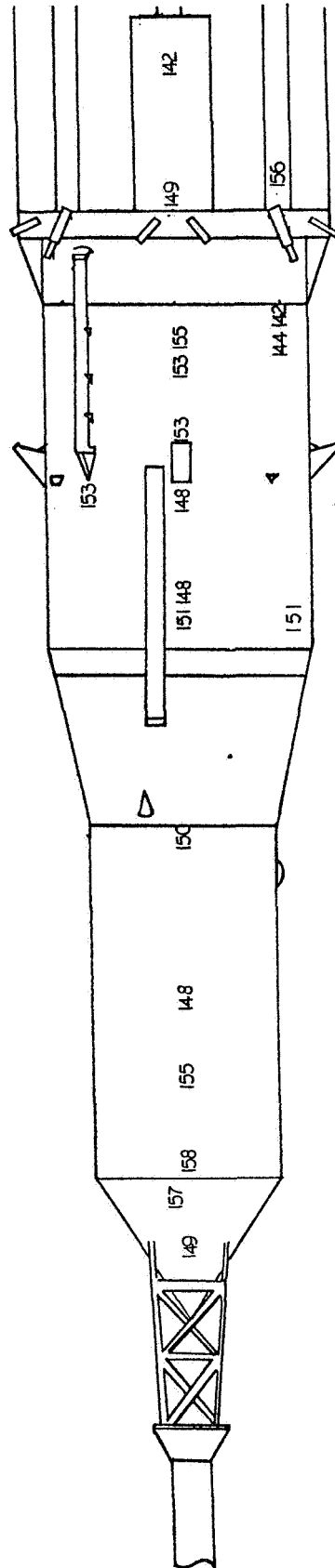


FIGURE 43

CONFIDENTIAL

OVERALL FLUCTUATING PRESSURE LEVEL DISTRIBUTION
OVER THE 2.75% SATURN MODEL

MACH NO. 1.05
ANGLE OF ATTACK 0°
CONFIGURATION C

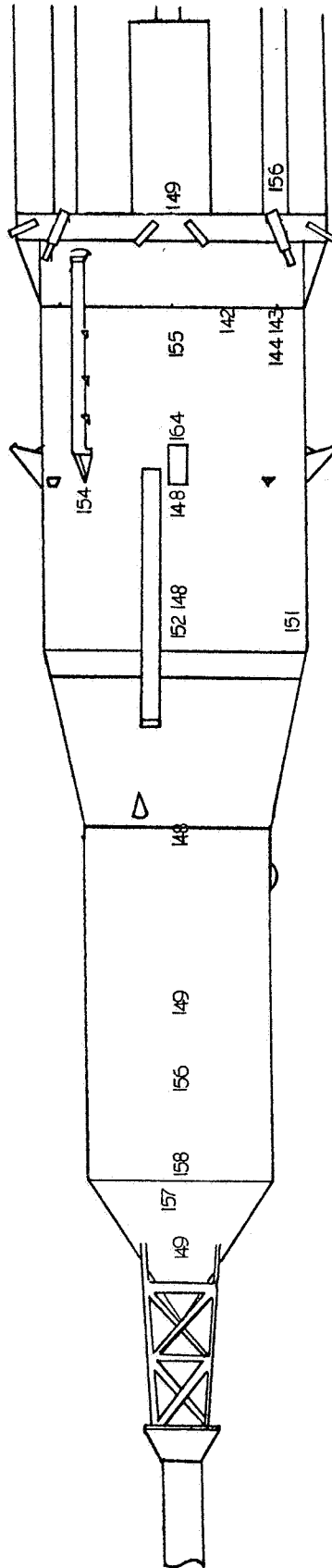


FIGURE 44

CONFIDENTIAL

CONFIDENTIAL

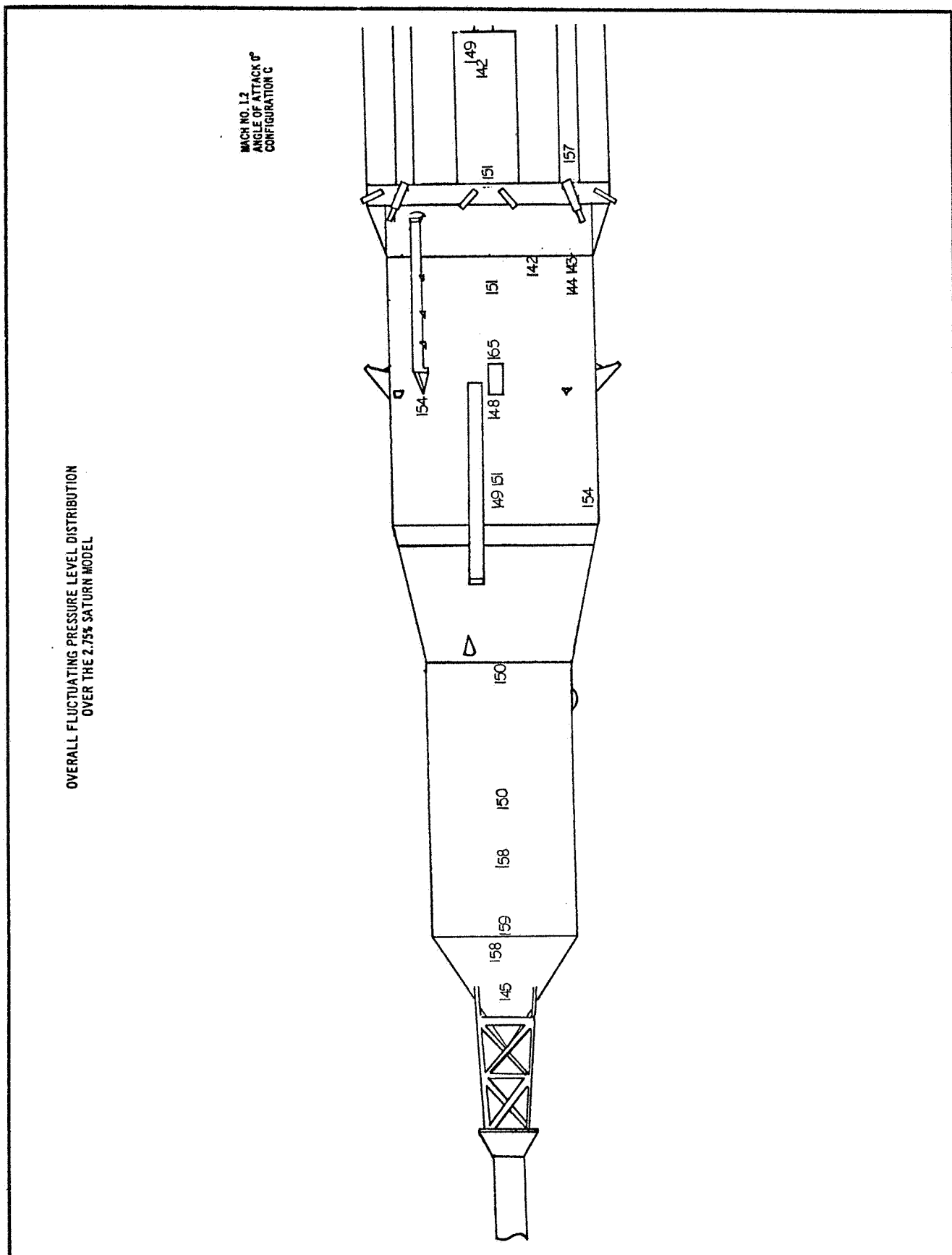


FIGURE 45

CONFIDENTIAL

OVERALL FLUCTUATING PRESSURE LEVEL DISTRIBUTION
OVER THE 2.75% SATURN MODEL

MACH NO. 1.6
ANGLE OF ATTACK 0°
CONFIGURATION C

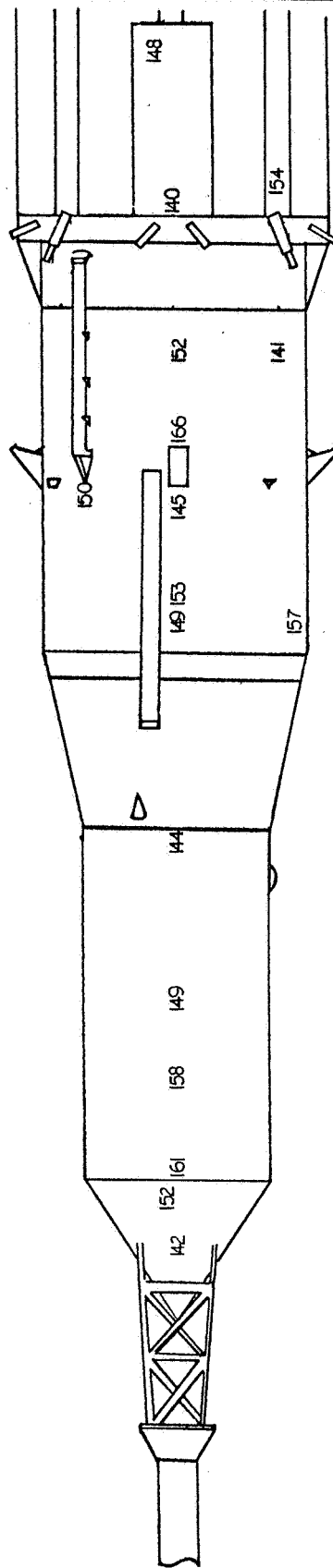


FIGURE 46

OVERALL FLUCTUATING PRESSURE LEVEL DISTRIBUTION
OVER THE 2.75% SATURN MODEL

MACH NO. 1.8
ANGLE OF ATTACK 0°
CONFIGURATION C

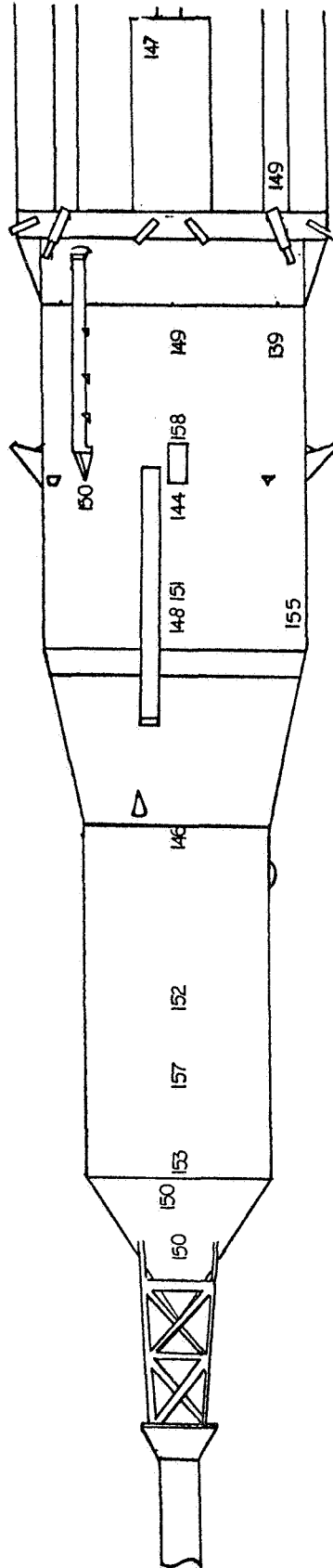


FIGURE 47

CONFIDENTIAL

CONFIDENTIAL

OVERALL FLUCTUATING PRESSURE LEVEL DISTRIBUTION
OVER THE 2.75% SATURN MODEL

MACH NO. 2.8
ANGLE OF ATTACK 0°
CONFIGURATION C

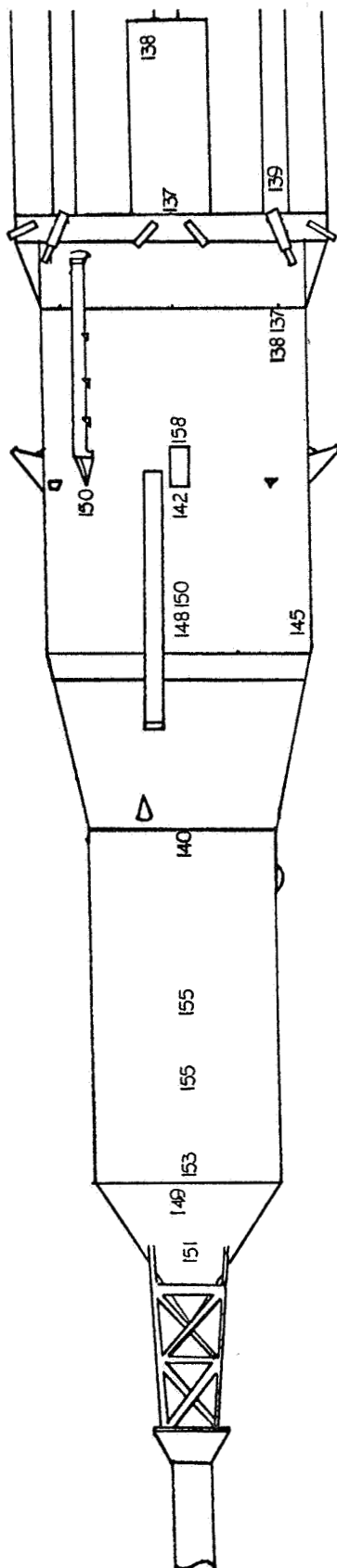


FIGURE 48

CONFIDENTIAL

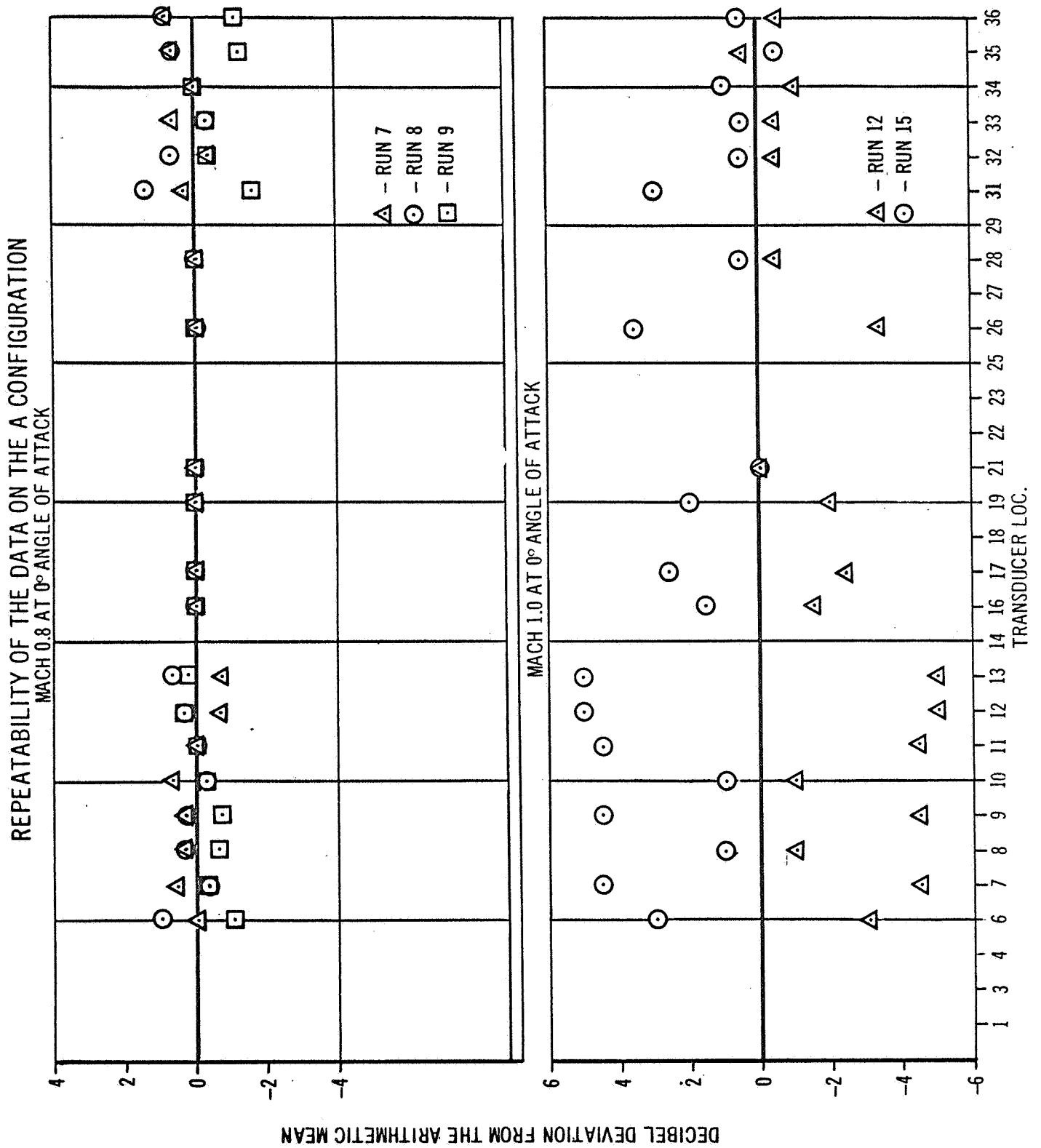
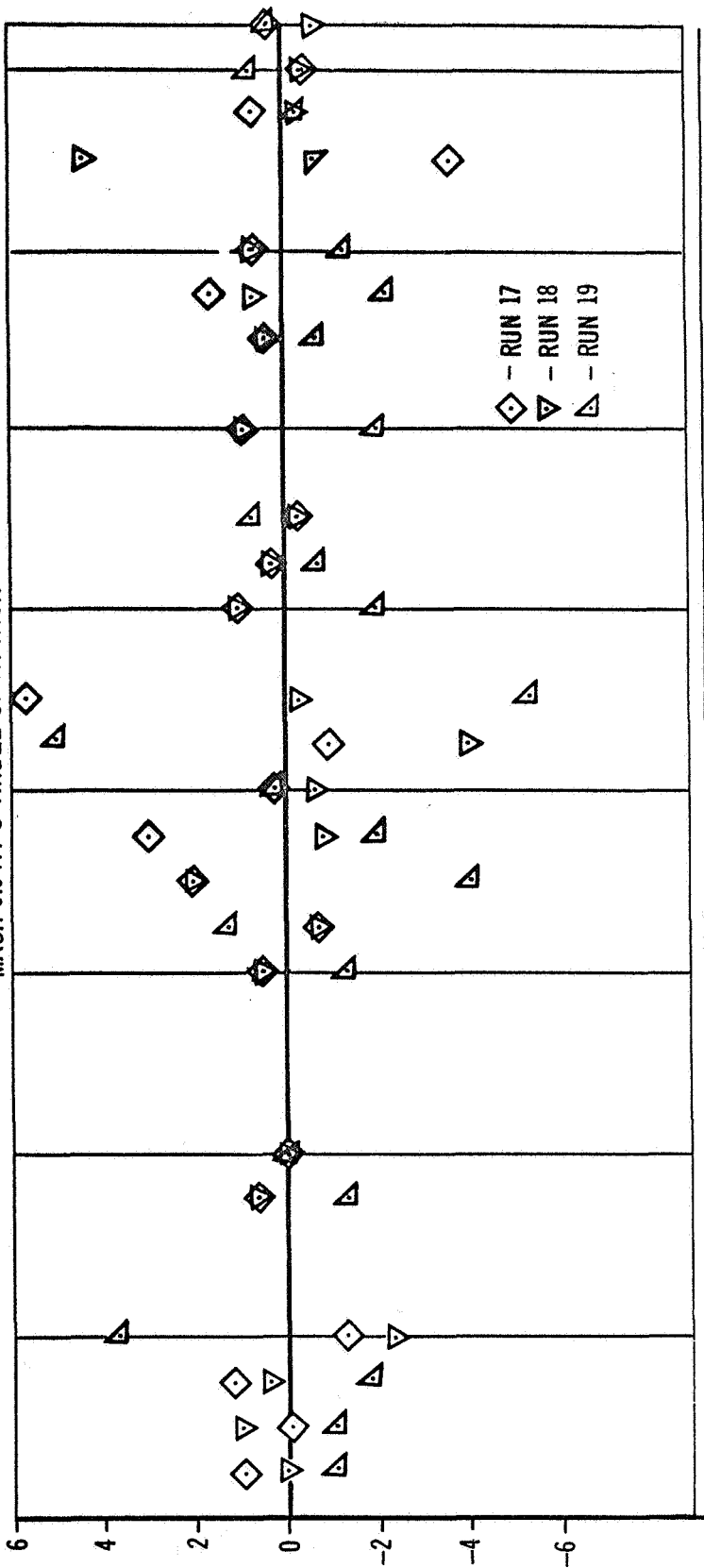


FIGURE 49

REPEATABILITY OF THE DATA ON THE B CONFIGURATION

MACH 0.9 AT 0° ANGLE OF ATTACK



MACH 1.6 AT 0° ANGLE OF ATTACK

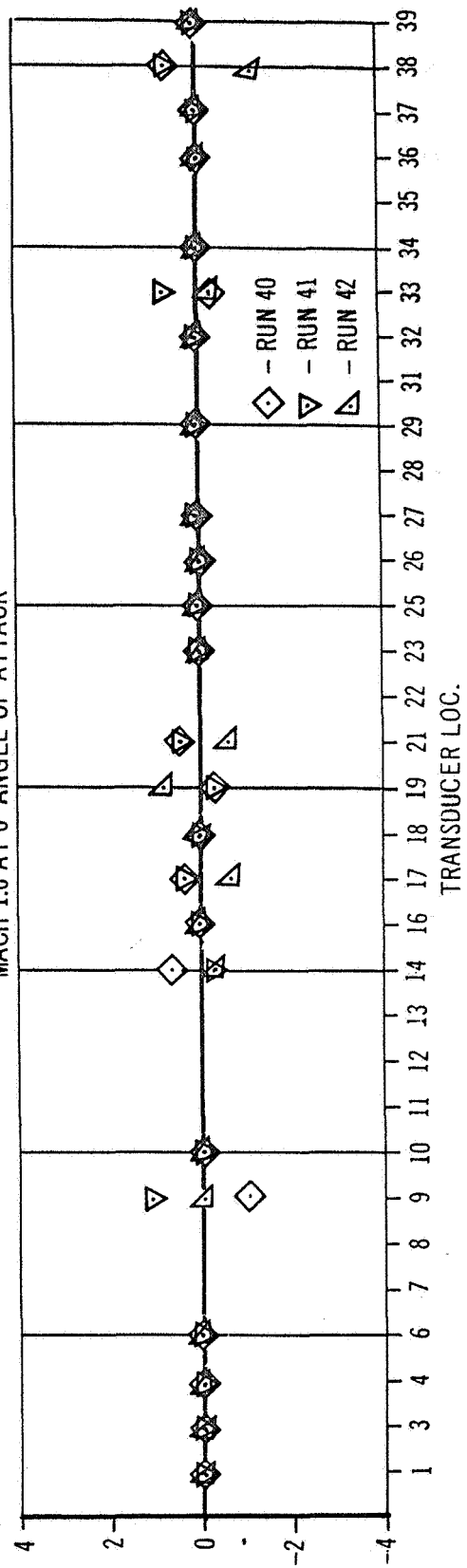


FIGURE 50

CONFIDENTIAL

COMPARISON OF TWO TRANSDUCERS 180° APART AT STATION NUMBER 1637 FOR DIFFERENT CONFIGURATIONS

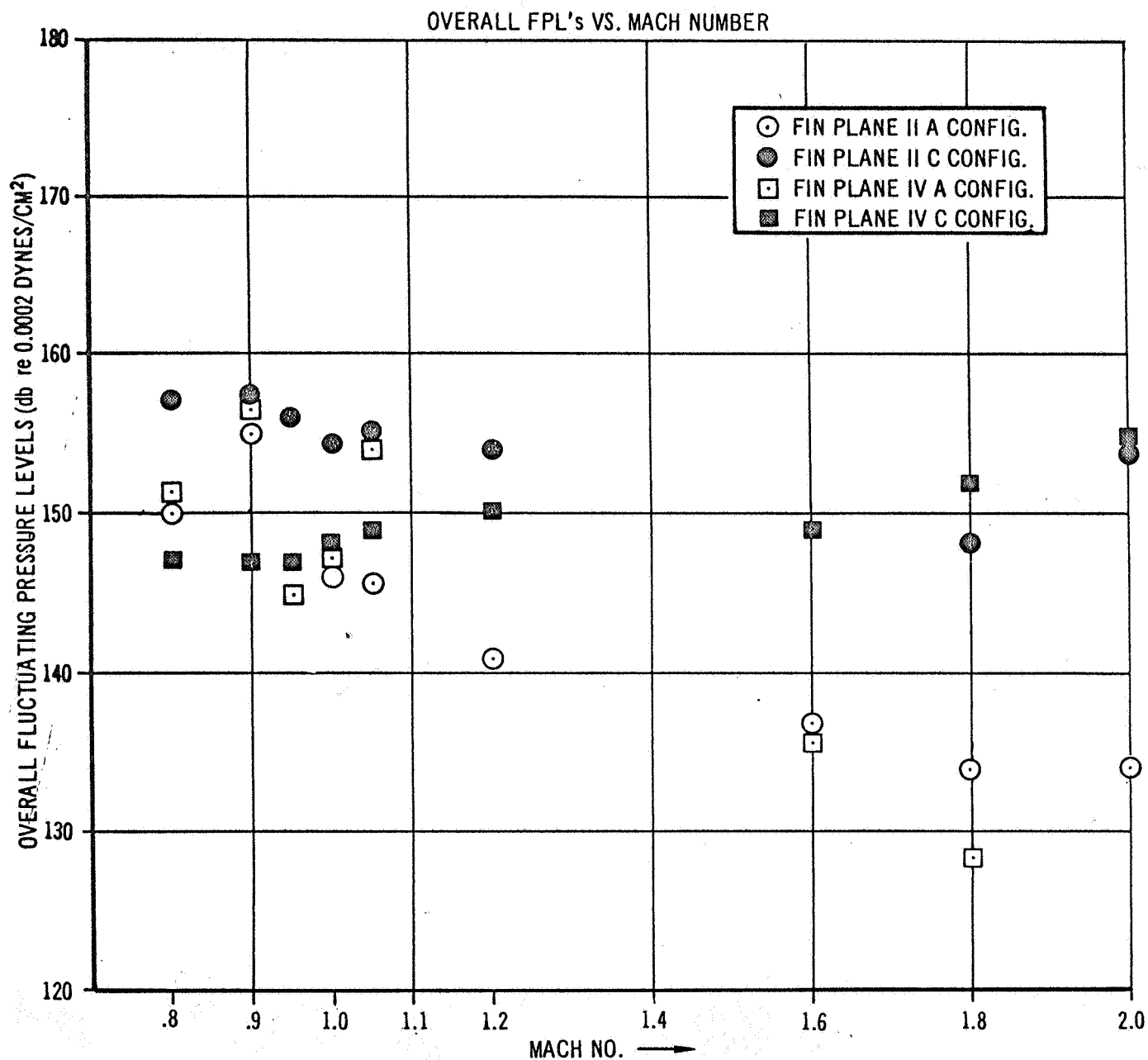
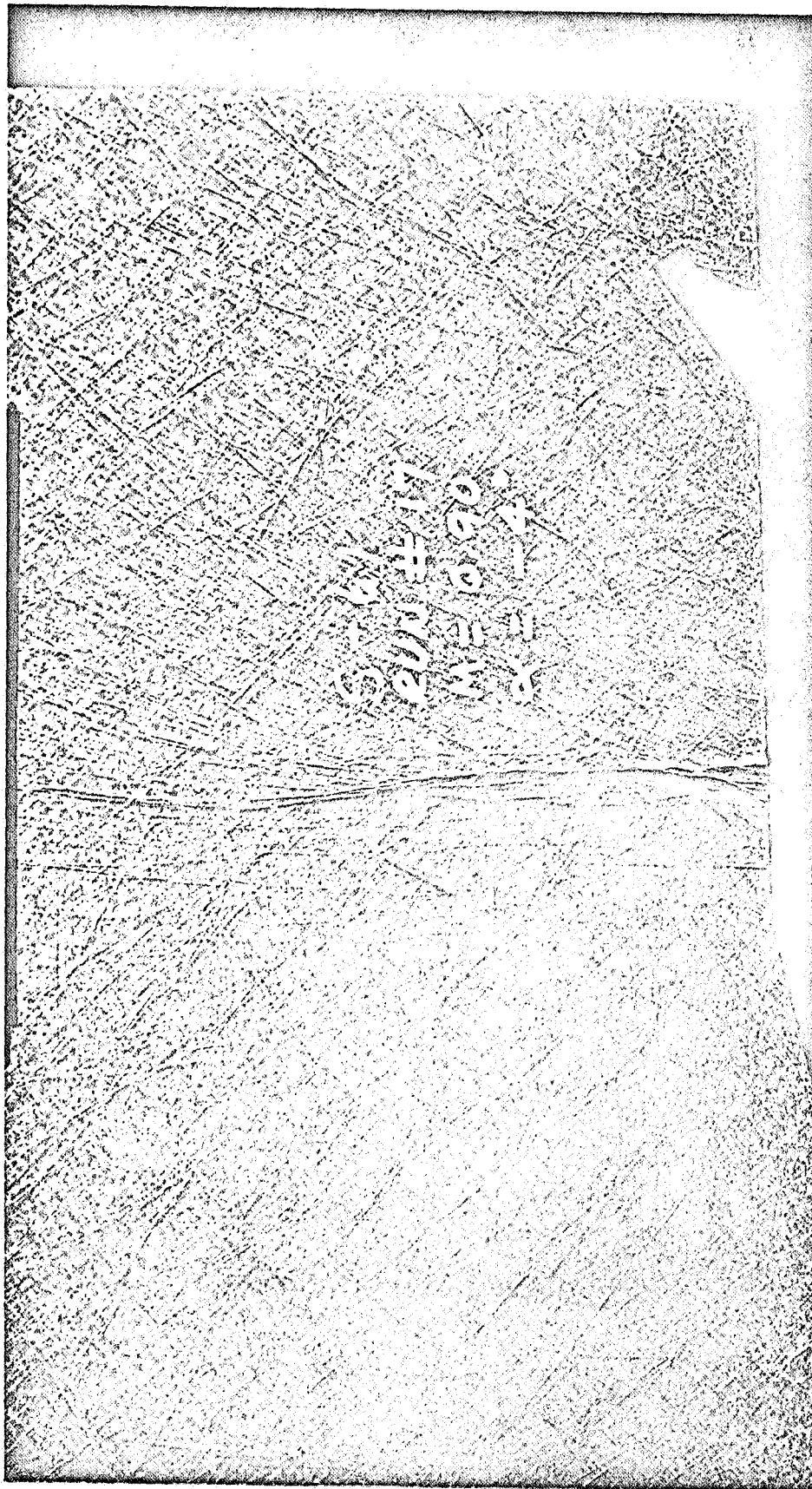


FIGURE 51

CONFIDENTIAL

CONFIDENTIAL

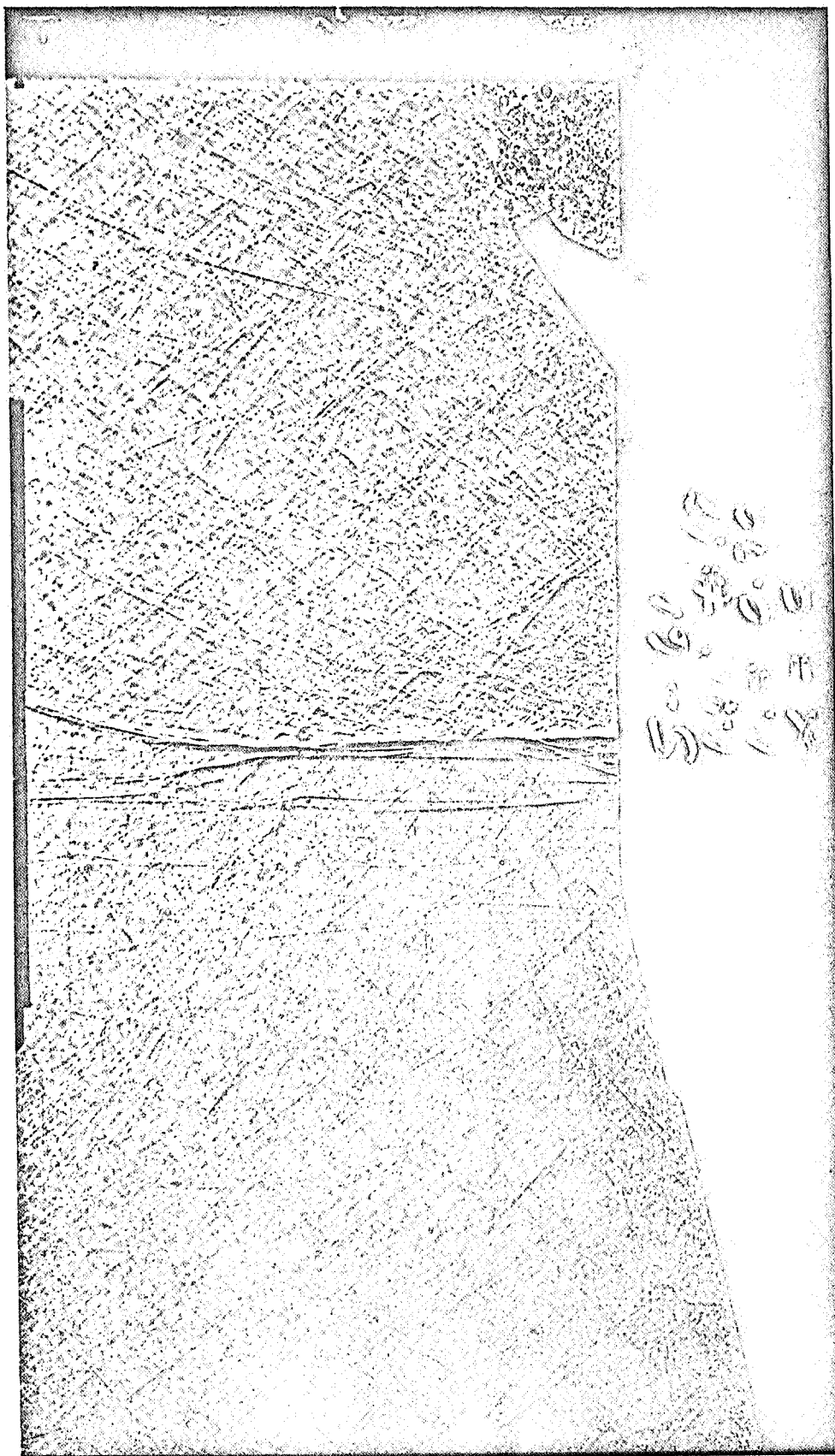


SHOCK ON THE FORWARD INTERSTAGE SHOULDER OF THE S-IV STAGE

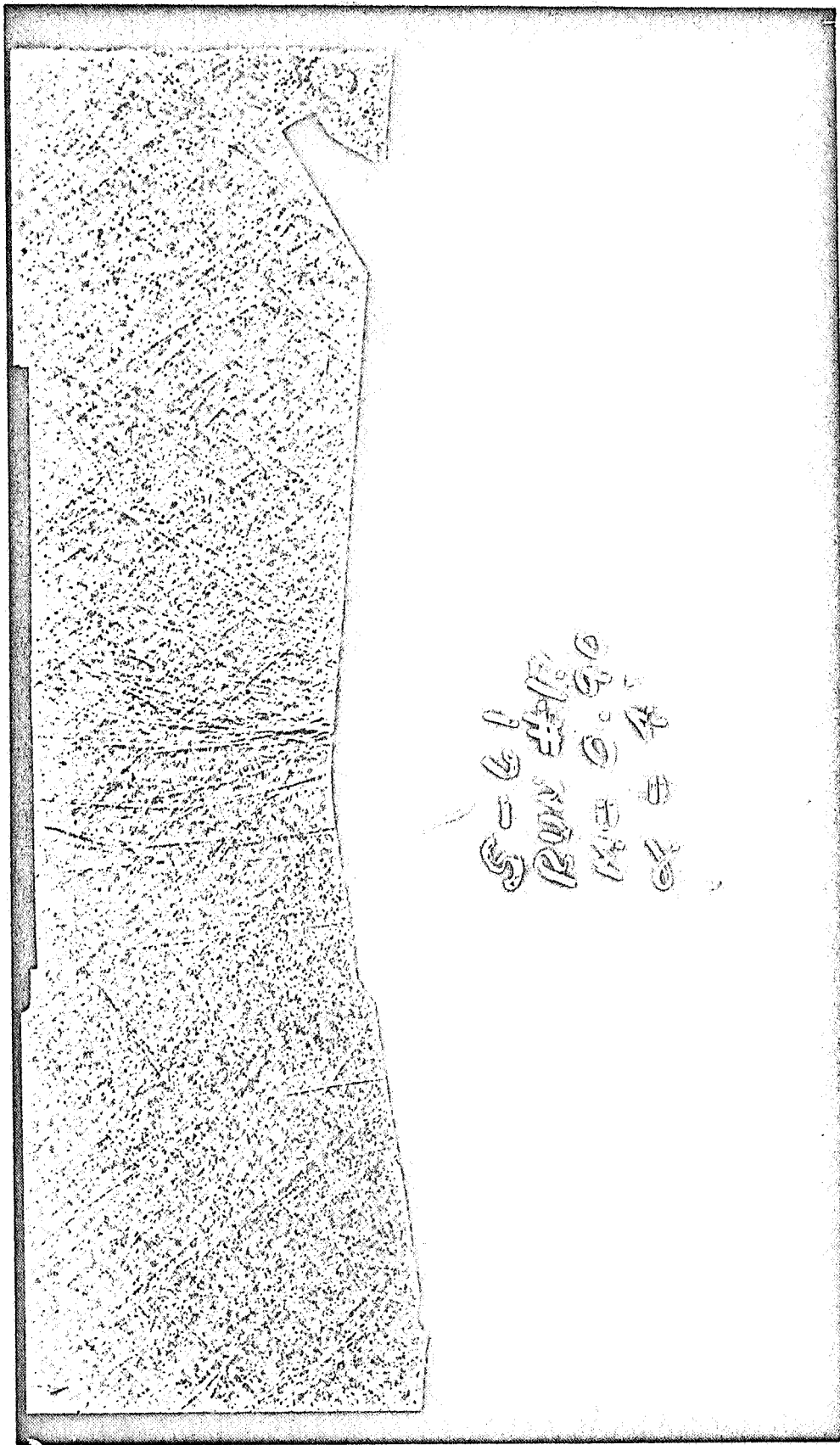
FIGURE 52

CONFIDENTIAL

~~CONFIDENTIAL~~

**FIGURE 53**

CONFIDENTIAL

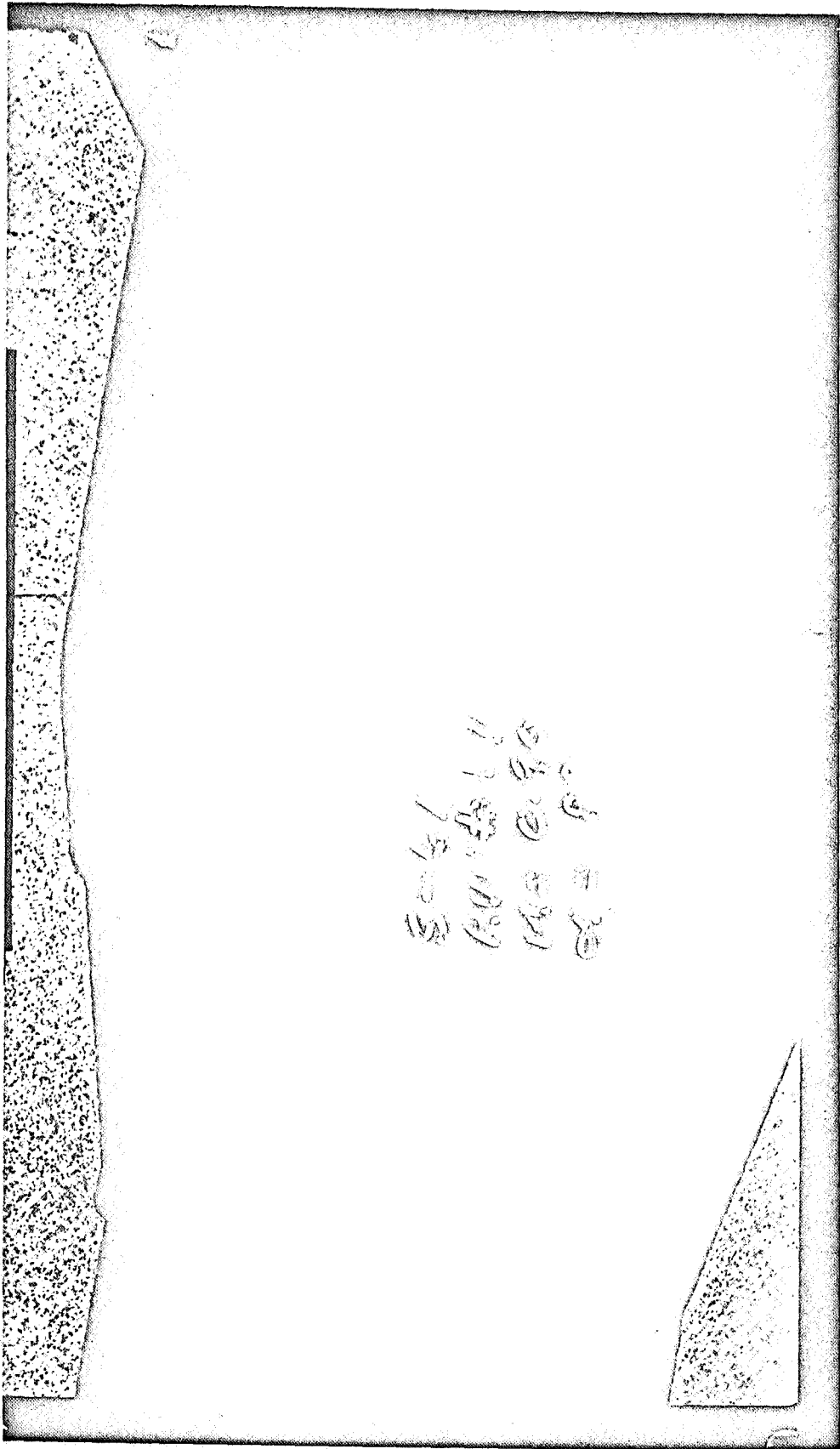


S-61
RUN #17
M. E. 90
04 4

SHOCK ON THE FORWARD INTERSTAGE SHOULDER OF THE S-IV STAGE

FIGURE 54

CONFIDENTIAL



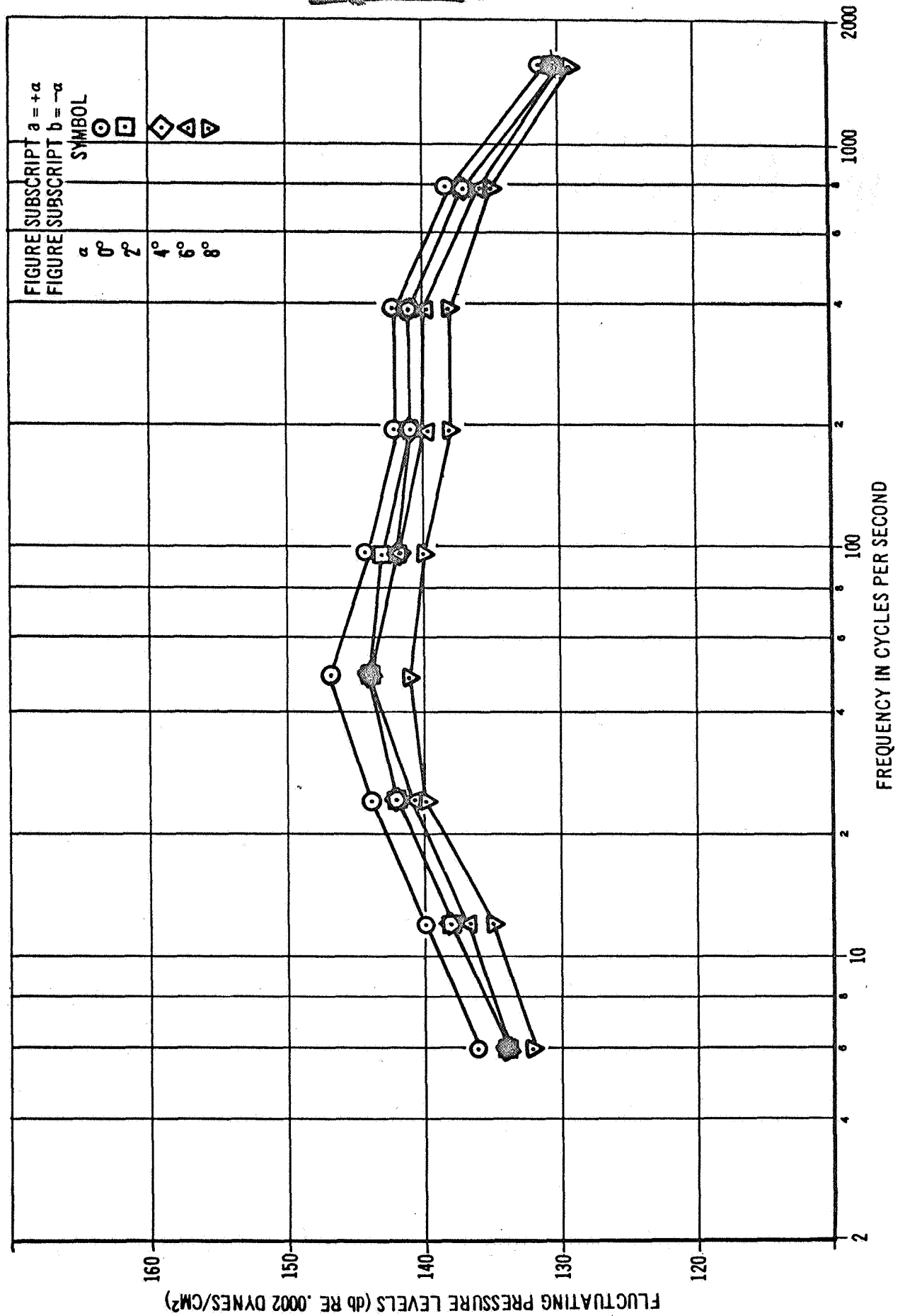
SHOCK ON THE FORWARD INTERSTAGE SHOULDER OF THE S-IV STAGE

FIGURE 55

CONFIDENTIAL

CONFIDENTIAL

VARIATION OF SPECTRUM SHAPE WITH ANGLE OF ATTACK α
FOR CONFIGURATION B, LOCATION 4, MACH NO. 1.8



CONFIDENTIAL

CONFIDENTIAL

VARIATION OF SPECTRUM SHAPE WITH ANGLE OF ATTACK α

FOR CONFIGURATION B, LOCATION 4, MACH NO. 1.8

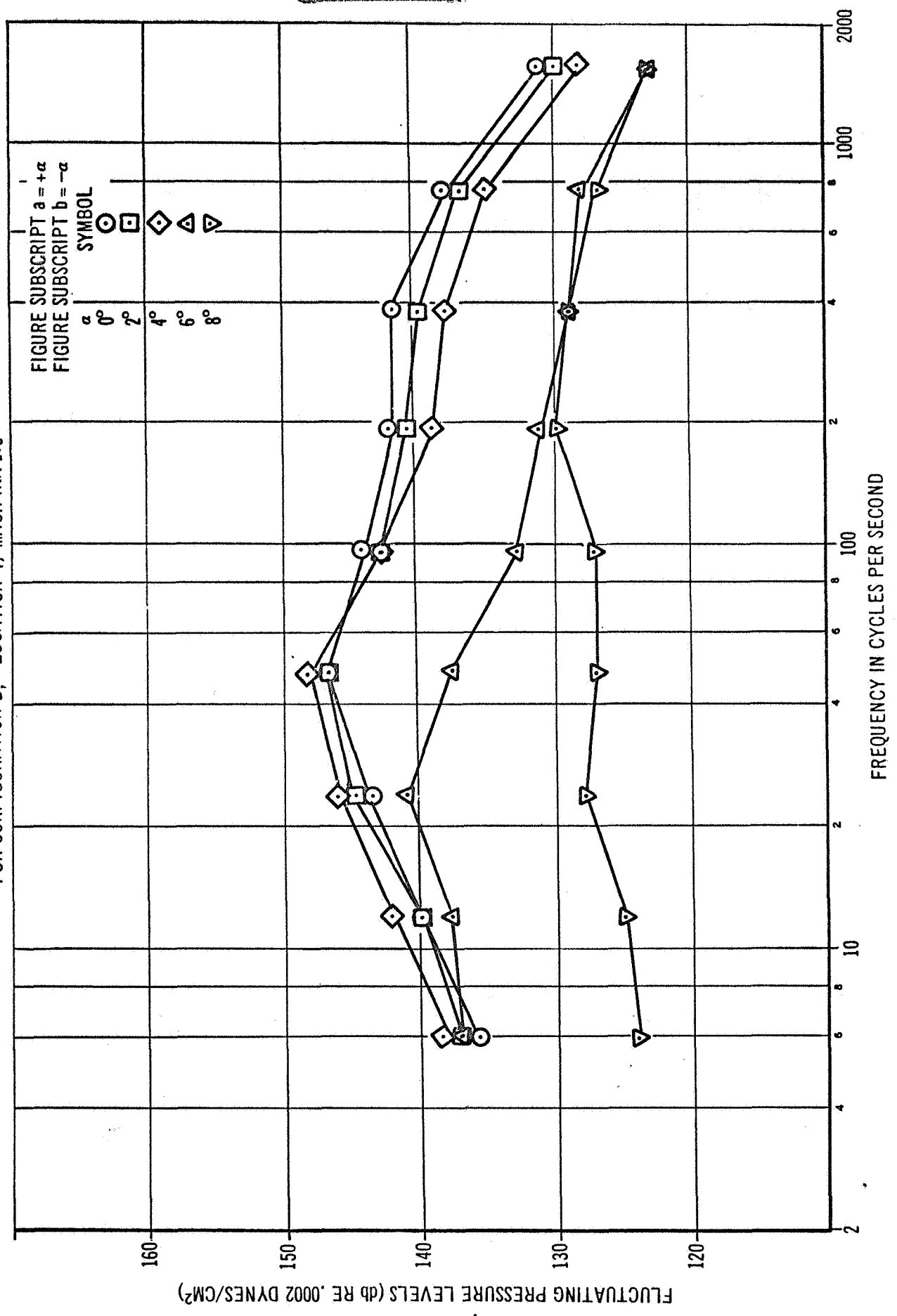


FIGURE 56 b

CONFIDENTIAL

CONFIDENTIAL

VARATION OF SPECTRUM SHAPE WITH ANGLE OF ATTACK α

FOR CONFIGURATION B, LOCATION 4, MACH NO. 2.0

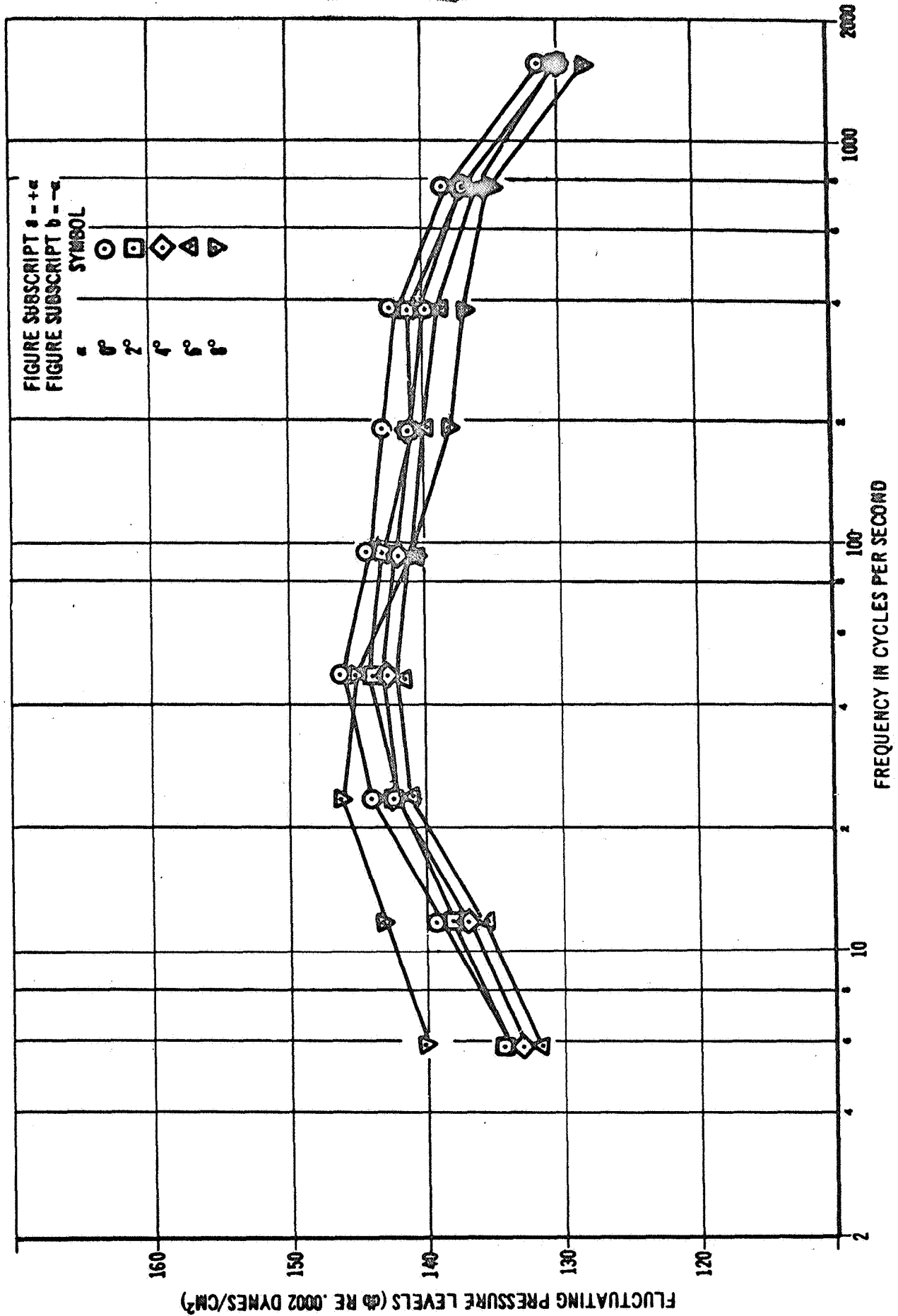


FIGURE 57a

FLUCTUATING PRESSURE LEVELS (ϕ RE .0002 DYNES/CM²)

FREQUENCY IN CYCLES PER SECOND

CONFIDENTIAL

CONFIDENTIAL

VARIAION OF SPECTRUM SHAPE WITH ANGLE OF ATTACK α

FOR CONFIGURATION B, LOCATION 4, MACH NO. 2.0

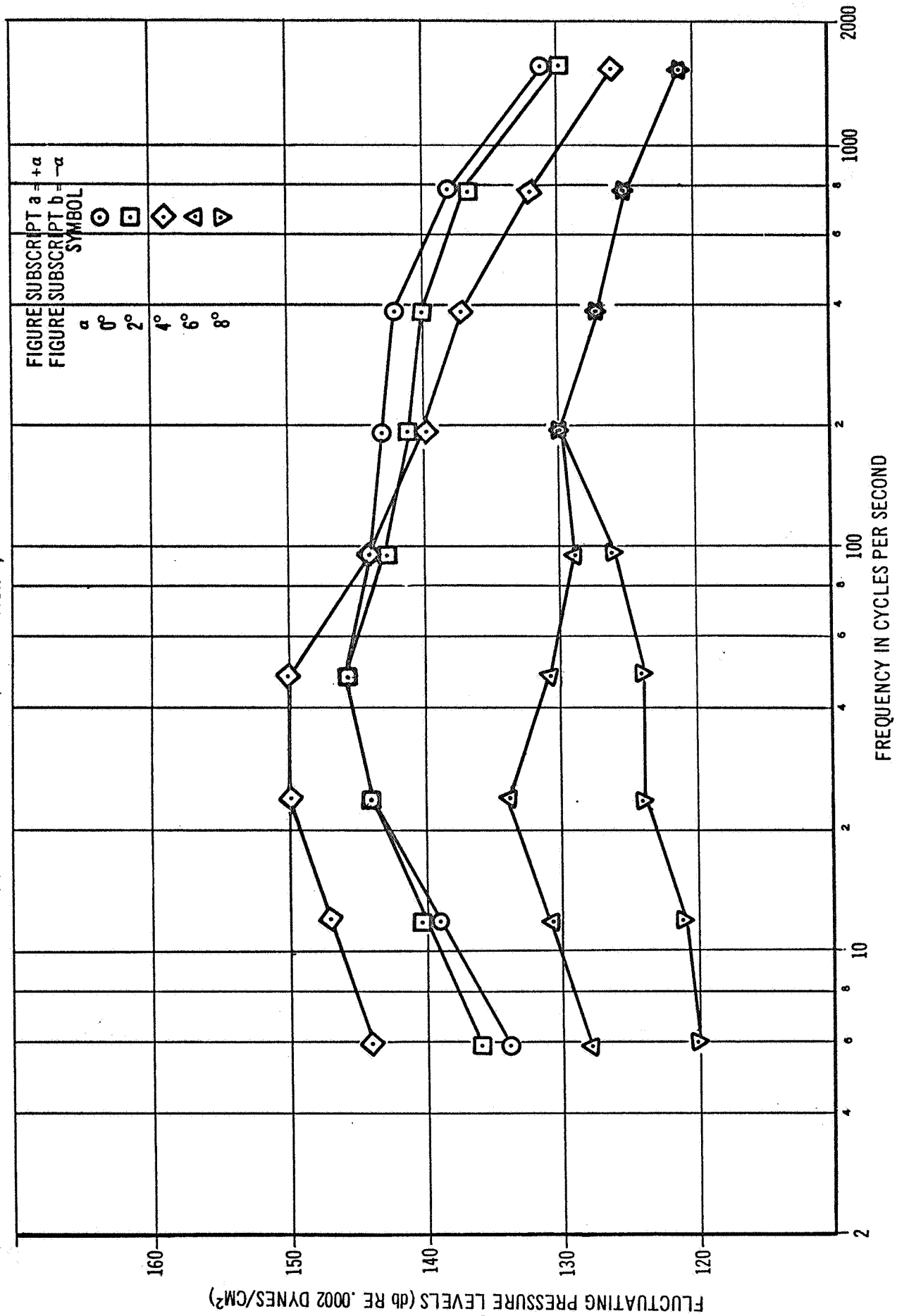


FIGURE 57b

CONFIDENTIAL

CONFIDENTIAL

VARIATION OF SPECTRUM SHAPE WITH ANGLE OF ATTACK α
FOR CONFIGURATION B₇, LOCATION 7, MACH NO. 1.6

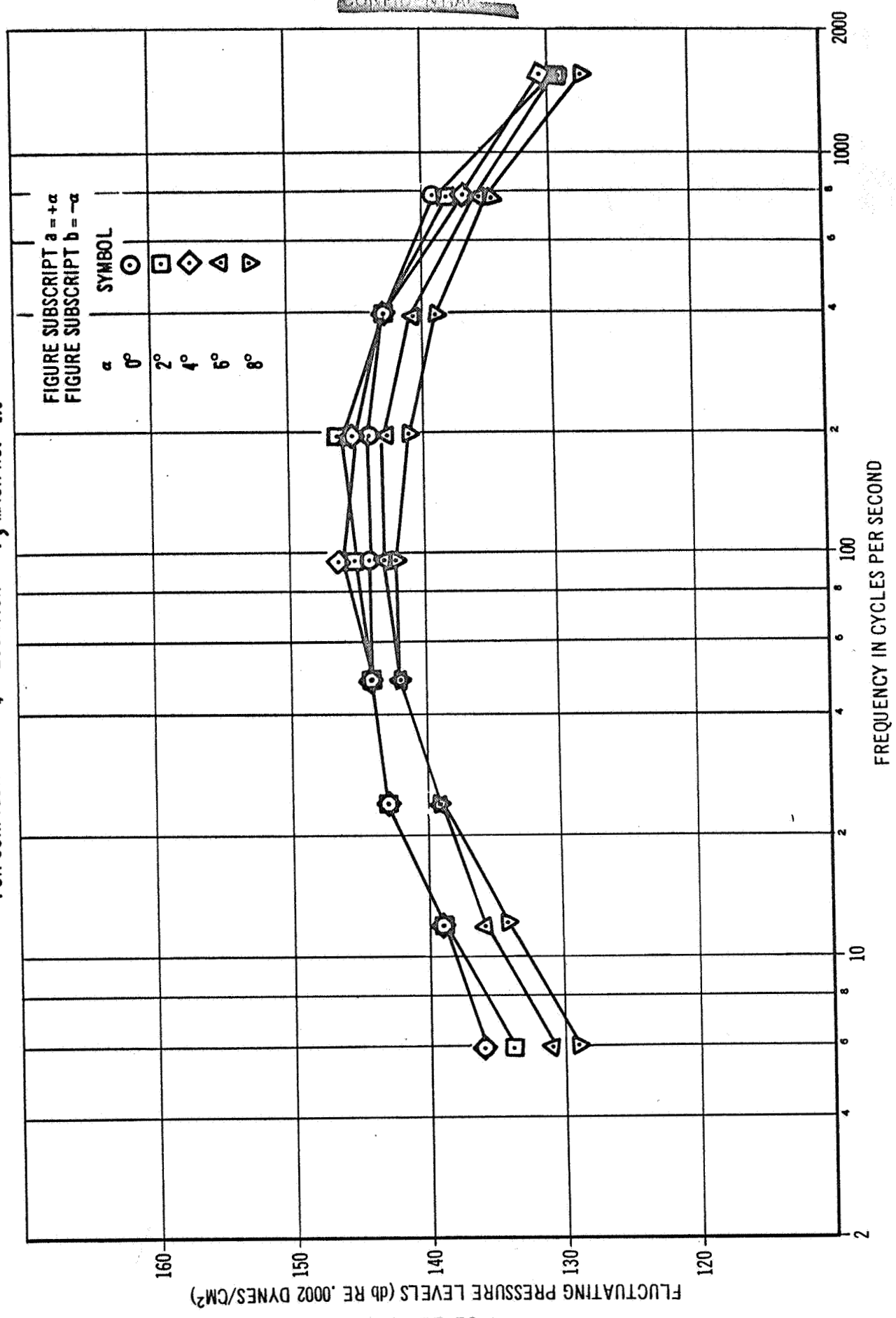


FIGURE 58a

CONFIDENTIAL

CONFIDENTIAL

VARIATION OF SPECTRUM SHAPE WITH ANGLE OF ATTACK α

FOR CONFIGURATION A, LOCATION 7, MACH NO. 1.6

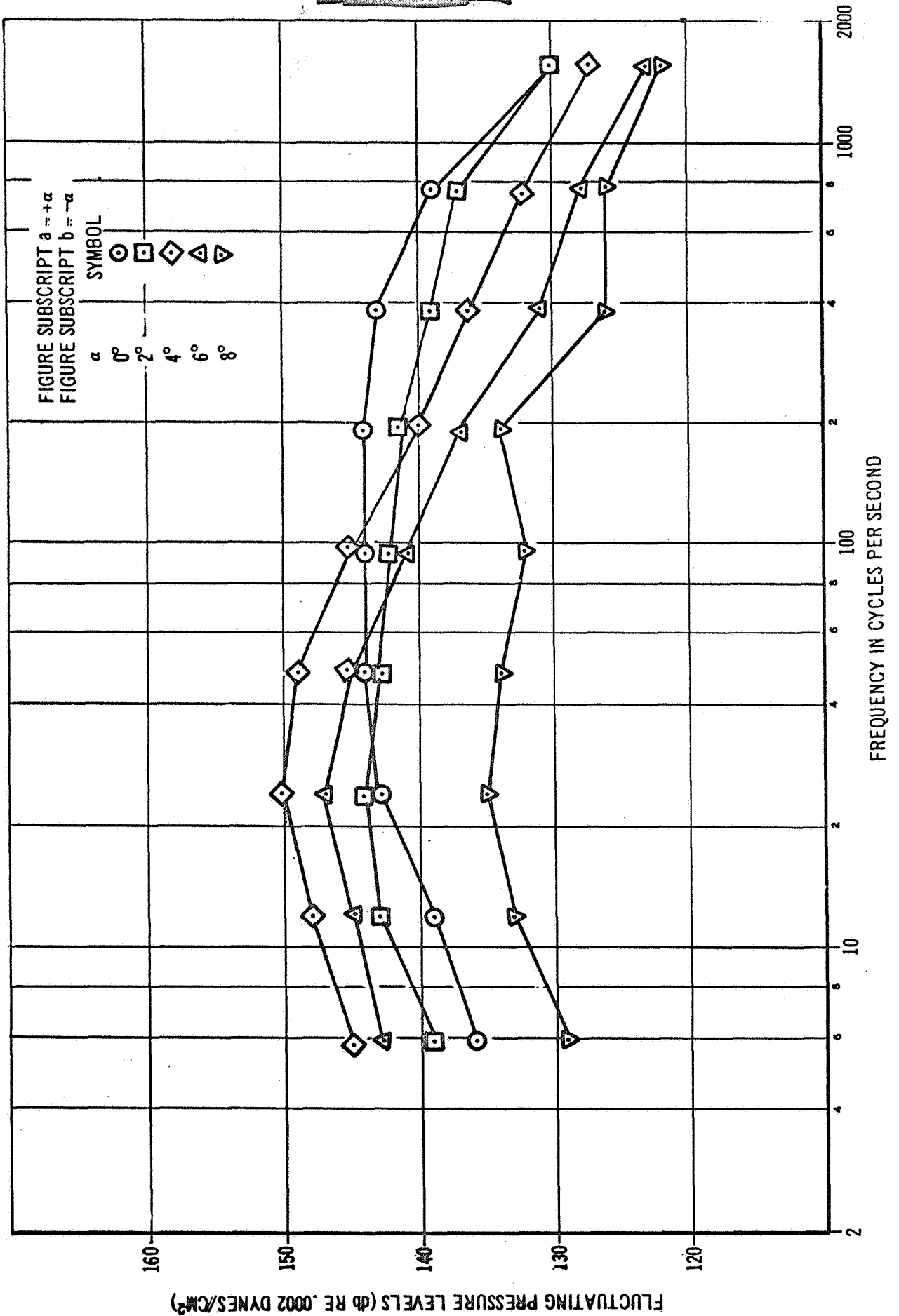


FIGURE 58b

CONFIDENTIAL

CONFIDENTIAL

VARIAION OF SPECTRUM SHAPE WITH ANGLE OF ATTACK α°

FOR CONFIGURATION A, LOCATION 7, MACH NO. 1.8

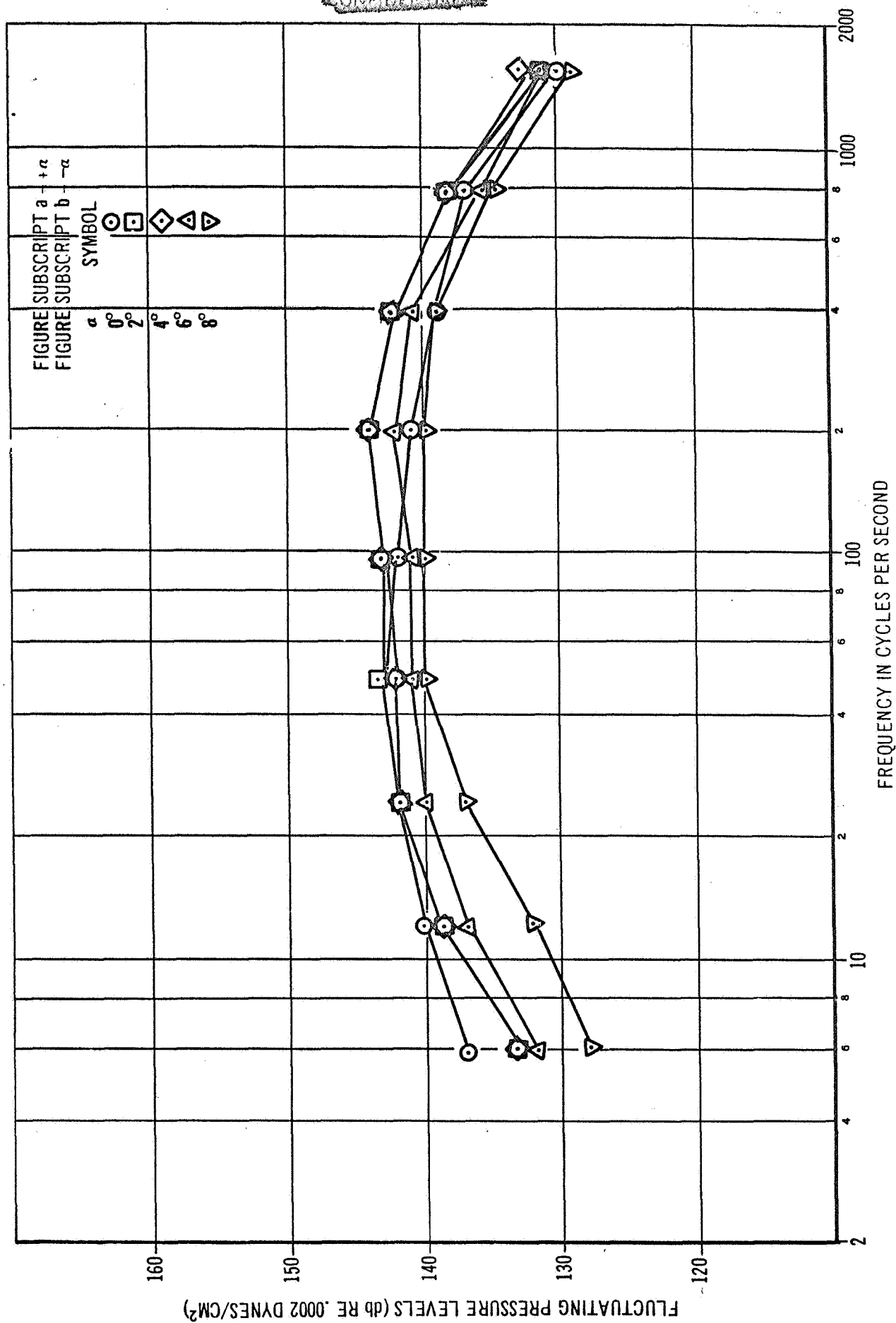


FIGURE 59a

CONFIDENTIAL

CONFIDENTIAL

VARIATION OF SPECTRUM SHAPE WITH ANGLE OF ATTACK α

FOR CONFIGURATION A, LOCATION 7, MACH NO. 1.8

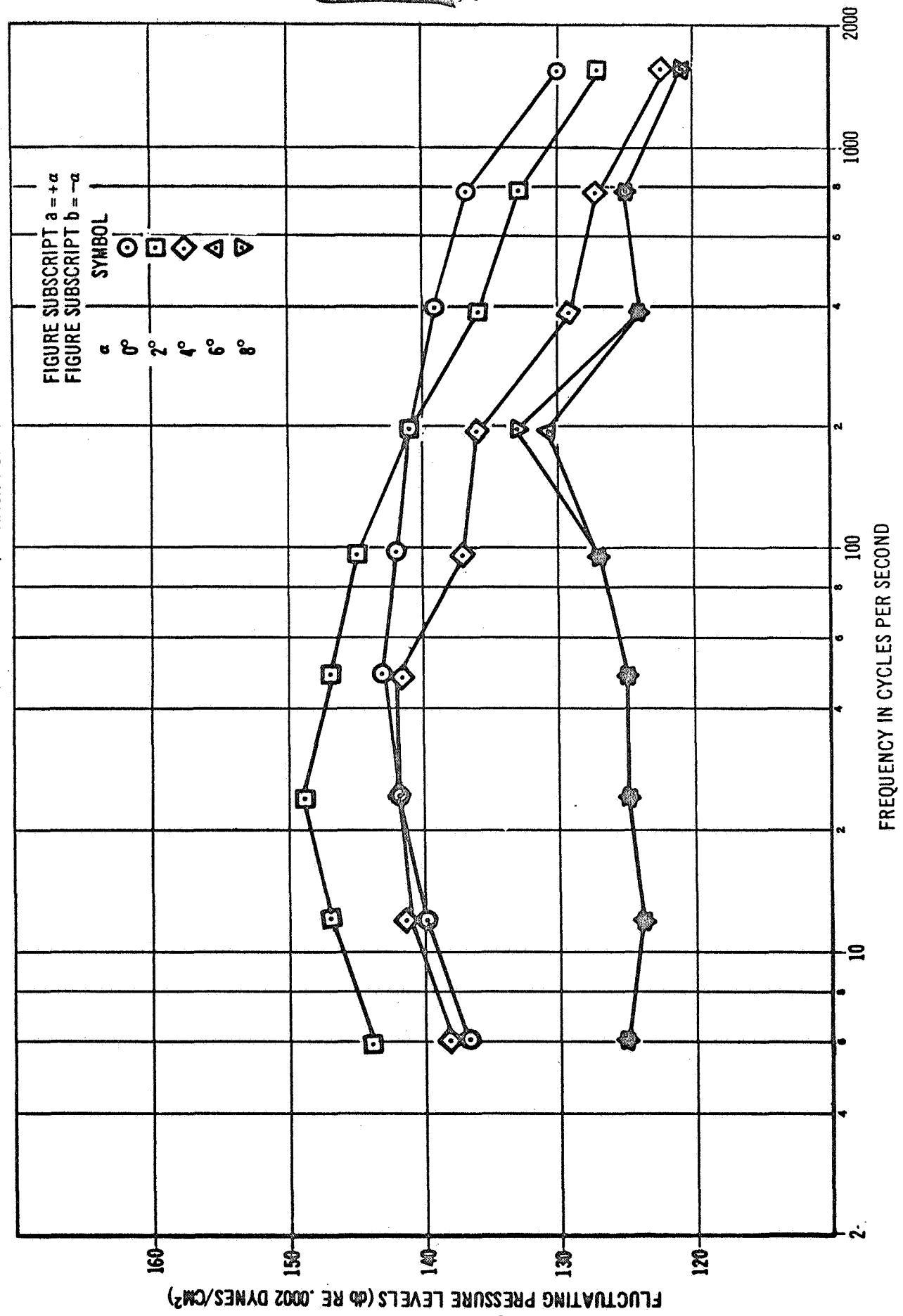


FIGURE 59b

CONFIDENTIAL

CONFIDENTIAL

1
VARIATION OF SPECTRUM SHAPE WITH ANGLE OF ATTACK α
FOR CONFIGURATION A, LOCATION 7, MACH NO. 2.0

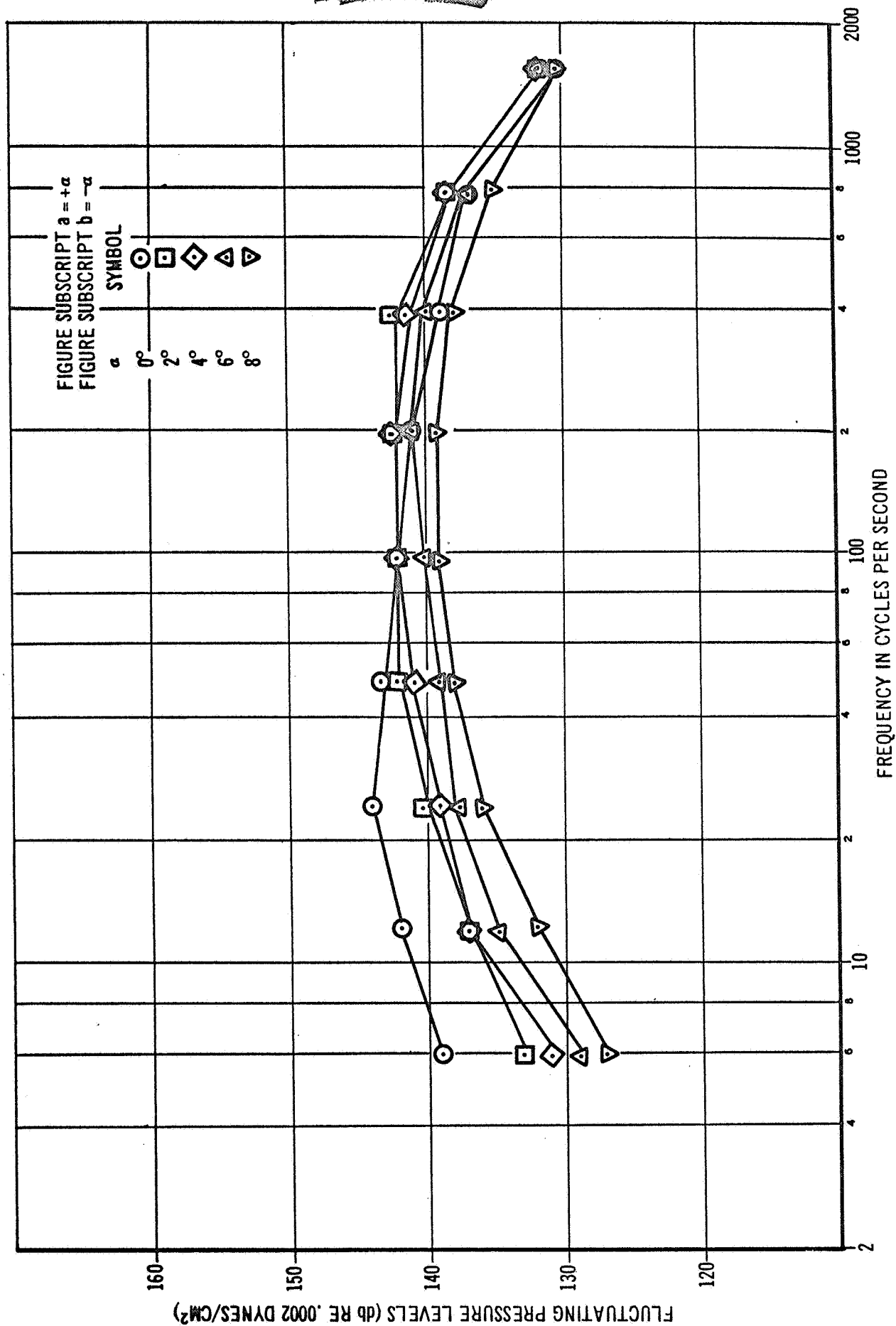


FIGURE 60 a

CONFIDENTIAL

VARIATION OF SPECTRUM SHAPE WITH ANGLE OF ATTACK α

FOR CONFIGURATION A, LOCATION 7, MACH NO. 2.0

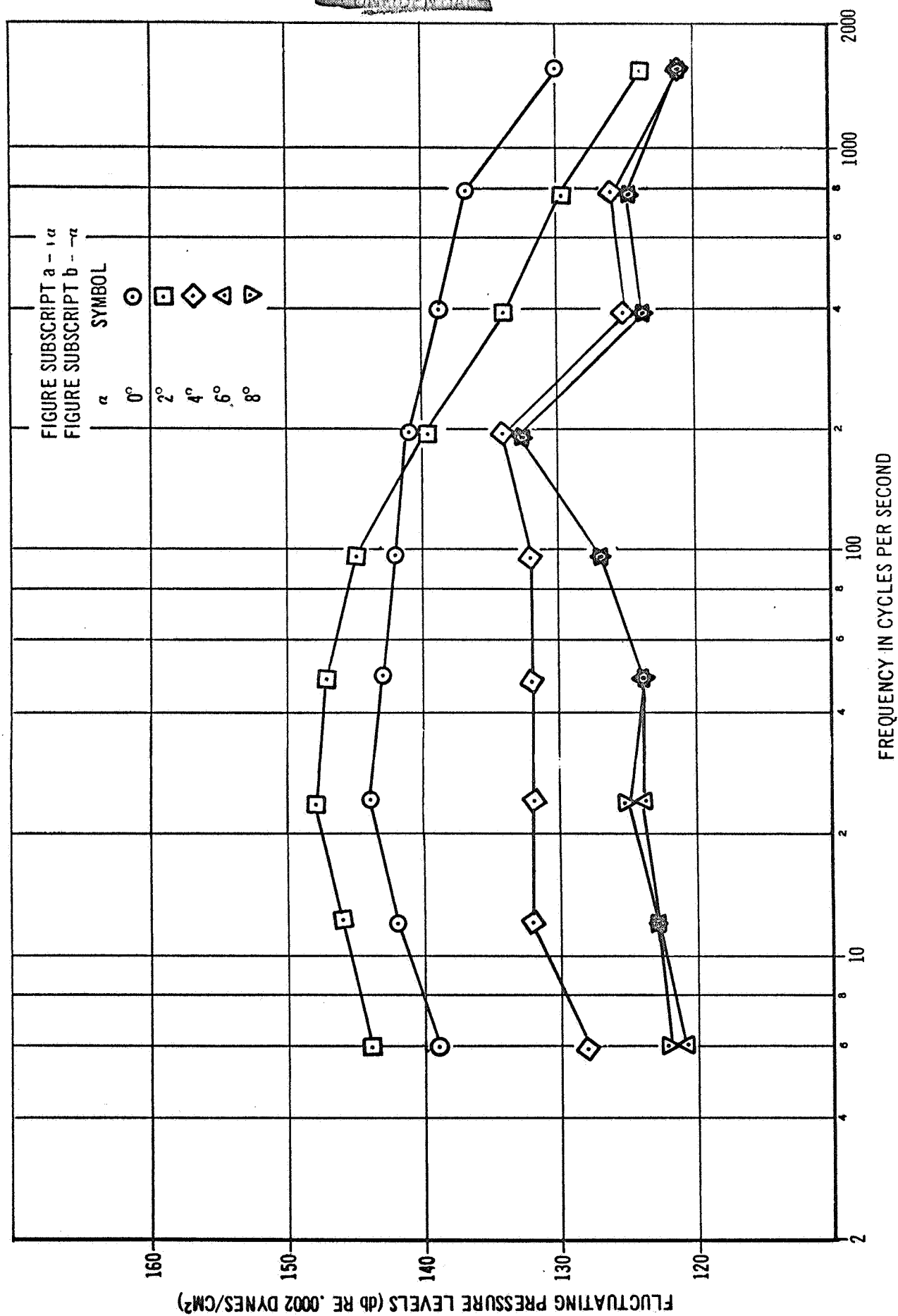


FIGURE 60 b

VARIATION OF SPECTRUM SHAPE WITH ANGLE OF ATTACK α

FOR CONFIGURATION A, LOCATION 21, MACH NO. 1.6

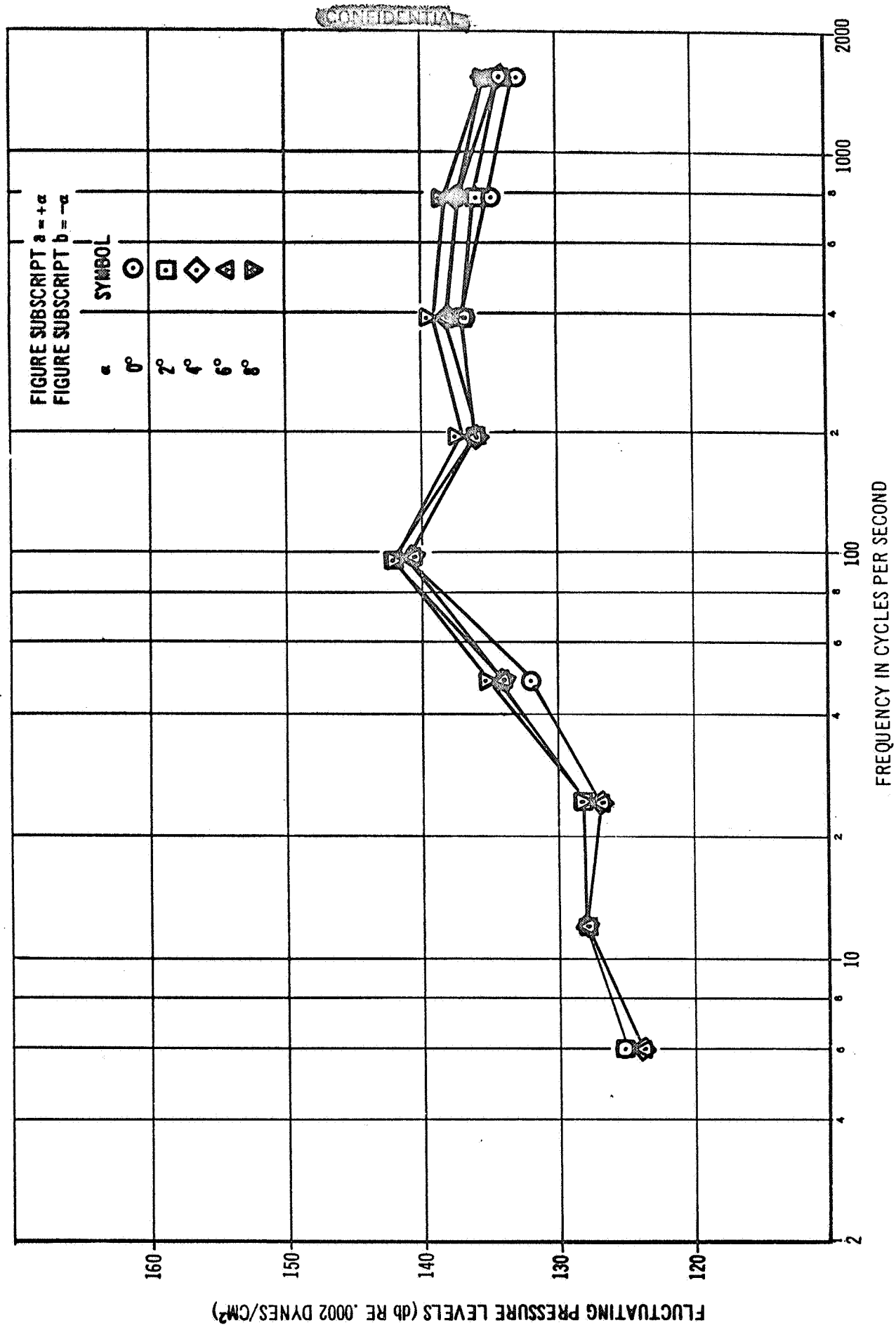


FIGURE 61 a

CONFIDENTIAL

CONFIDENTIAL

VARIATION OF SPECTRUM SHAPE WITH ANGLE OF ATTACK α
FOR CONFIGURATION A, LOCATION 21, MACH NO. 1.6

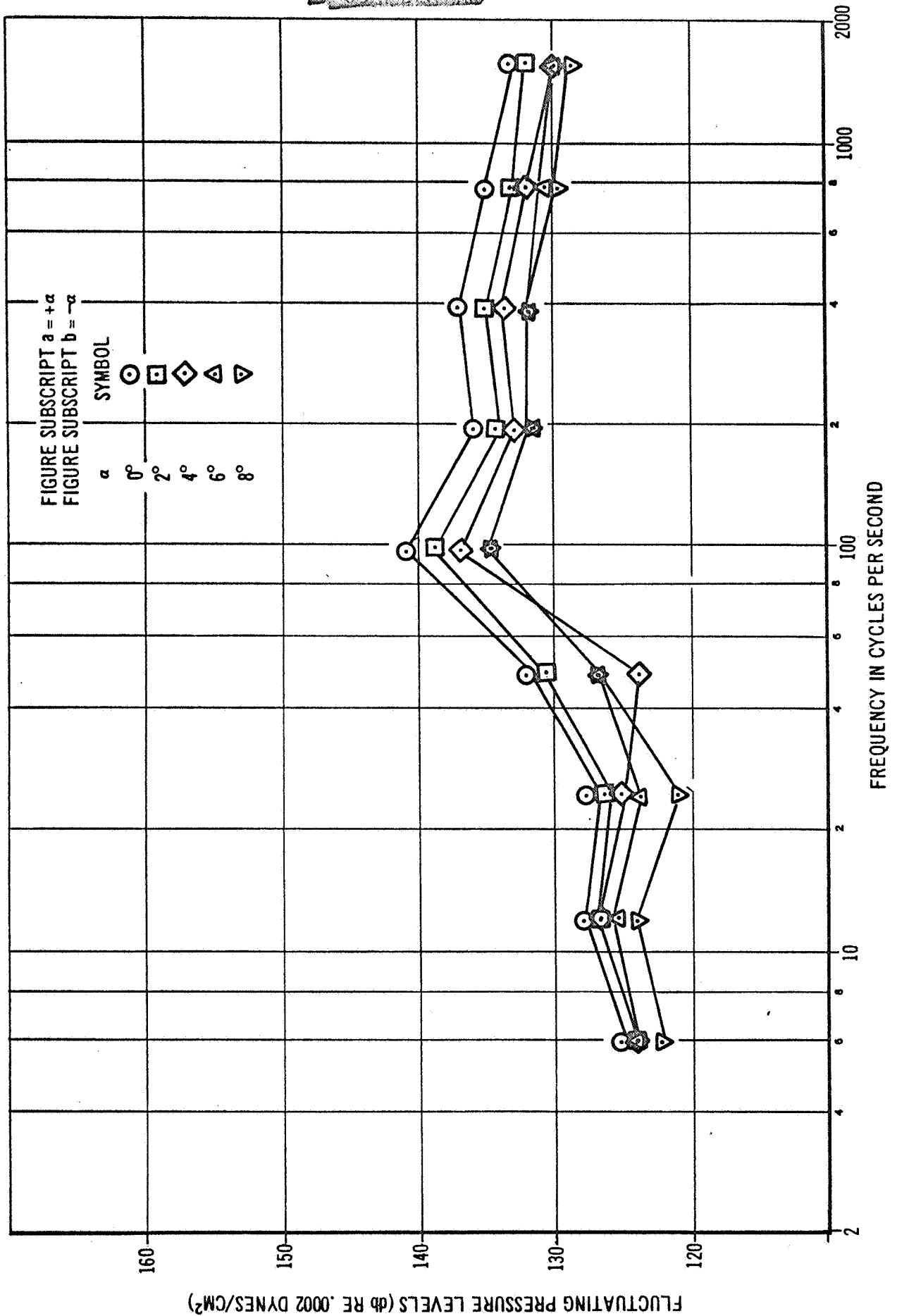


FIGURE 61b

CONFIDENTIAL

VARIATION OF SPECTRUM SHAPE WITH ANGLE OF ATTACK α

FOR CONFIGURATION A, LOCATION 21, MACH NO. 1.8

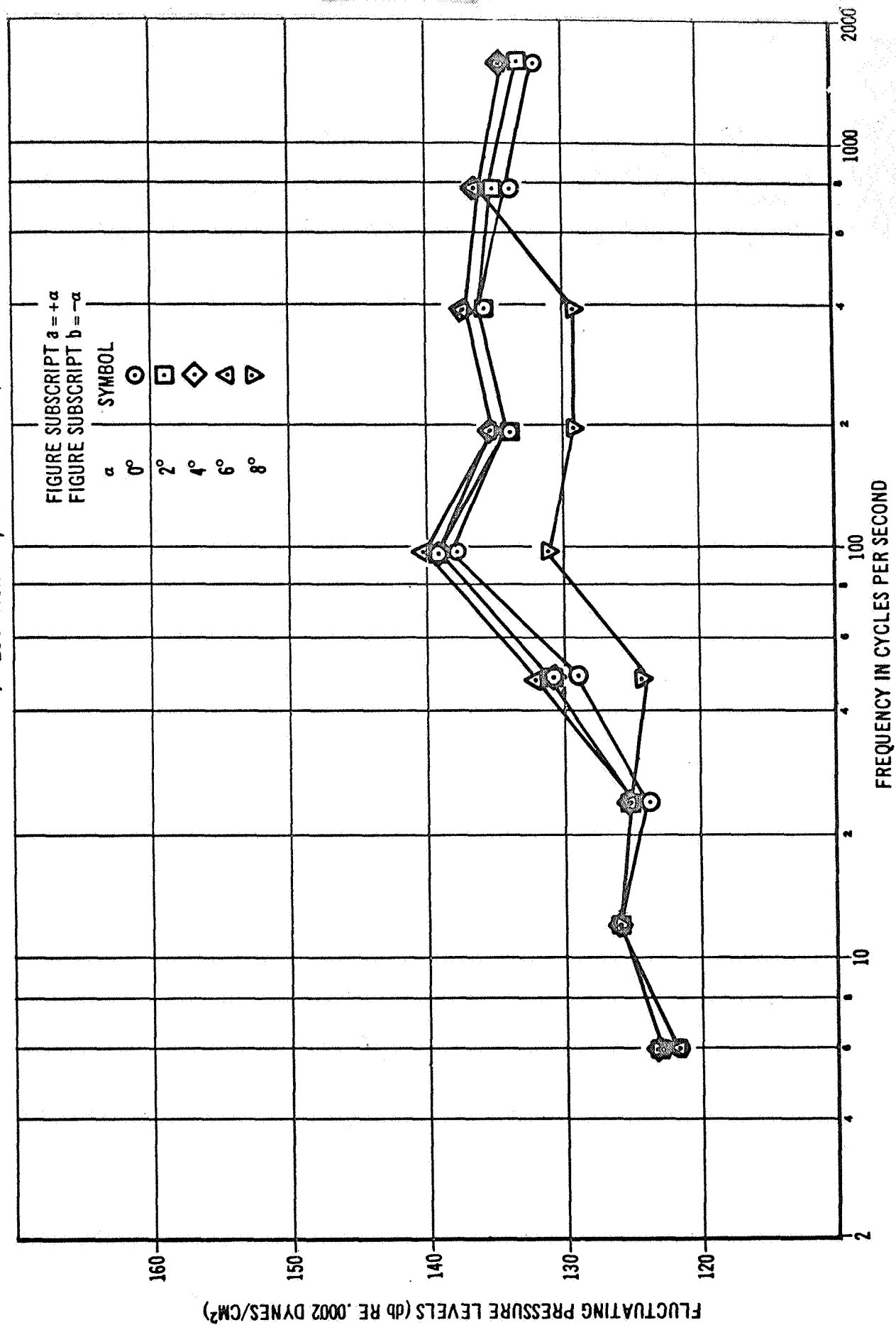


FIGURE 62 a

CONFIDENTIAL

VARIATION OF SPECTRUM SHAPE WITH ANGLE OF ATTACK α

FOR CONFIGURATION A, LOCATION 21, MACH NO. 1.8

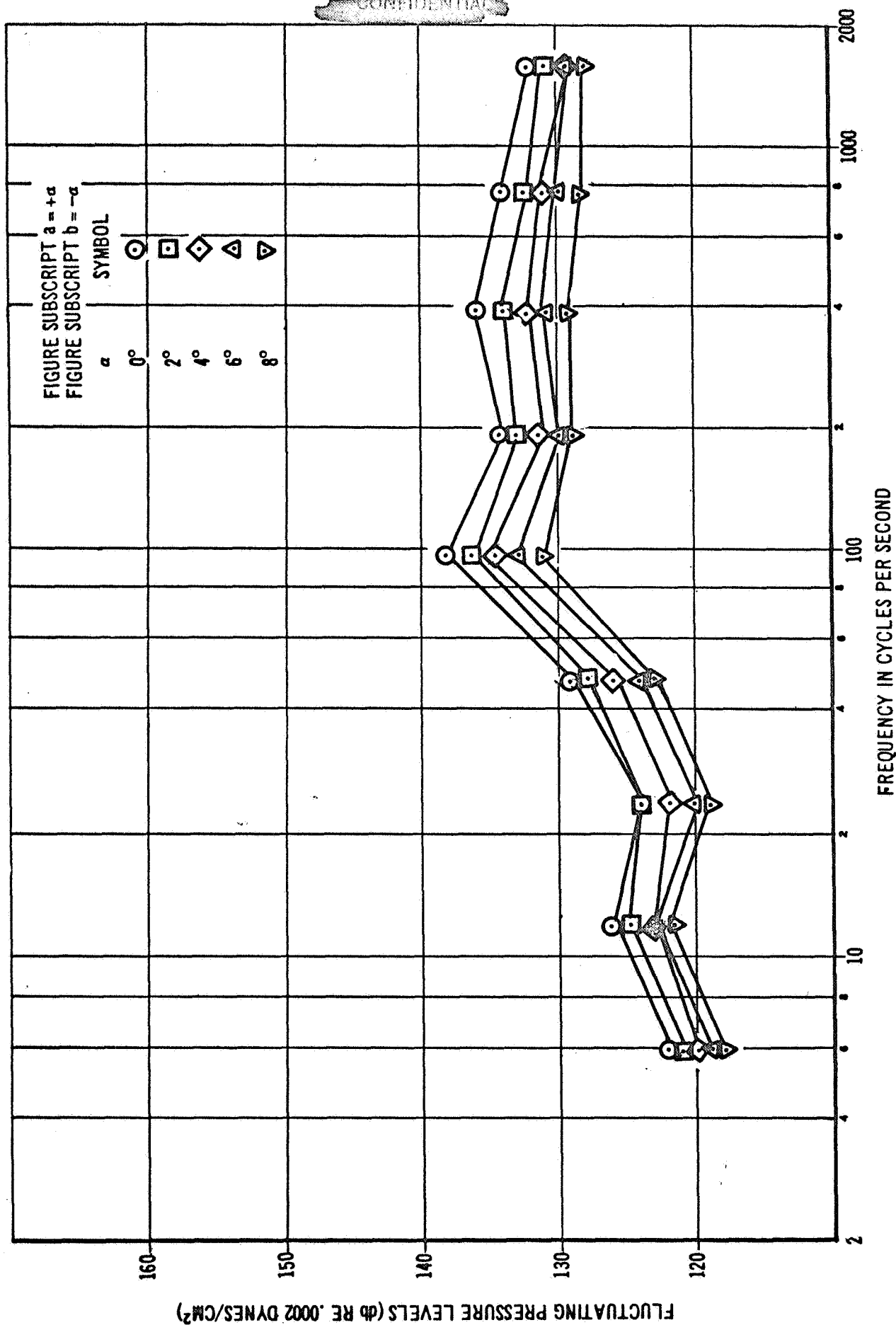


FIGURE 62 b

VARIATION OF SPECTRUM SHAPE WITH ANGLE OF ATTACK α

FOR CONFIGURATION C, LOCATION 3, MACH NO. 1.8

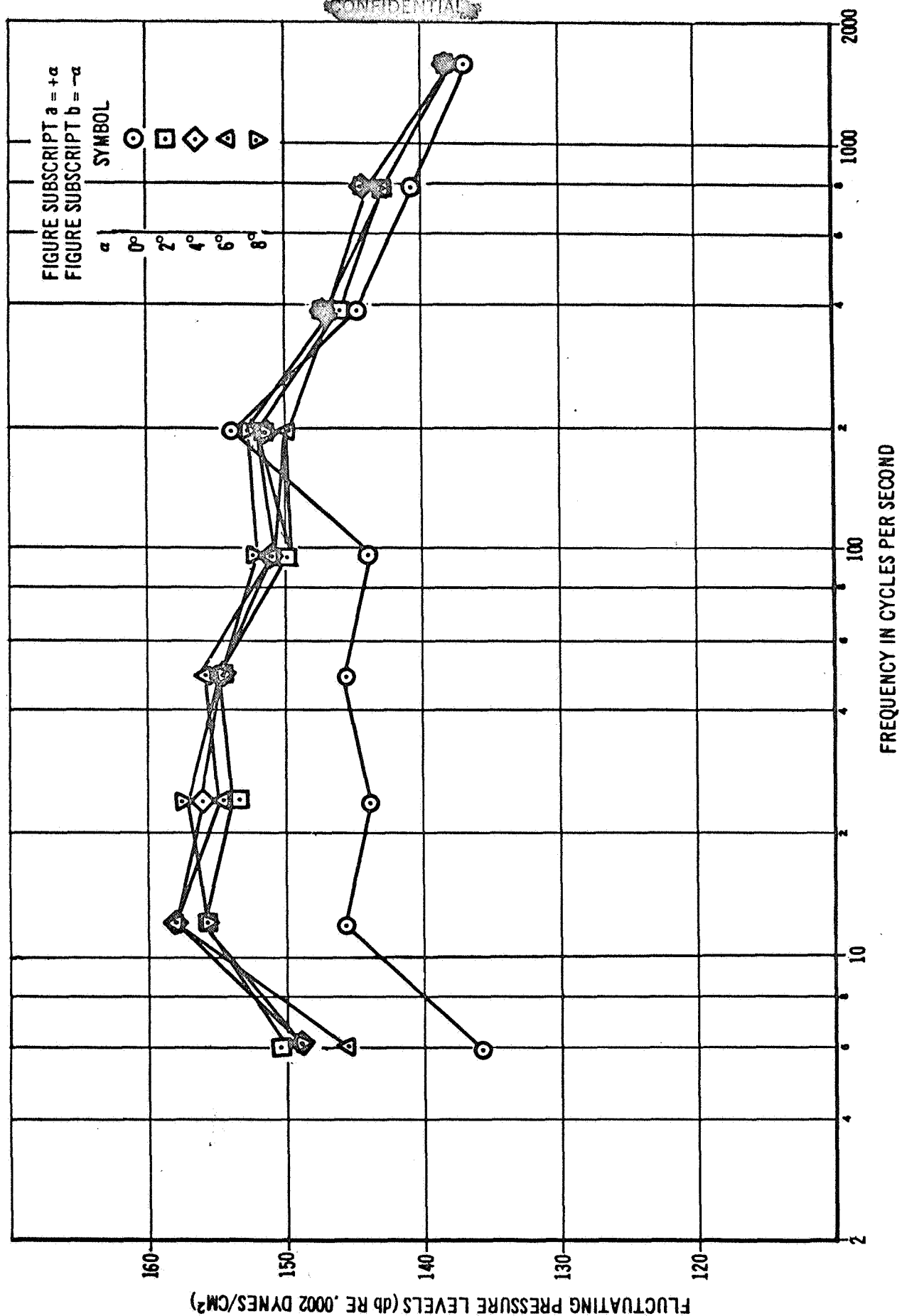


FIGURE 63a

CONFIDENTIAL

CONFIDENTIAL

VARIAION OF SPECTRUM SHAPE WITH ANGLE OF ATTACK α

FOR CONFIGURATION C, LOCATION 3, MACH NO. 1.8

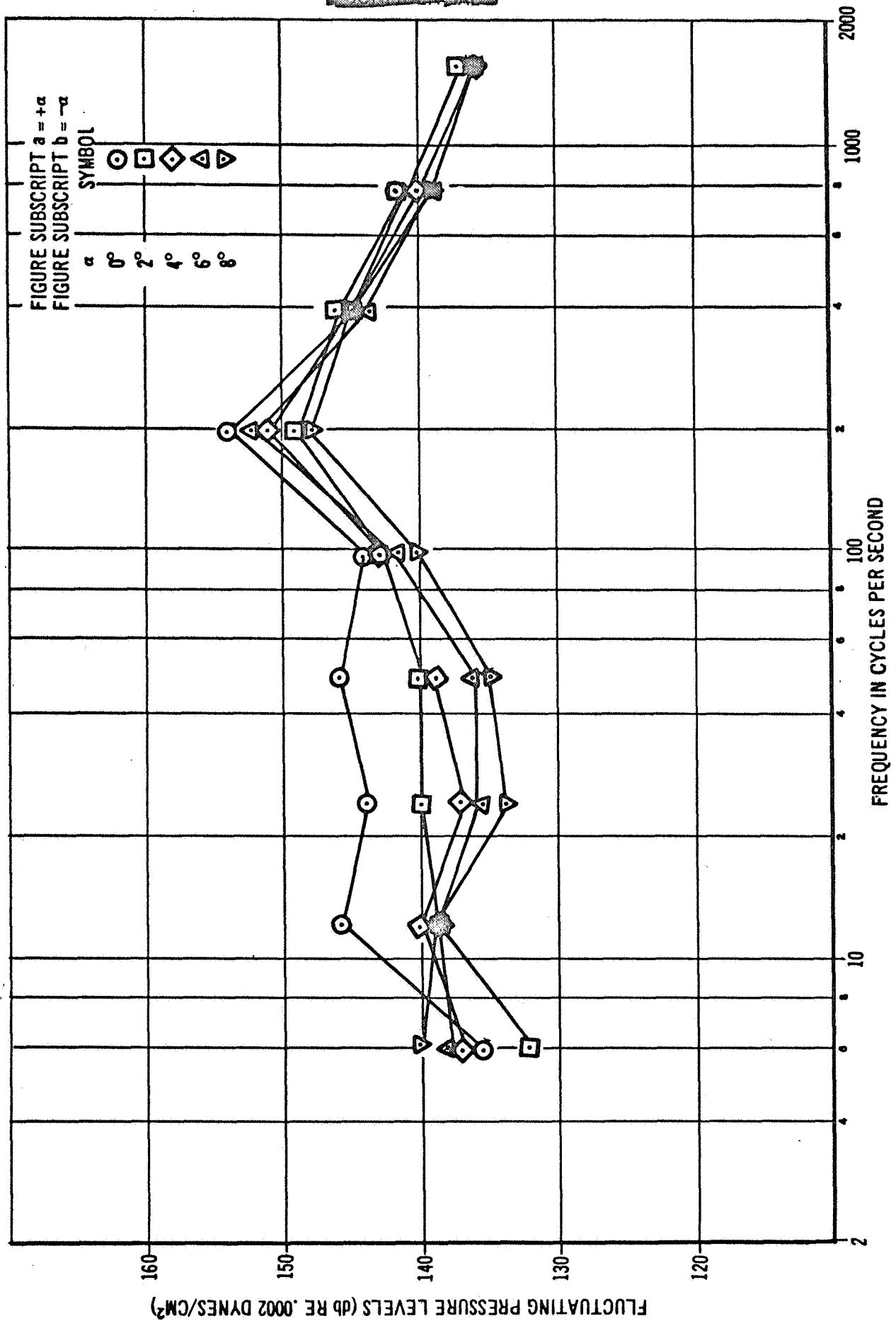


FIGURE 63b

CONFIDENTIAL

CONFIDENTIAL

OVERALL FLUCTUATING PRESSURE LEVEL DISTRIBUTION IN FIN PLANE II
OF CONFIGURATION A VS. MACH NUMBER

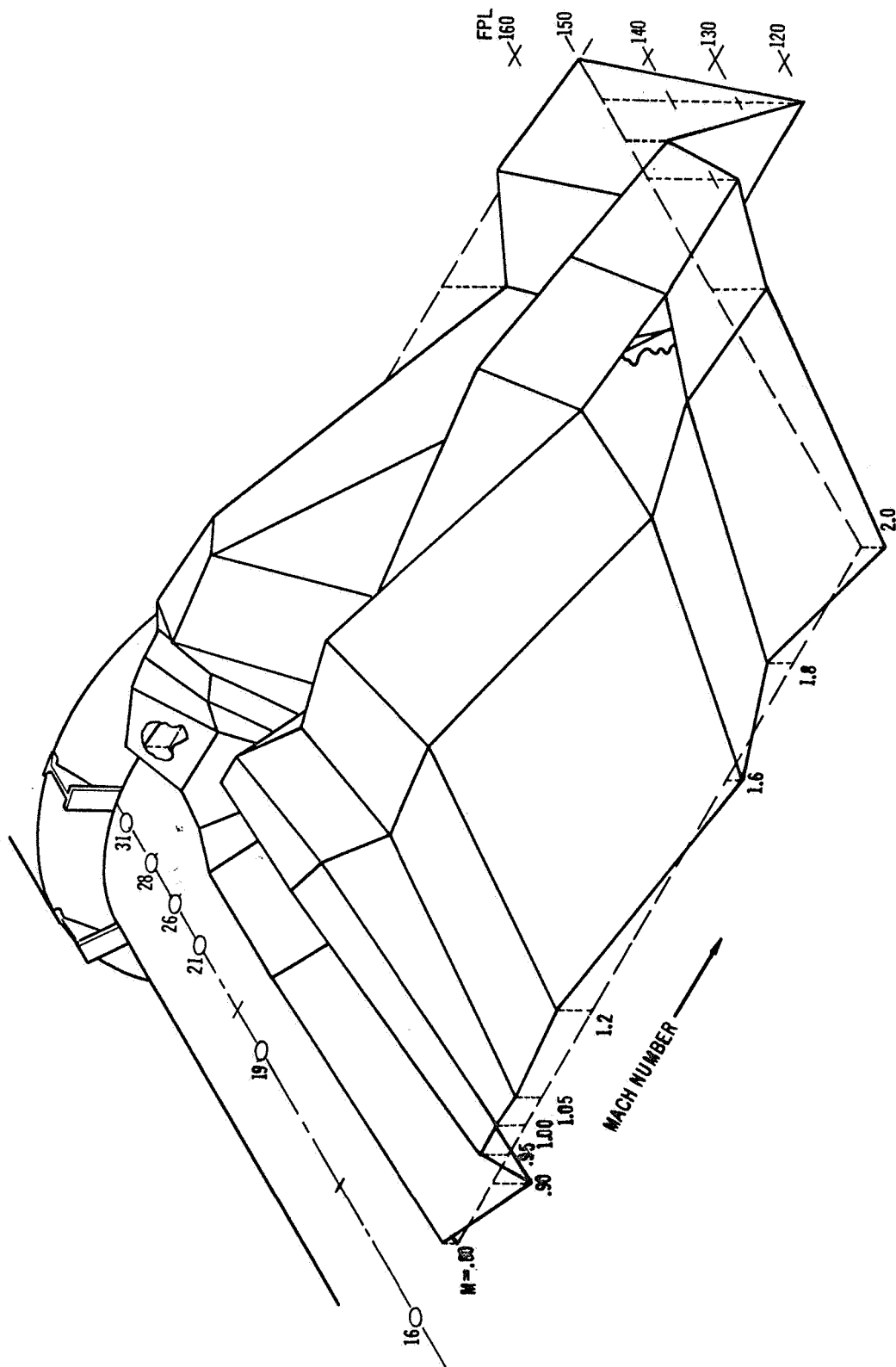


FIGURE 64

CONFIDENTIAL

OVERALL FLUCTUATING PRESSURE LEVEL DISTRIBUTION IN FIN PLANE II
CONFIGURATION B VERSUS MACH NUMBER

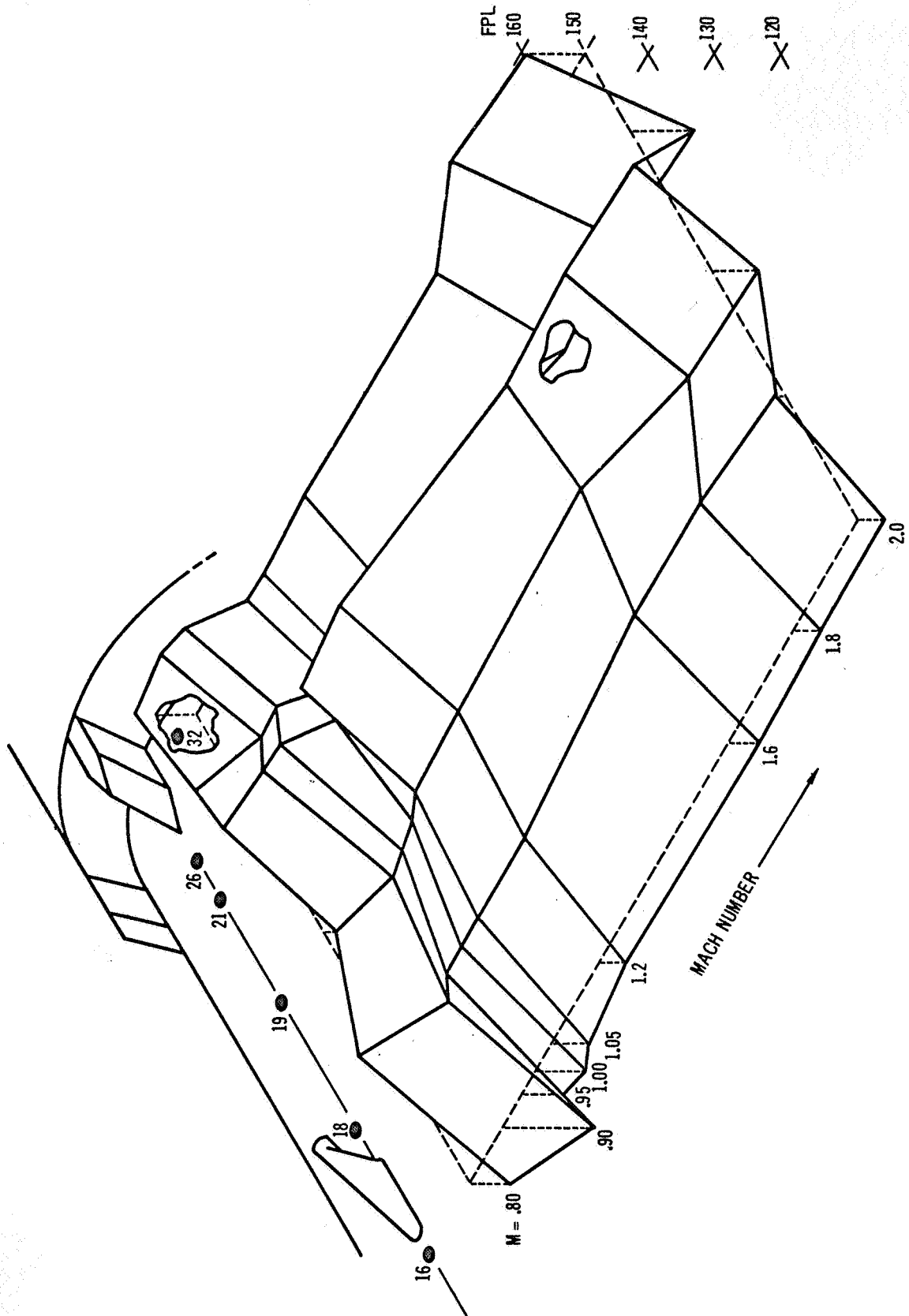


FIGURE 65

CONFIDENTIAL

OVERALL FLUCTUATING PRESSURE LEVEL DISTRIBUTION IN
FIN PLANE II OF CONFIGURATION C VERSUS
MACH NUMBER

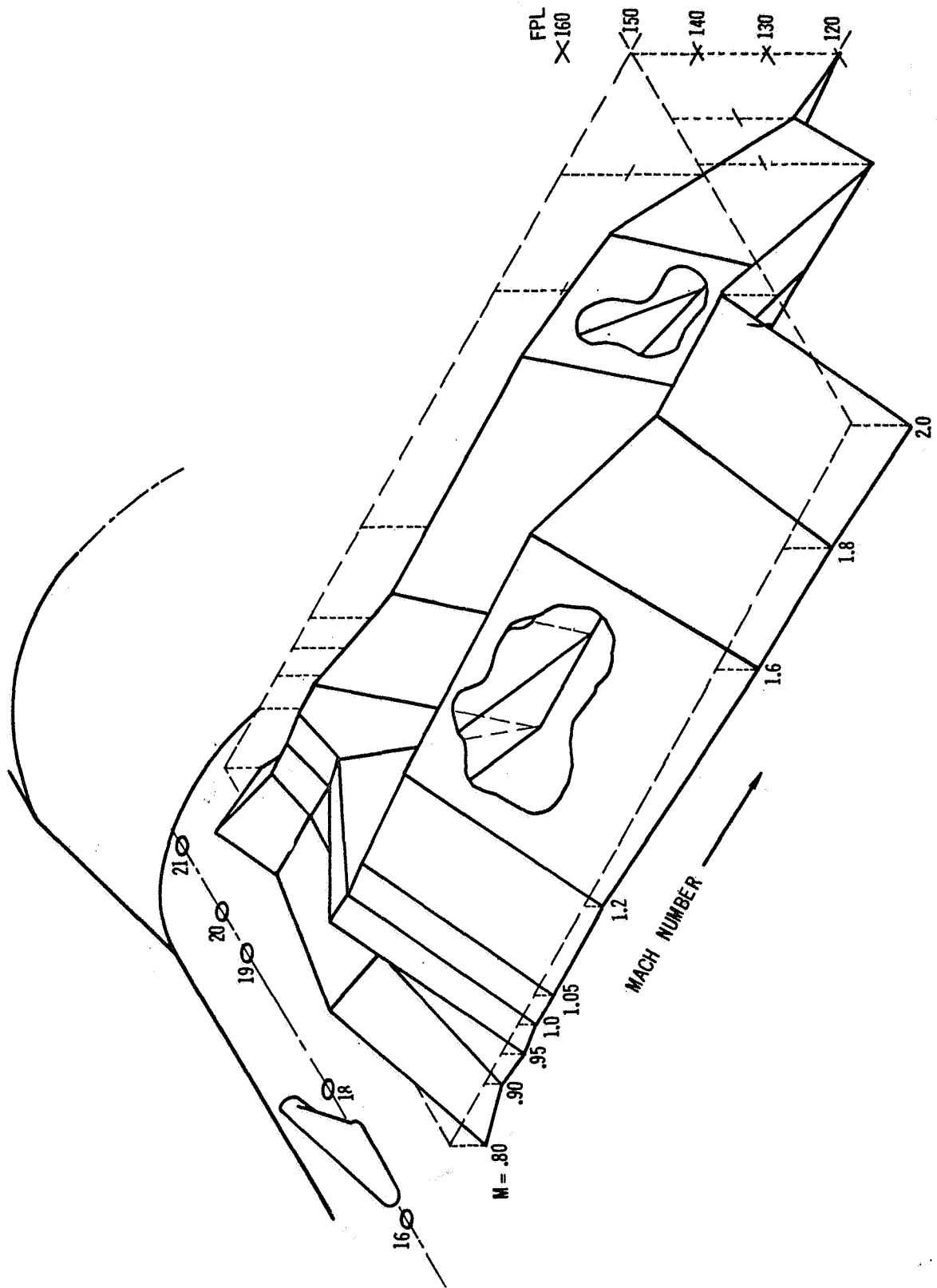
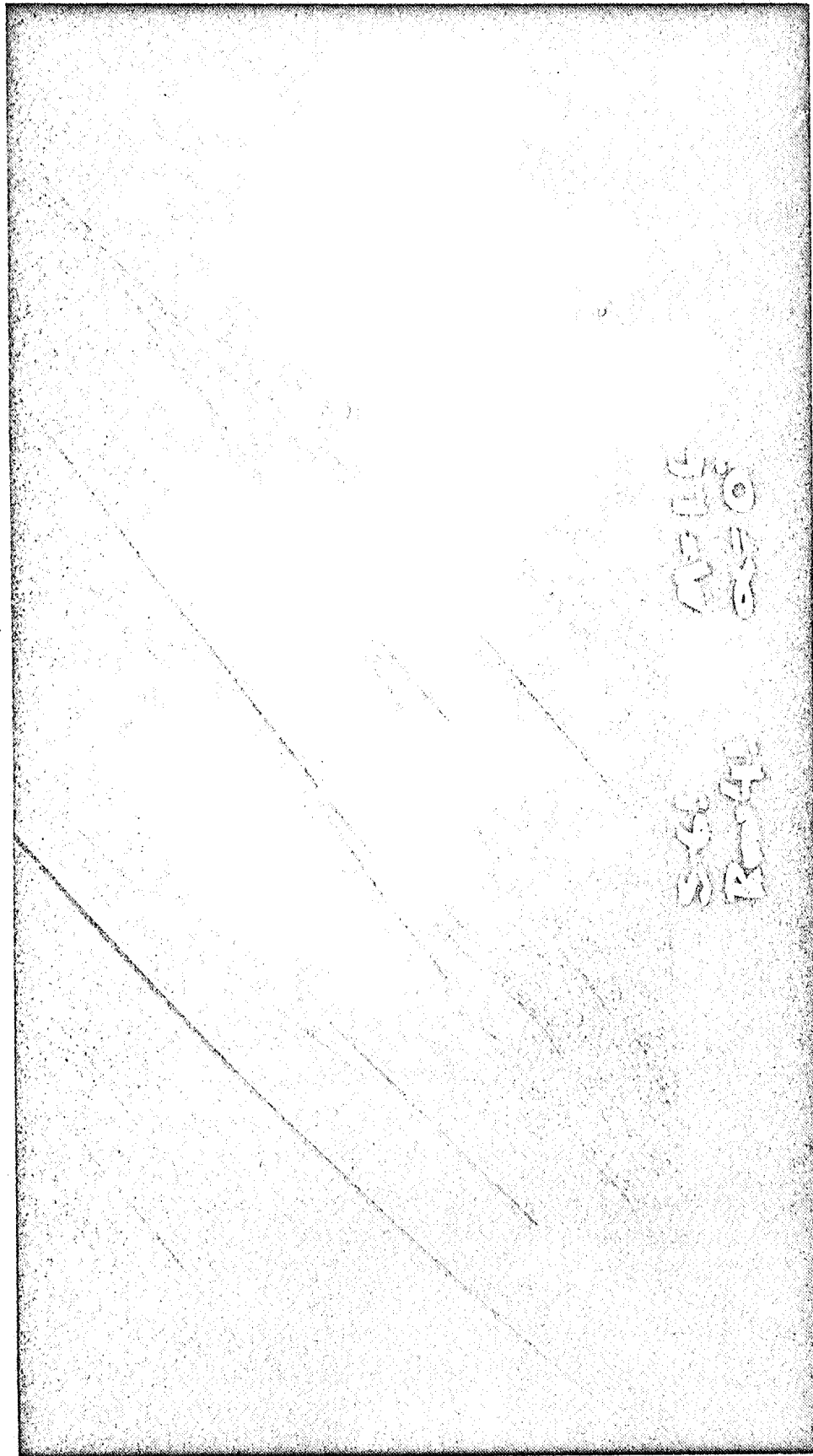


FIGURE 66

CONFIDENTIAL

CONFIDENTIAL

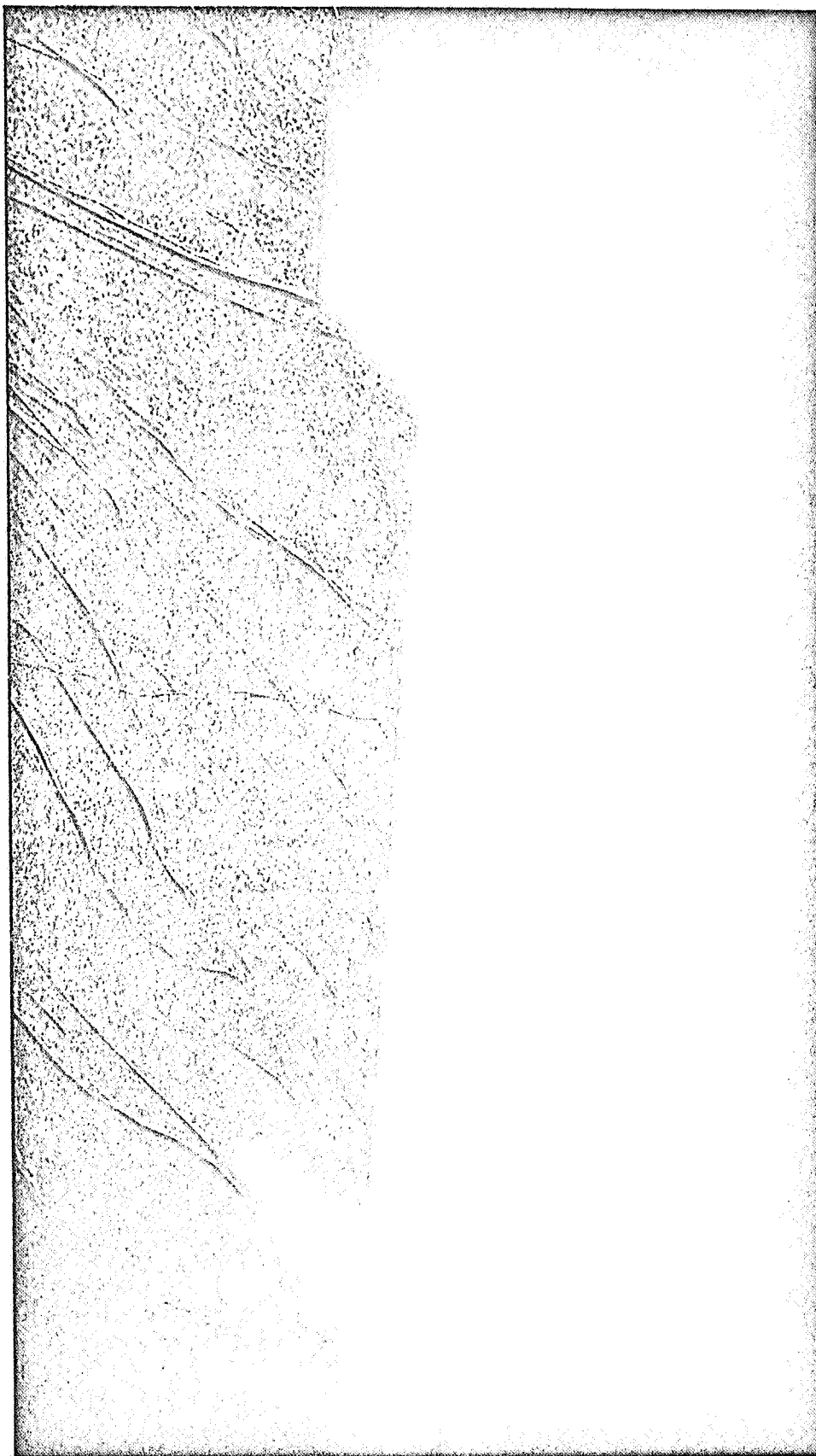


SHADOWGRAPH OF THE B CONFIGURATION

FIGURE 67

CONFIDENTIAL

CONFIDENTIAL

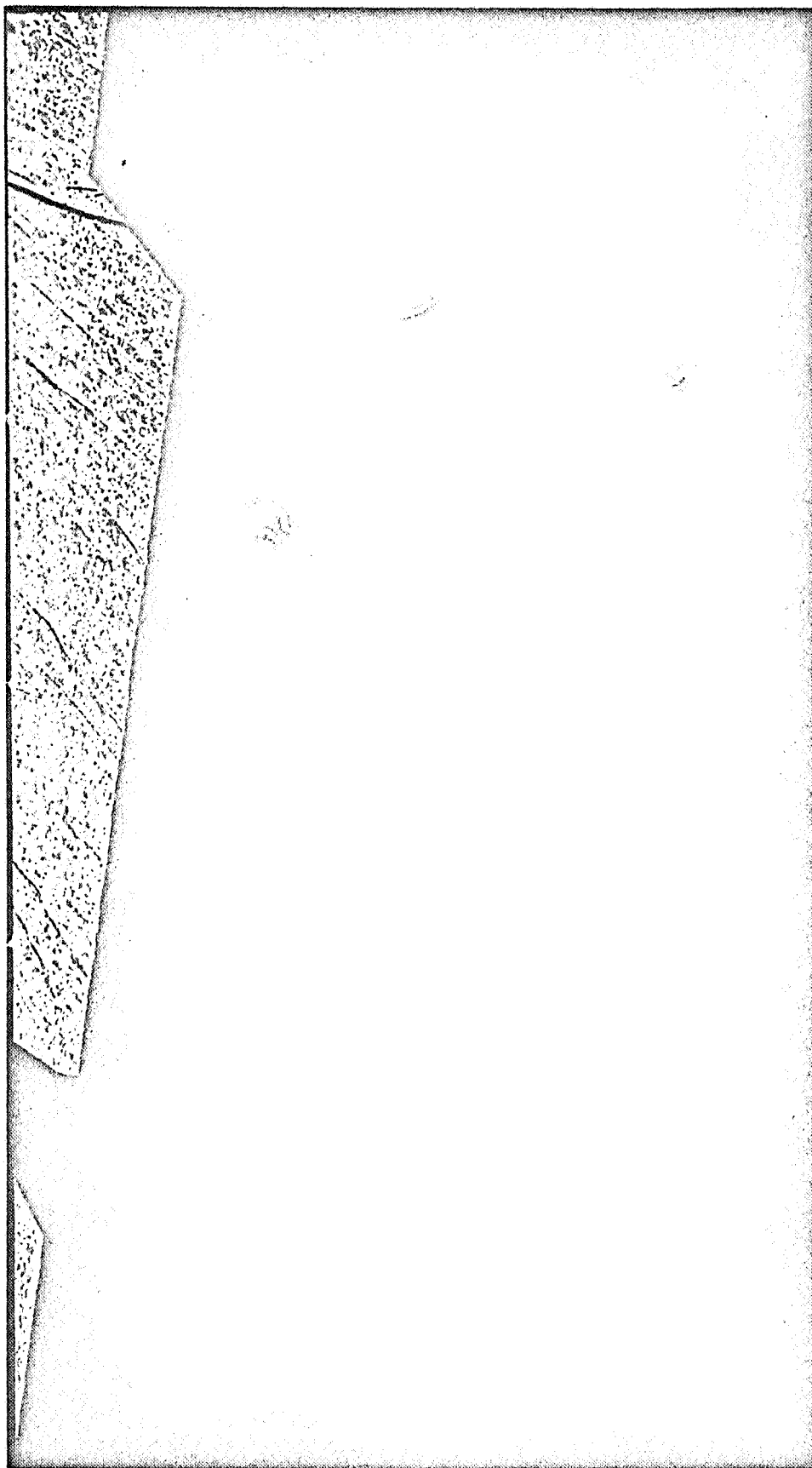


SHADOWGRAPH OF THE B CONFIGURATION

FIGURE 68

CONFIDENTIAL

~~CONFIDENTIAL~~



SHADOWGRAPH OF THE B CONFIGURATION

FIGURE 69

~~CONFIDENTIAL~~

VARIATION OF SPECTRUM SHAPE WITH ANGLE OF ATTACK α

FOR CONFIGURATION B, LOCATION 21, MACH NO. 1.0,

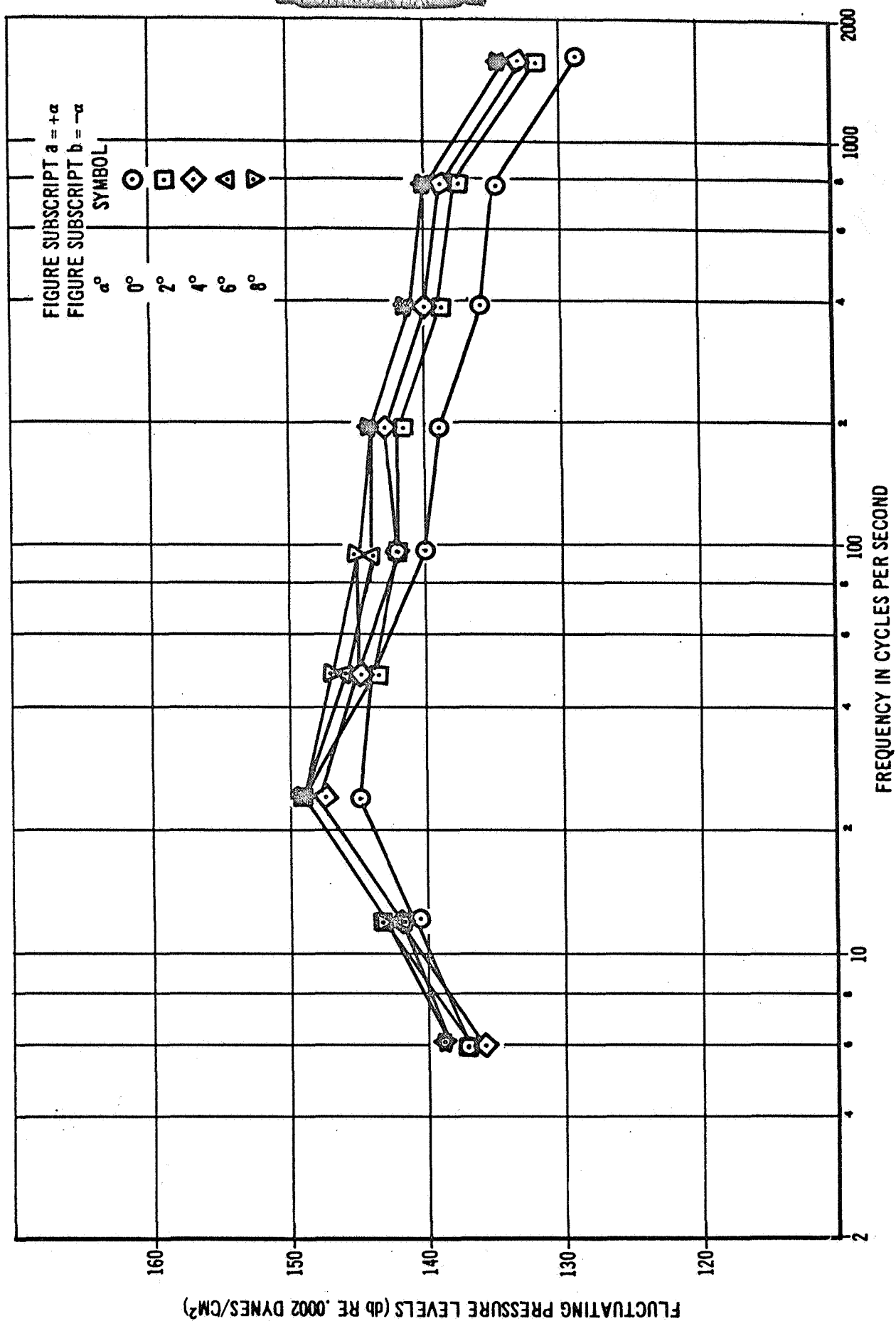


FIGURE 70 a

CONFIDENTIAL

VARIATION OF SPECTRUM SHAPE WITH ANGLE OF ATTACK α

FOR CONFIGURATION B, LOCATION 21, MACH NO. 1.0

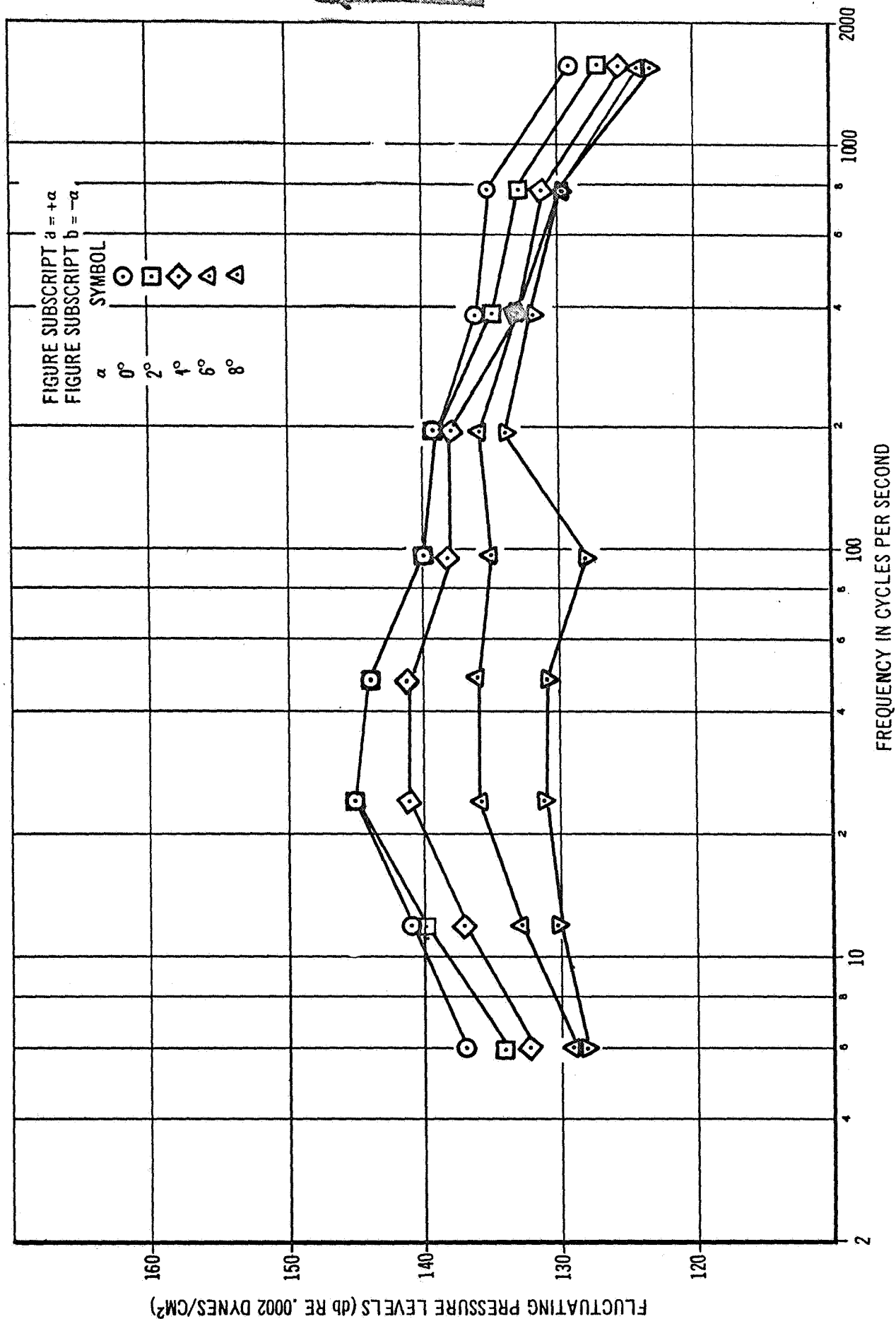


FIGURE 70b

VARIATION OF SPECTRUM SHAPE WITH ANGLE OF ATTACK α

FOR CONFIGURATION B, LOCATION 21, MACH NO. 1.2

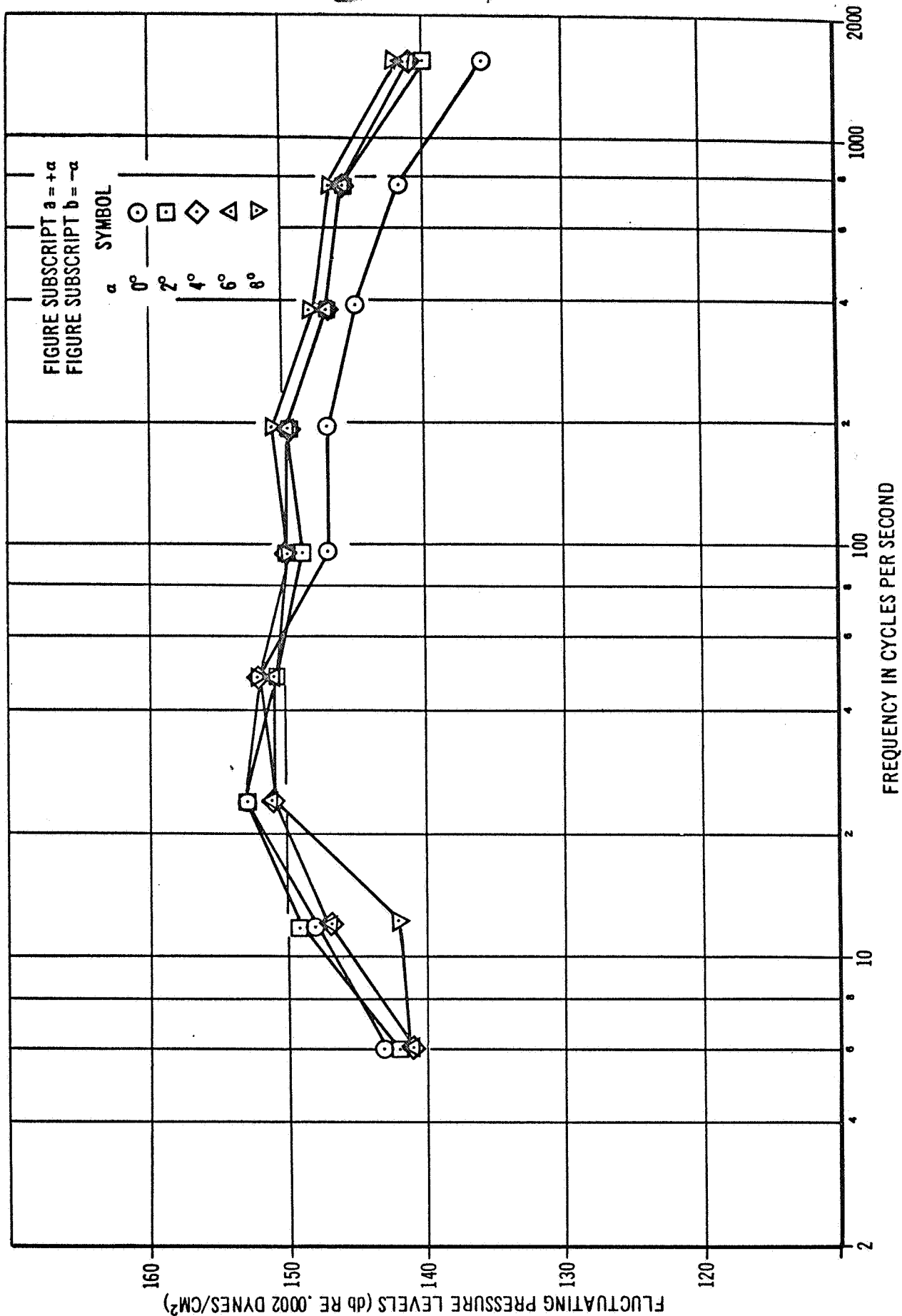


FIGURE 71a

~~CONFIDENTIAL~~

CONFIDENTIAL

VARIATION OF SPECTRUM SHAPE WITH ANGLE OF ATTACK α
FOR CONFIGURATION B, LOCATION 21, MACH NO. 1.2

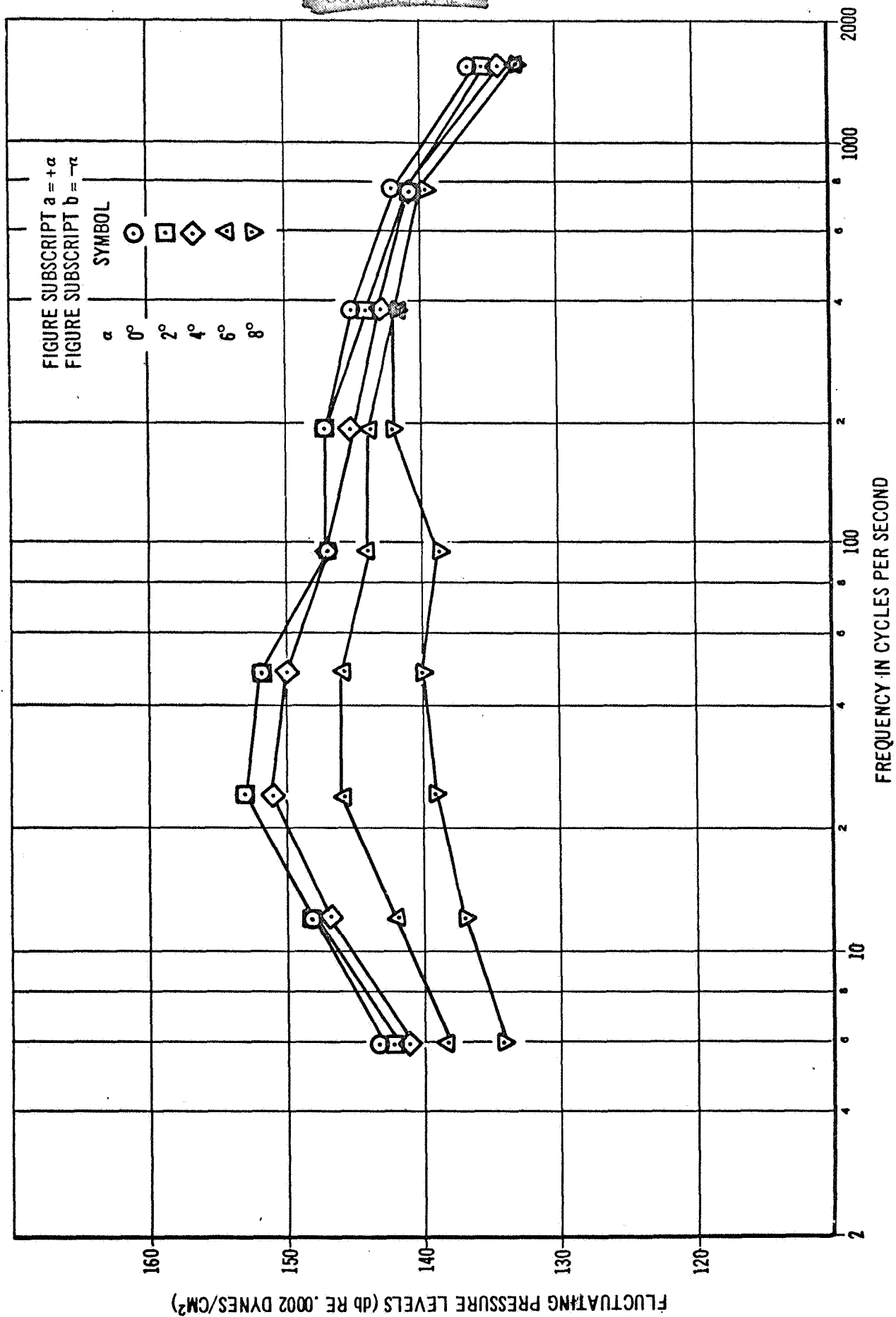


FIGURE 71b

CONFIDENTIAL

CONFIDENTIAL

VARIAION OF SPECTRUM SHAPE WITH ANGLE OF ATTACK α

FOR CONFIGURATION B, LOCATION 21, MACH NO. 1.6

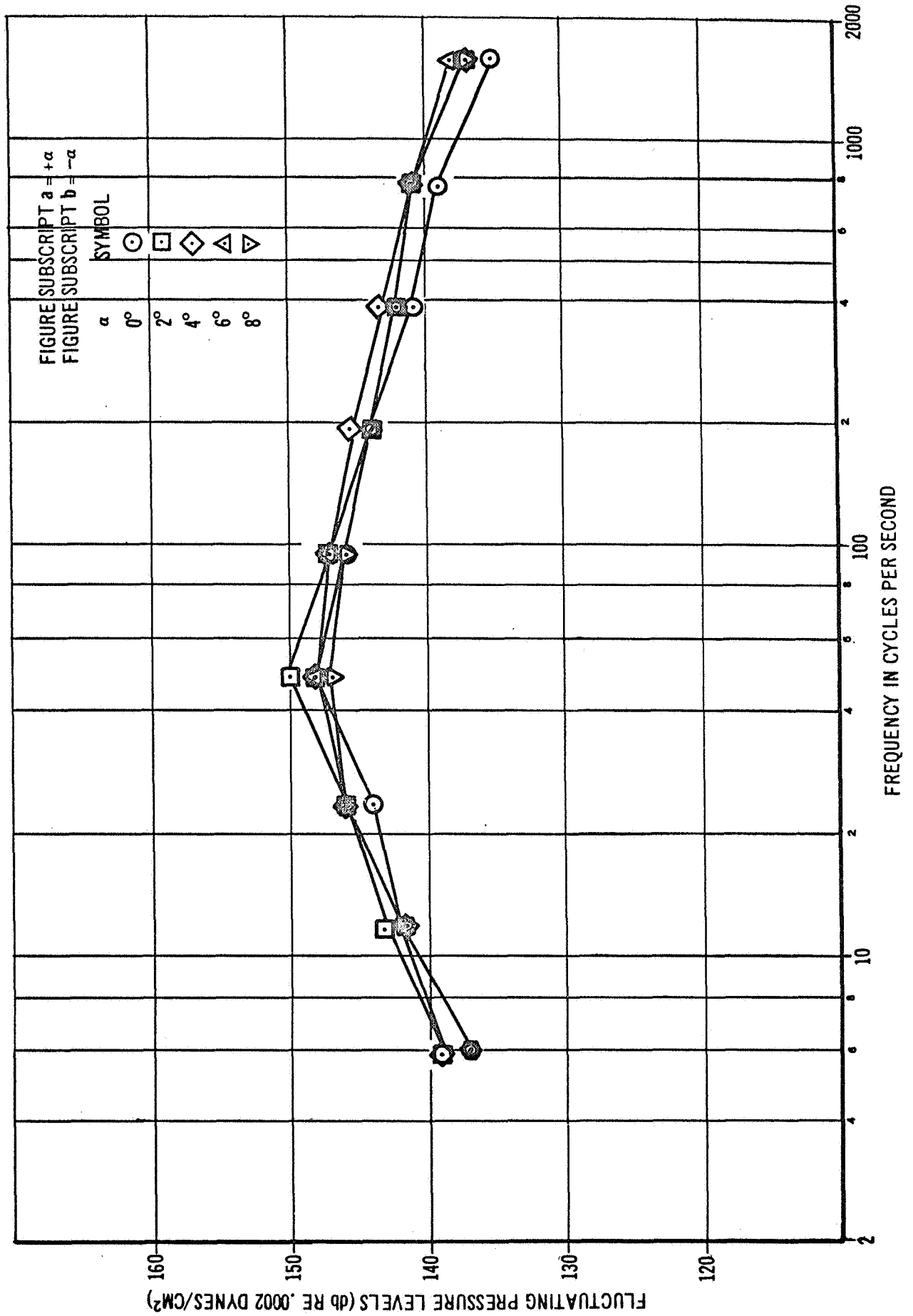


FIGURE 72 a

CONFIDENTIAL

CONFIDENTIAL

VARIATION OF SPECTRUM SHAPE WITH ANGLE OF ATTACK α

FOR CONFIGURATION B, LOCATION 2.1, MACH NO. 1.6

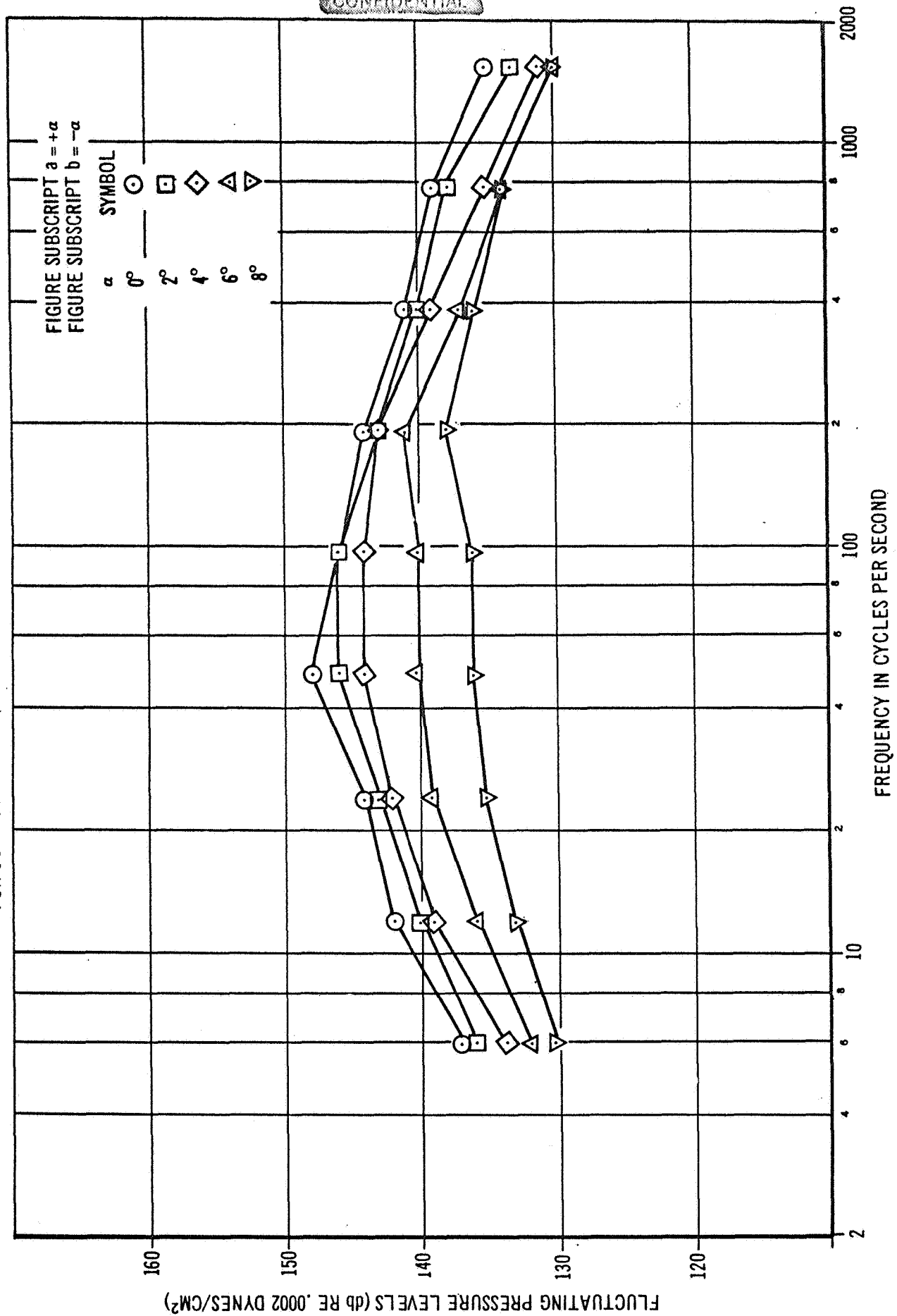


FIGURE 72b

CONFIDENTIAL

CONFIDENTIAL

VARIAION OF SPECTRUM SHAPE WITH ANGLE OF ATTACK α

FOR CONFIGURATION B, LOCATION 26, MACH NO. 1.0

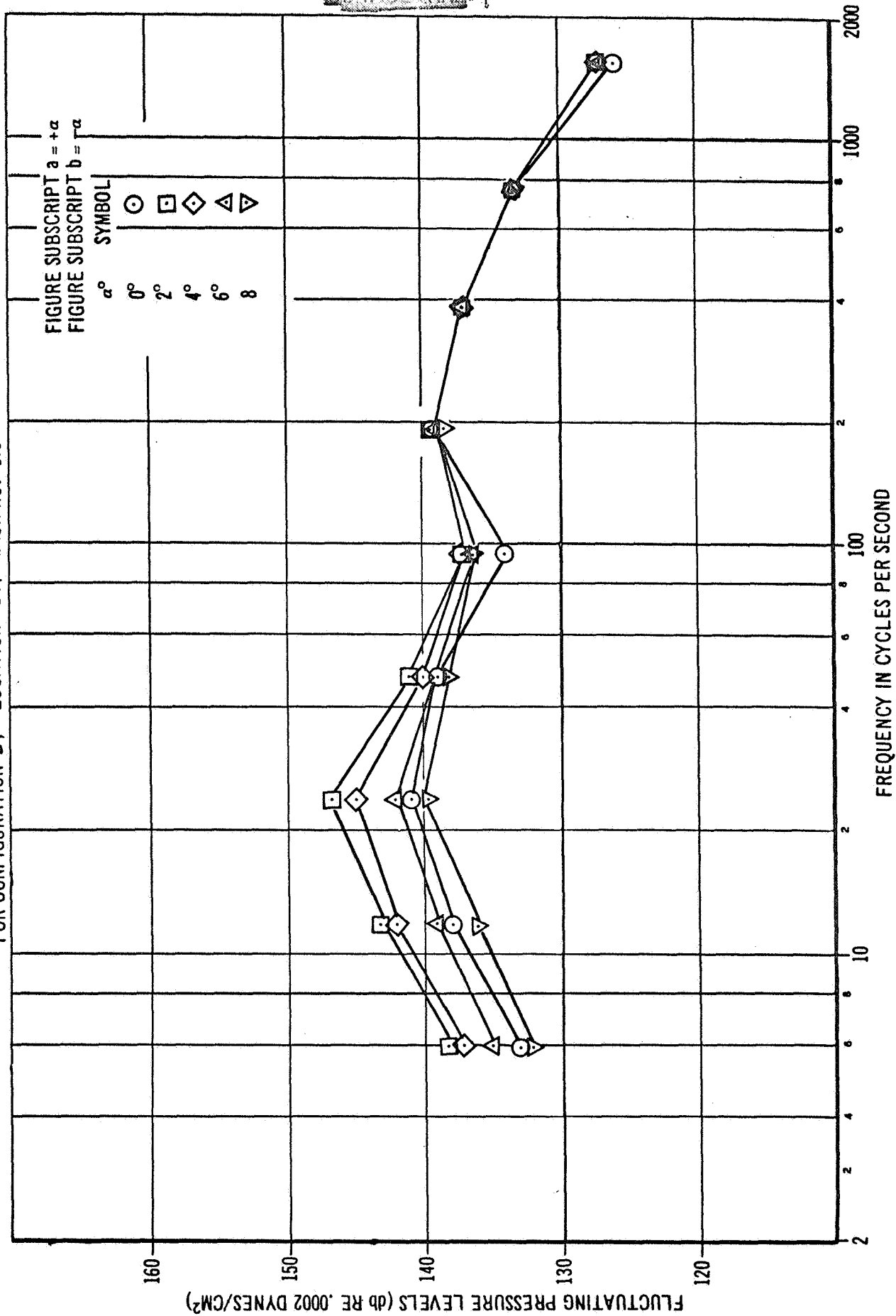


FIGURE 73a

CONFIDENTIAL

CONFIDENTIAL

VARIAION OF SPECTRUM SHAPE WITH ANGLE OF ATTACK α°

FOR CONFIGURATION B, LOCATION 26, MACH NO. 1.0

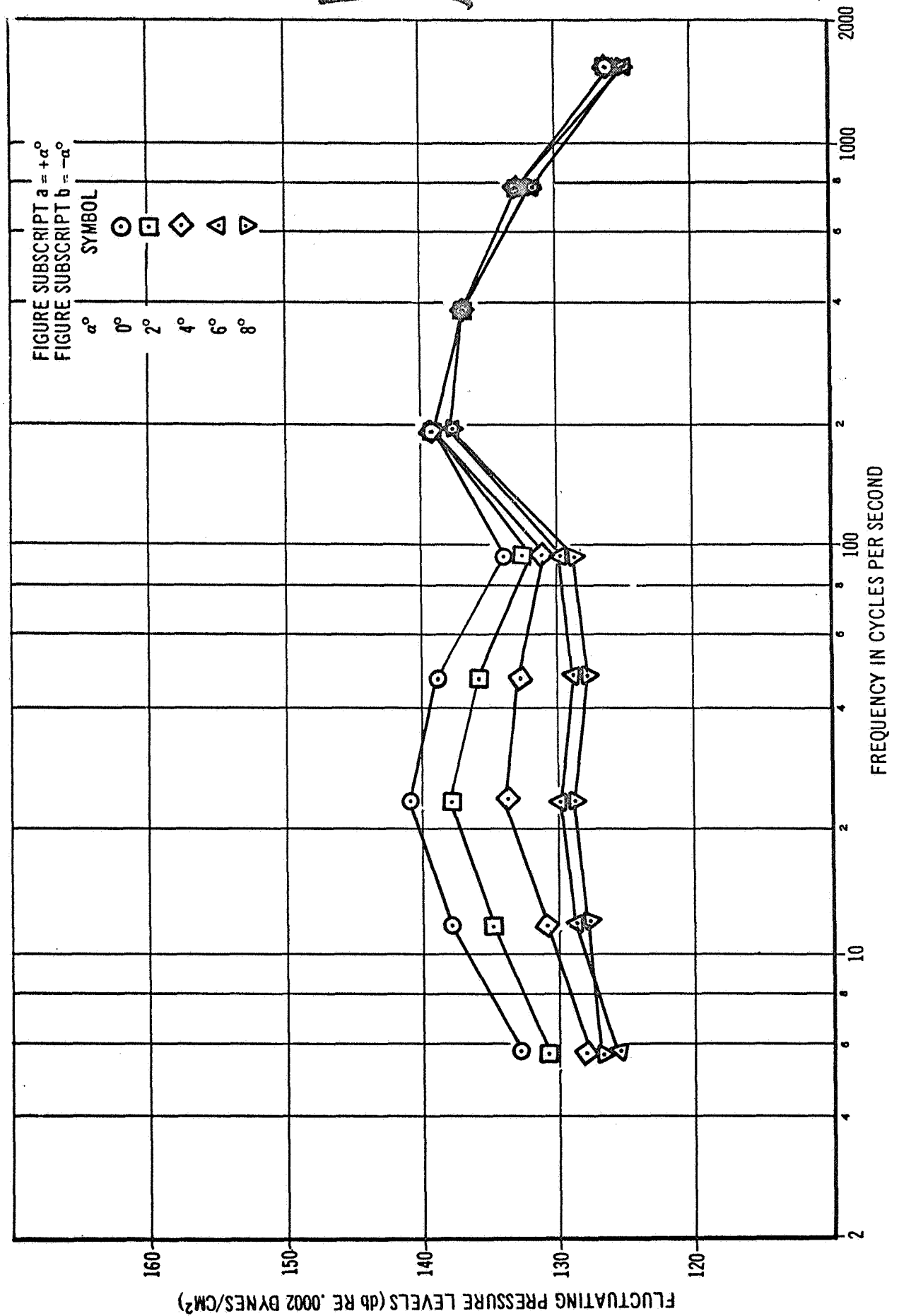


FIGURE 73b

CONFIDENTIAL

CONFIDENTIAL

VARIAION OF SPECTRUM SHAPE WITH ANGLE OF ATTACK α

FOR CONFIGURATION B, LOCATION 26, MACH NO. 1.2

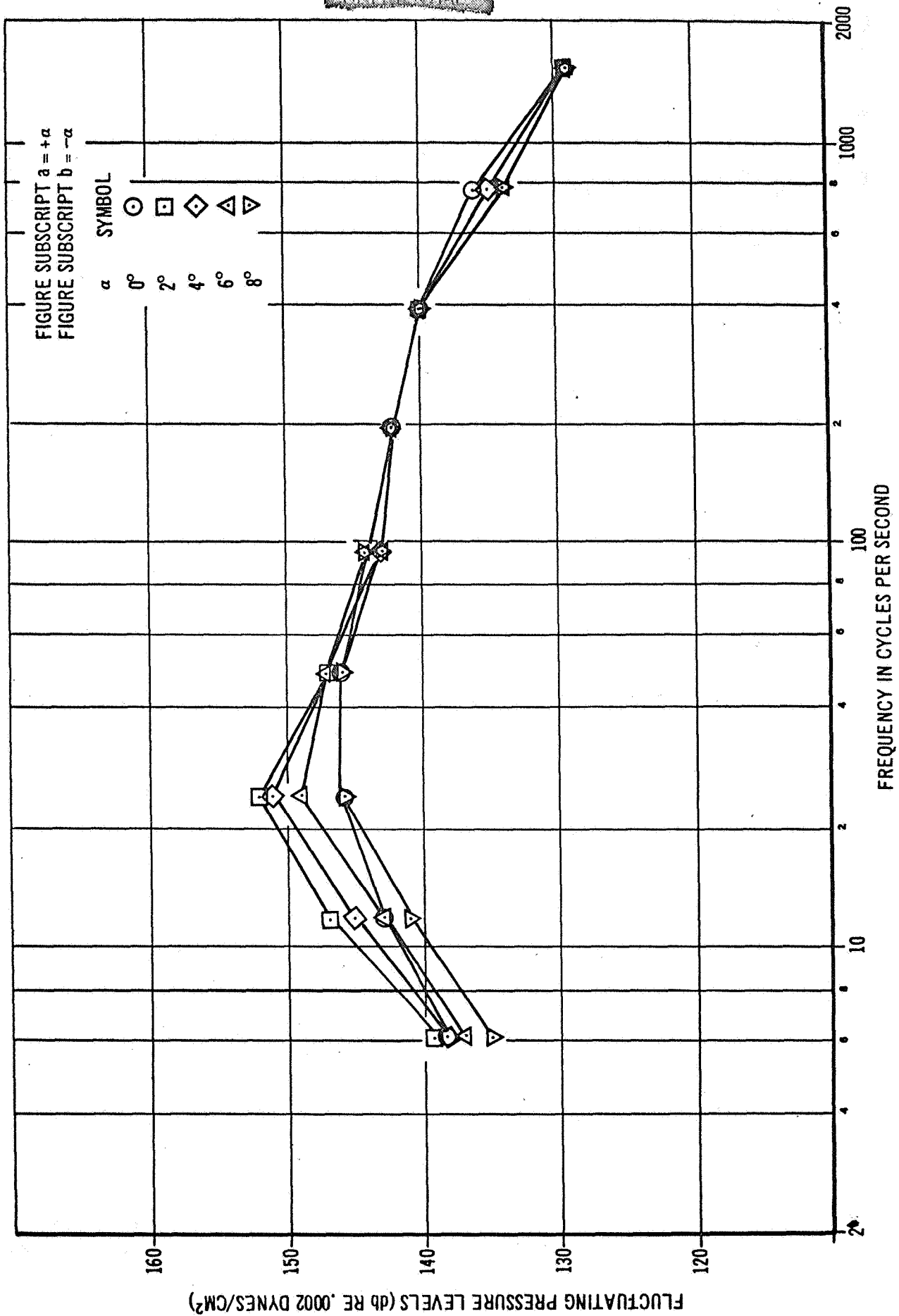


FIGURE 74a

CONFIDENTIAL

CONFIDENTIAL VARIATION OF SPECTRUM SHAPE WITH ANGLE OF ATTACK α

FOR CONFIGURATION B LOCATION 26, MACH NO. 1.2

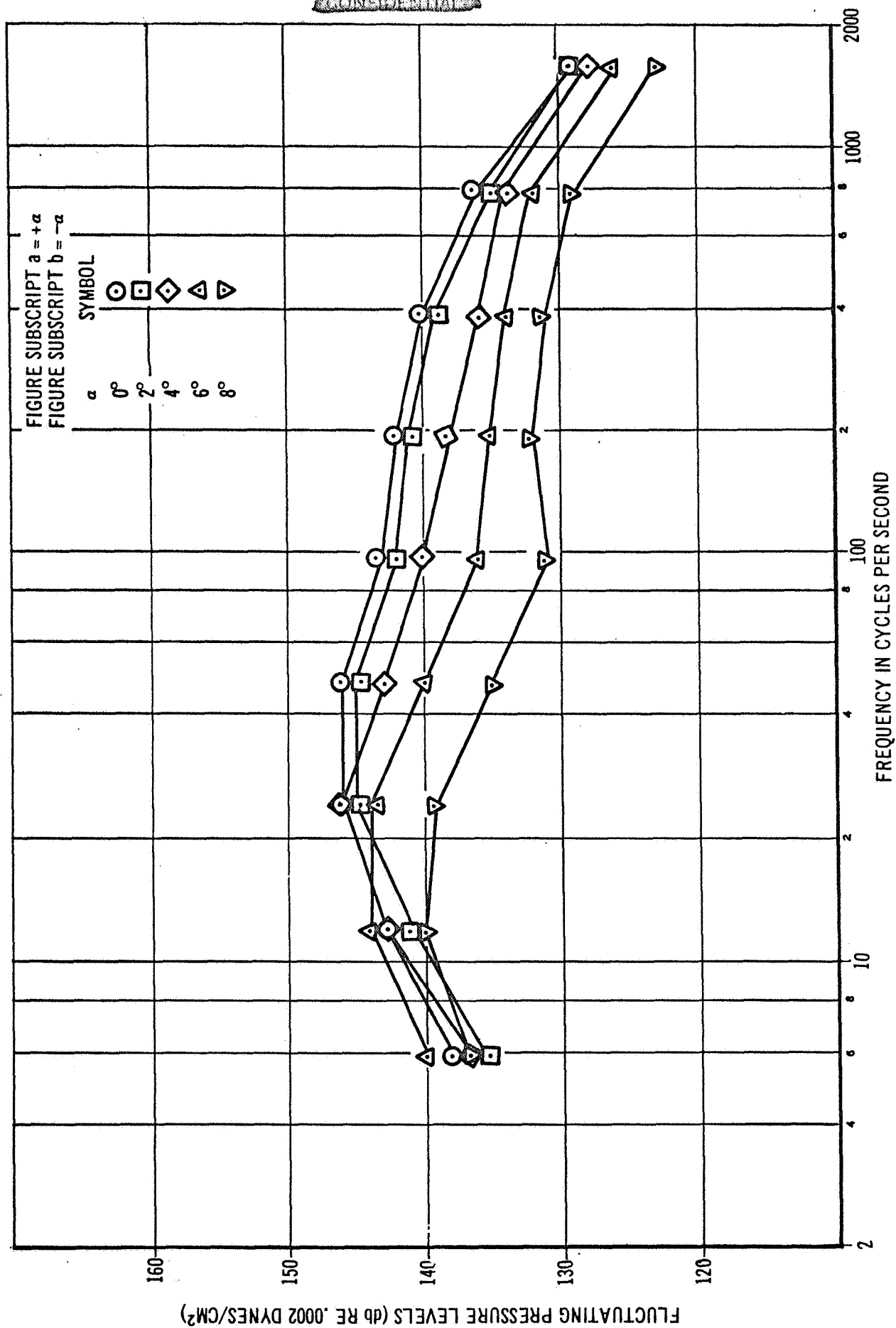


FIGURE 74b

CONFIDENTIAL

CONFIDENTIAL

VARIATION OF SPECTRUM SHAPE WITH ANGLE OF ATTACK α

FOR CONFIGURATION B, LOCATION 26, MACH NO. 1.6

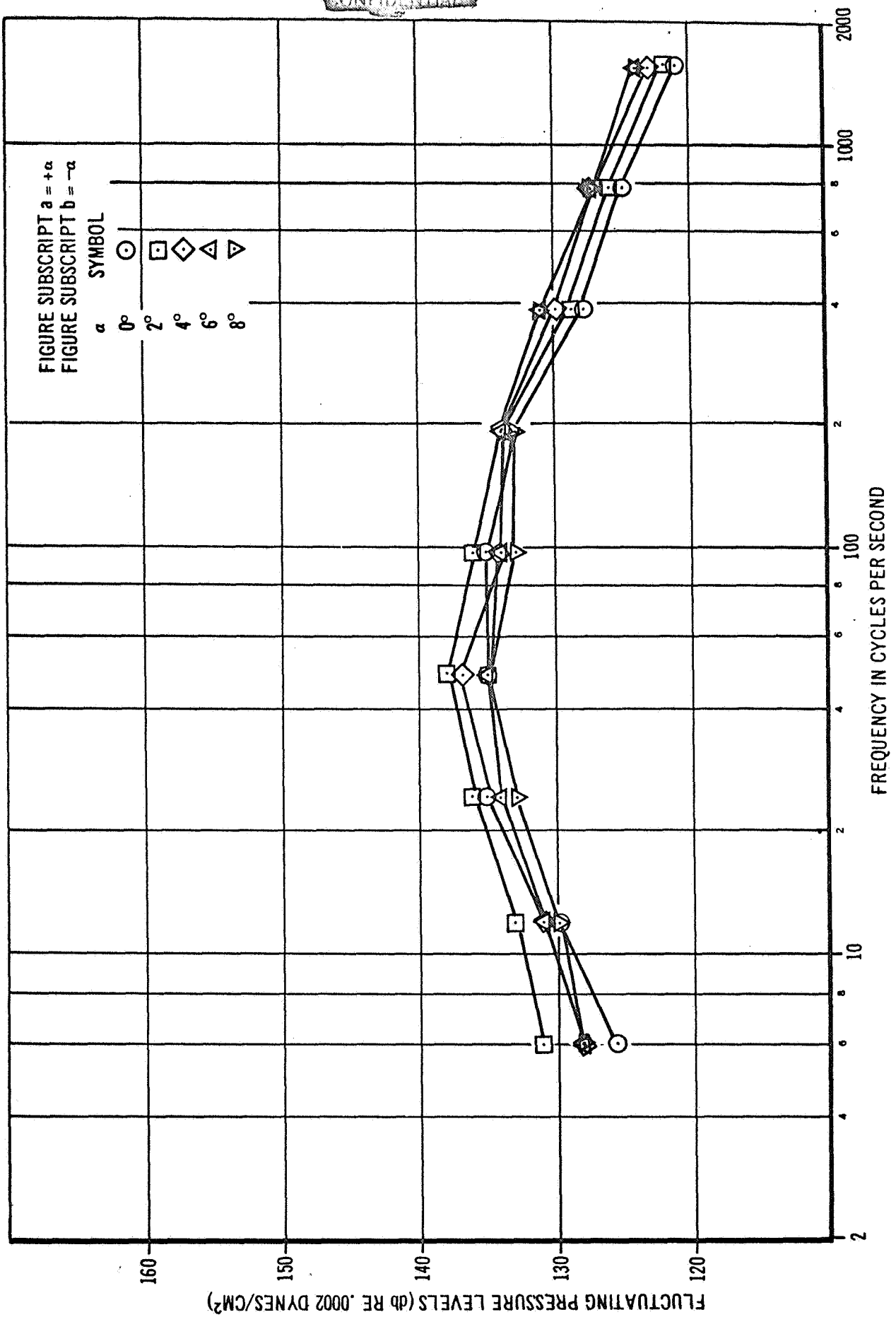


FIGURE 75a

CONFIDENTIAL

CONFIDENTIAL

VARIATION OF SPECTRUM SHAPE WITH ANGLE OF ATTACK α
 FOR CONFIGURATION B. LOCATION 26, MACH NO. 1.6

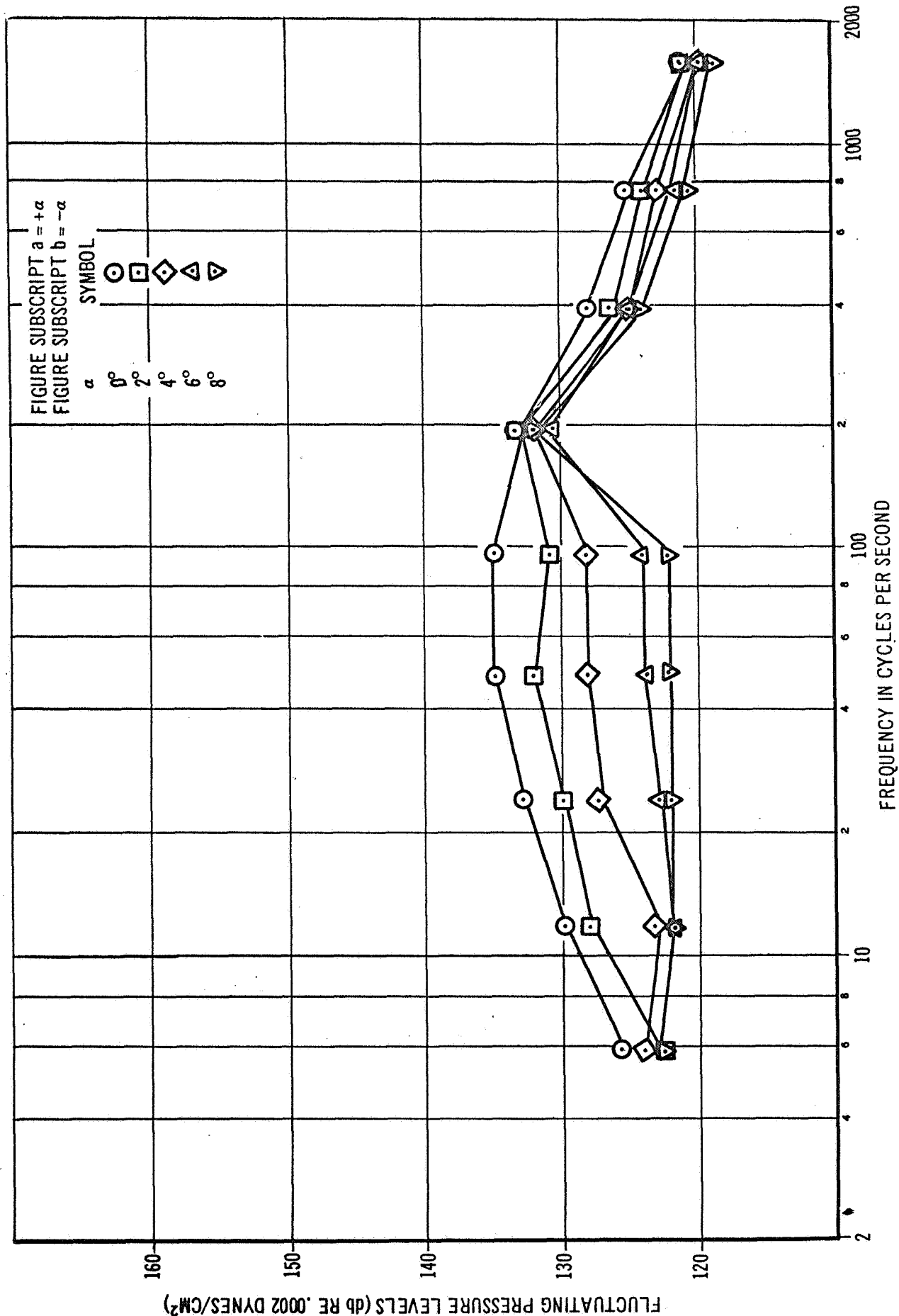


FIGURE 75b

CONFIDENTIAL

PERCENT OF MODEL FLUCTUATING PRESSURE MEASUREMENTS
GREATER THAN THE APPARENT NOISE LEVELS
OF THE WIND TUNNEL

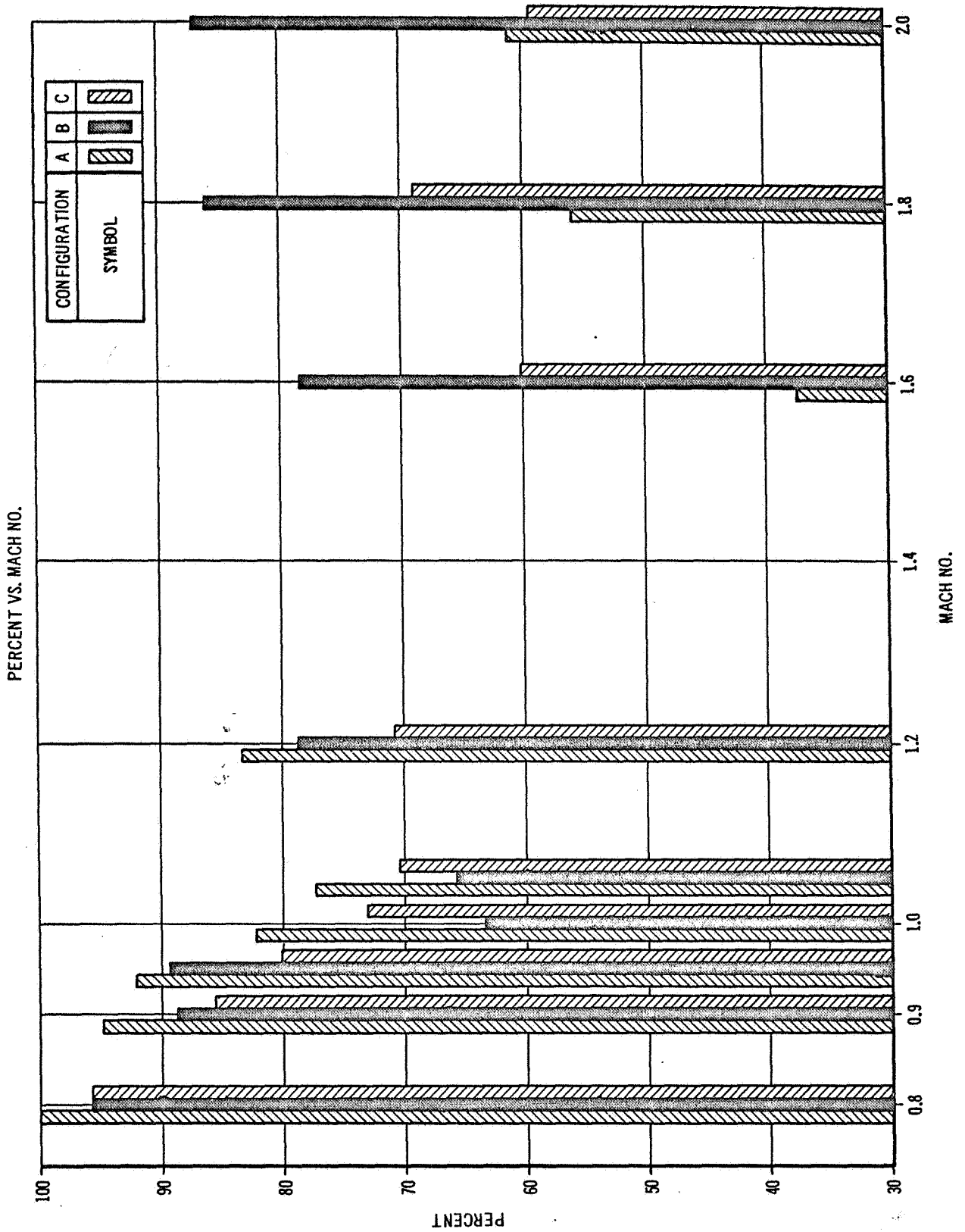


FIGURE 76

NON-DIMENSIONALIZED UNCORRECTED SPECTRA OF THE PRESSURE
AT THE SURFACE FOR "WELL BEHAVED" MODEL FLOW

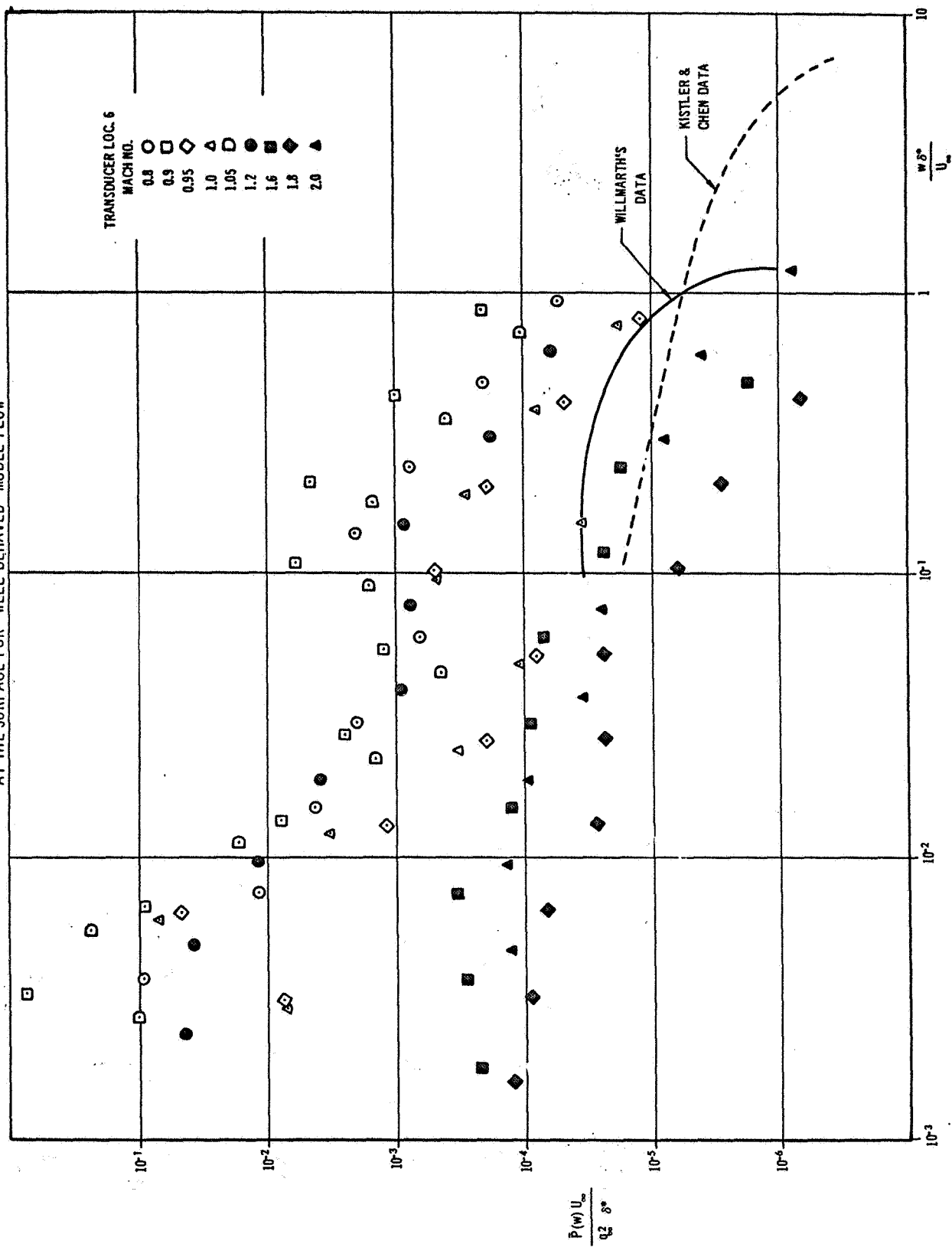


FIGURE 77

NON-DIMENSIONALIZED UNCORRECTED SPECTRA OF THE PRESSURE
AT THE SURFACE FOR "WELL BEHAVED" MODEL FLOW

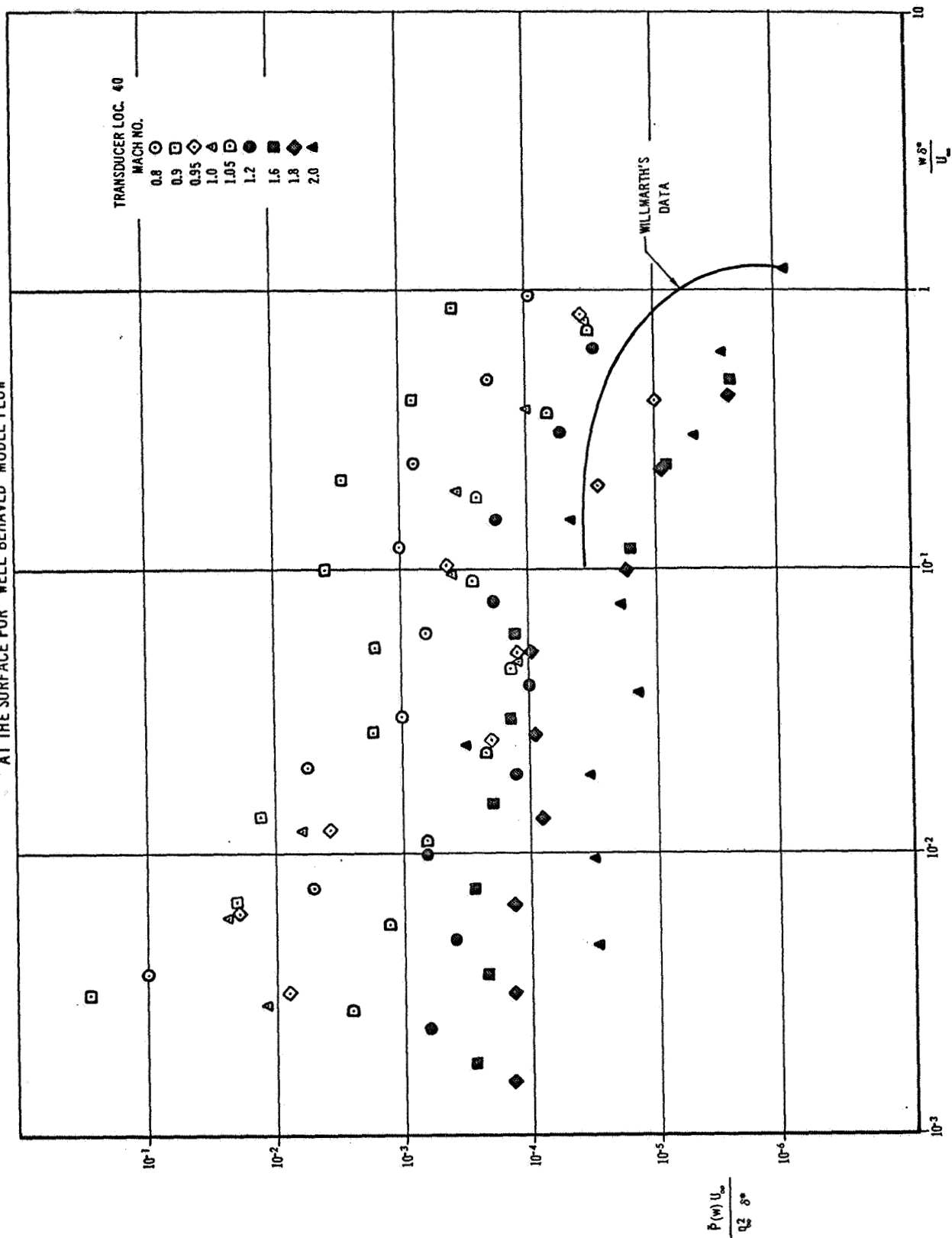


FIGURE 78

NON-DIMENSIONALIZED UNCORRECTED SPECTRA OF THE PRESSURE
AT THE SURFACE FOR "WELL BEHAVED" MODEL FLOW

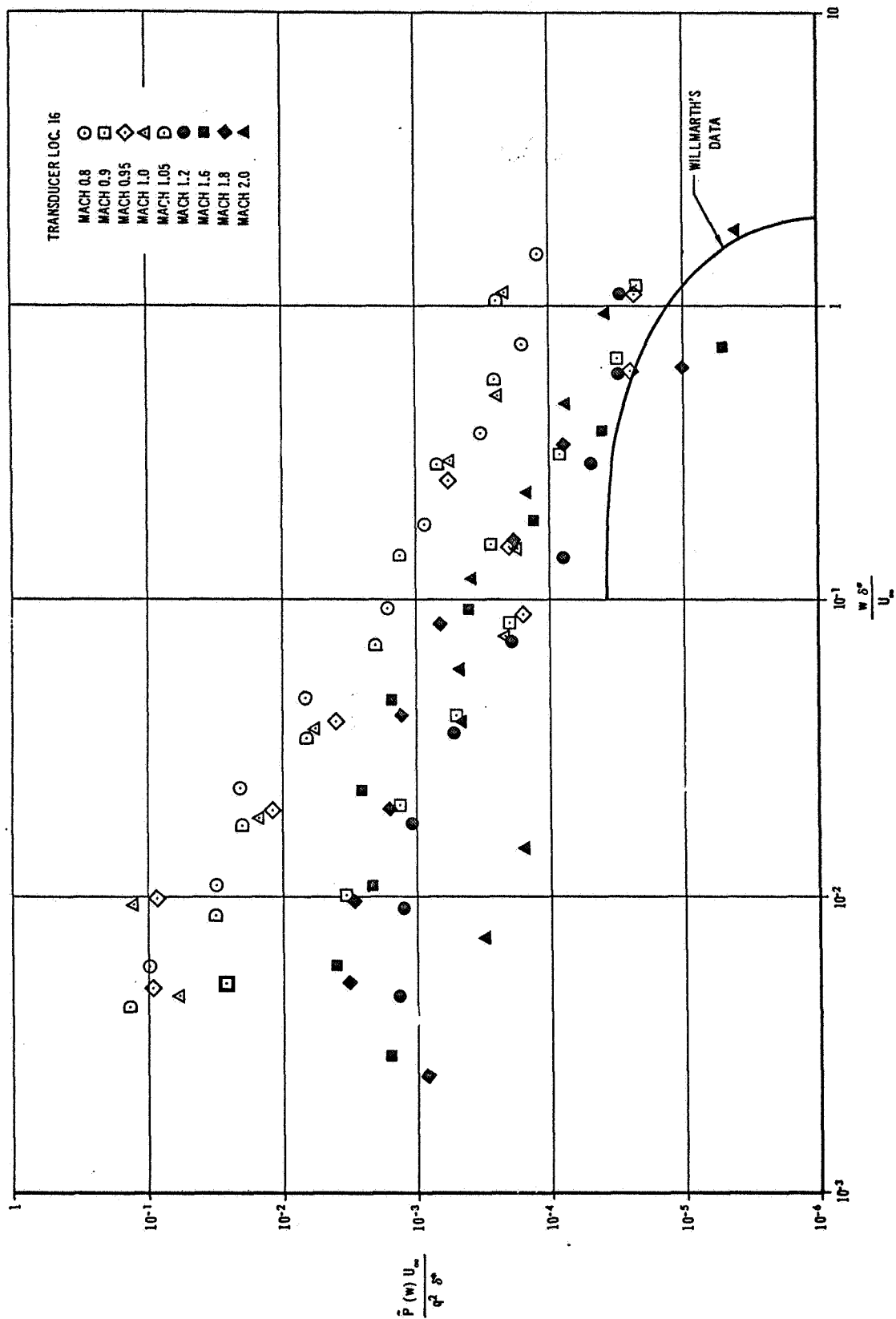


FIGURE 79

NON-DIMENSIONALIZED UNCORRECTED SPECTRA OF THE PRESSURE
AT THE SURFACE FOR "WELL BEHAVED" MODEL FLOW

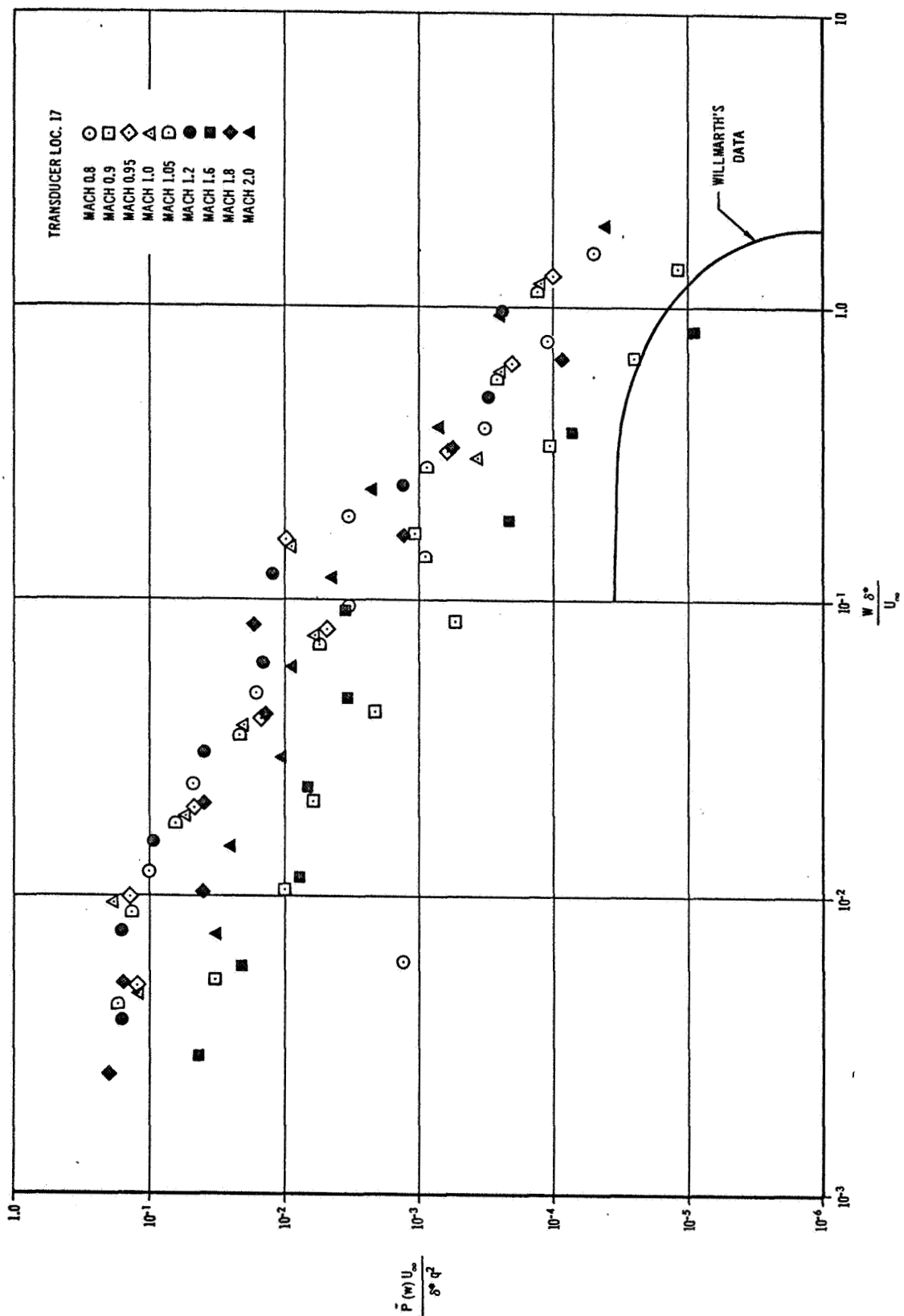


FIGURE 80

NON-DIMENSIONALIZED UNCORRECTED SPECTRA OF THE PRESSURE
AT THE SURFACE FOR "WELL BEHAVED" MODEL FLOW

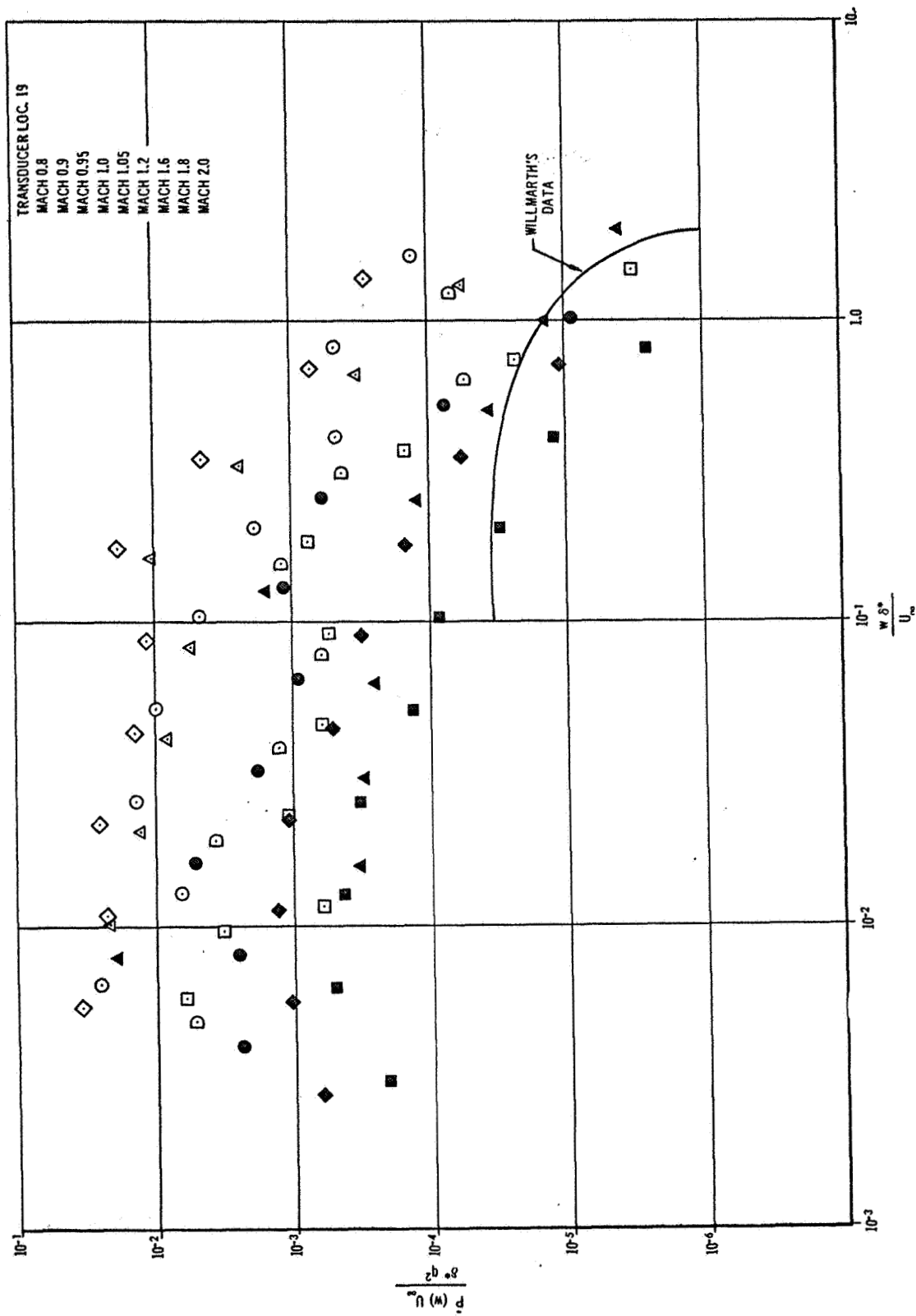


FIGURE 81

CONFIDENTIAL

NON-DIMENSIONALIZED UNCORRECTED SPECTRA OF THE PRESSURE
AT THE SURFACE FOR "WELL BEHAVED" MODEL FLOW

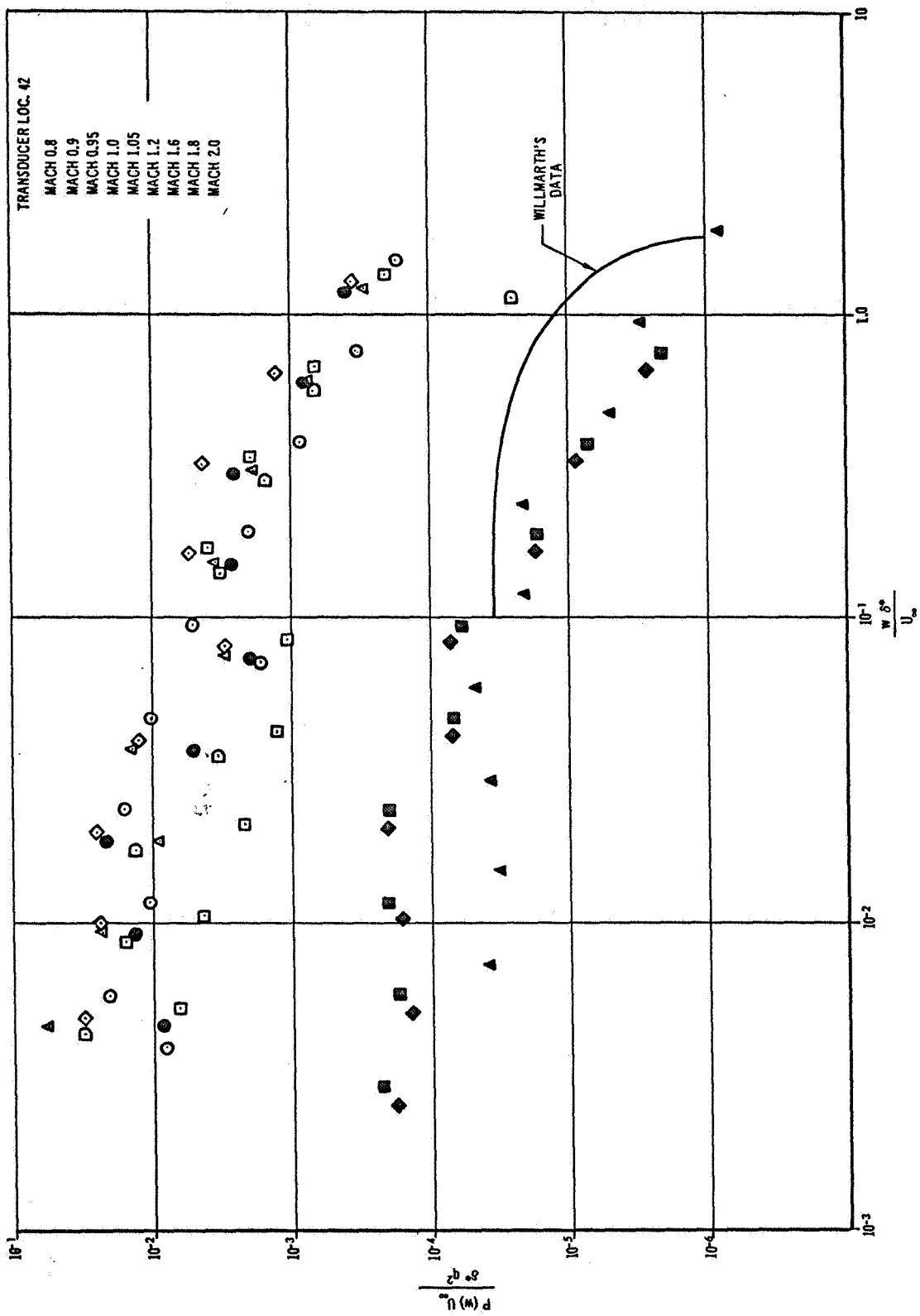


FIGURE 82

TIME HISTORY OF SA-4 FLUCTUATING PRESSURE LEVELS AND COMPARISON
WITH 2.75% SCALE MODEL WIND TUNNEL MEASUREMENTS

OVERALL FLUCTUATING PRESSURE LEVELS AT THE
SIV AFT INTERSTAGE VS TIME

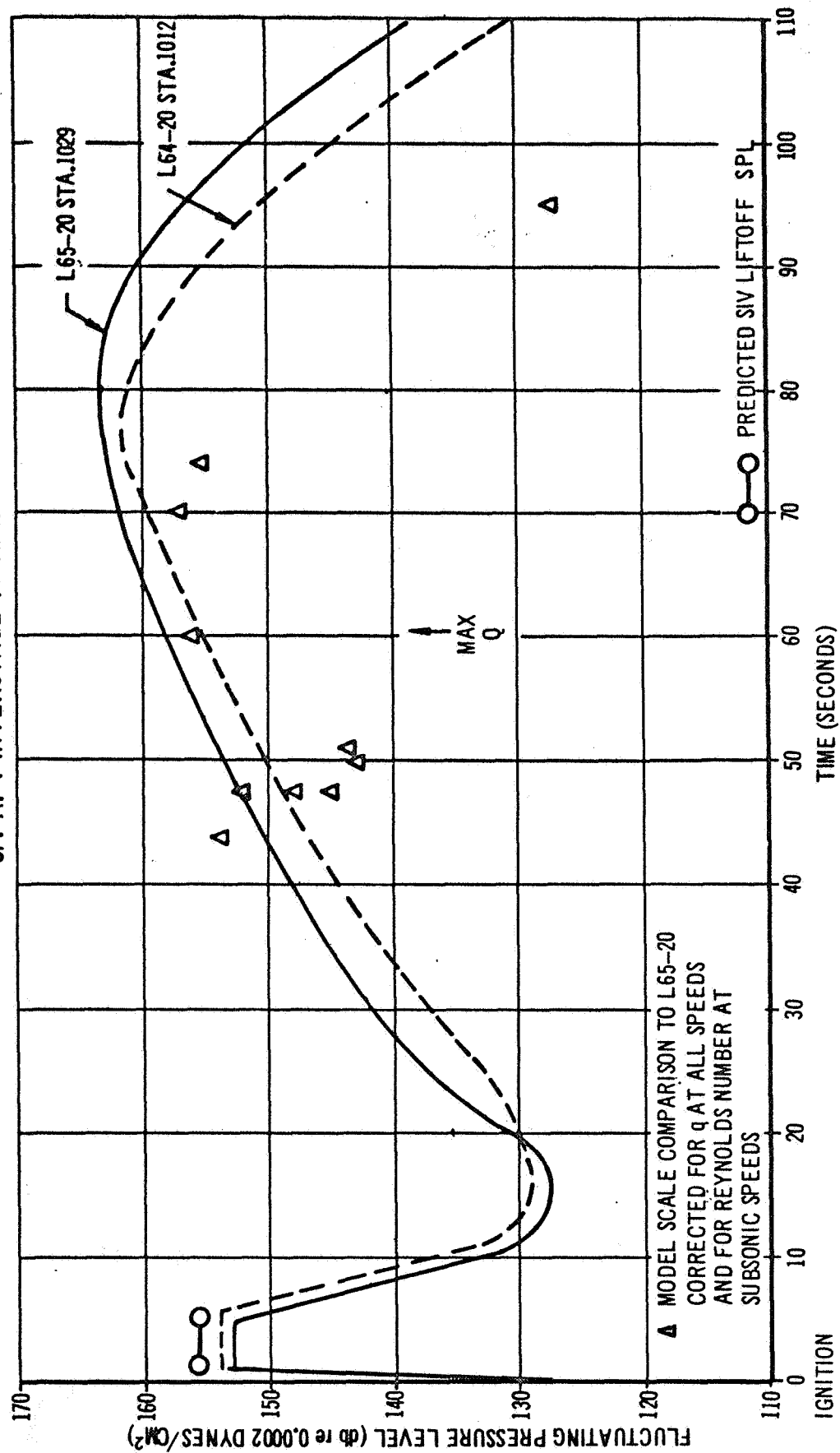
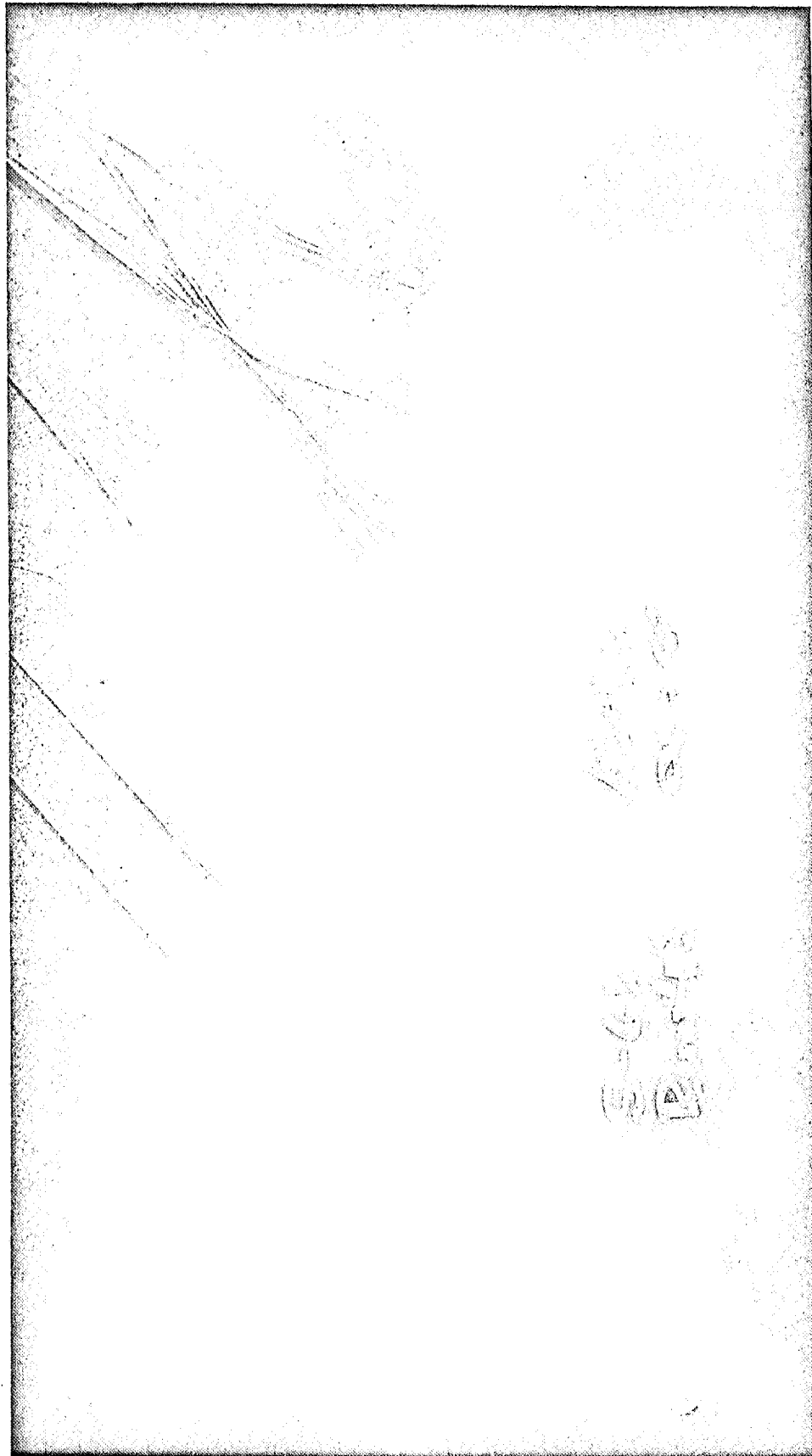


FIGURE 83

CONFIDENTIAL

CONFIDENTIAL



SHADOWGRAPH SHOWING THE INFLUENCE OF THE HYDROGEN CHILL DOWN
DUCT AT MACH 1.6

FIGURE 84

CONFIDENTIAL

COMPARISON OF SA-4 FLIGHT DATA AND 2.75% SCALE
MODEL WIND TUNNEL DATA DURING MAX q

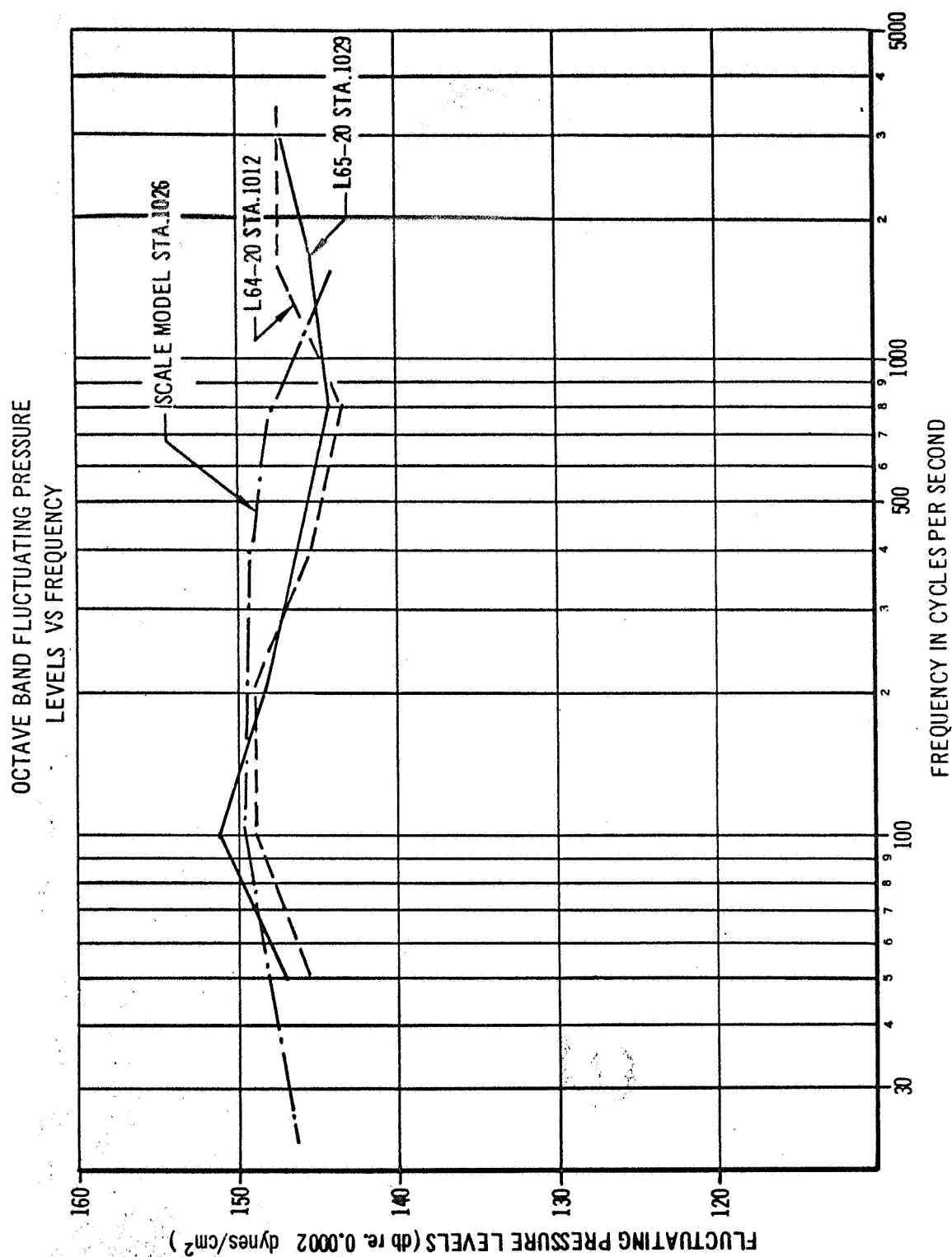


FIGURE 85

CONFIDENTIAL

COMPARISON OF SA-4 MEASUREMENT AT MAXIMUM LEVELS
WITH 2.75% MODEL SCALE DATA
OCTAVE BAND FLUCTUATING PRESSURE LEVEL VS FREQUENCY

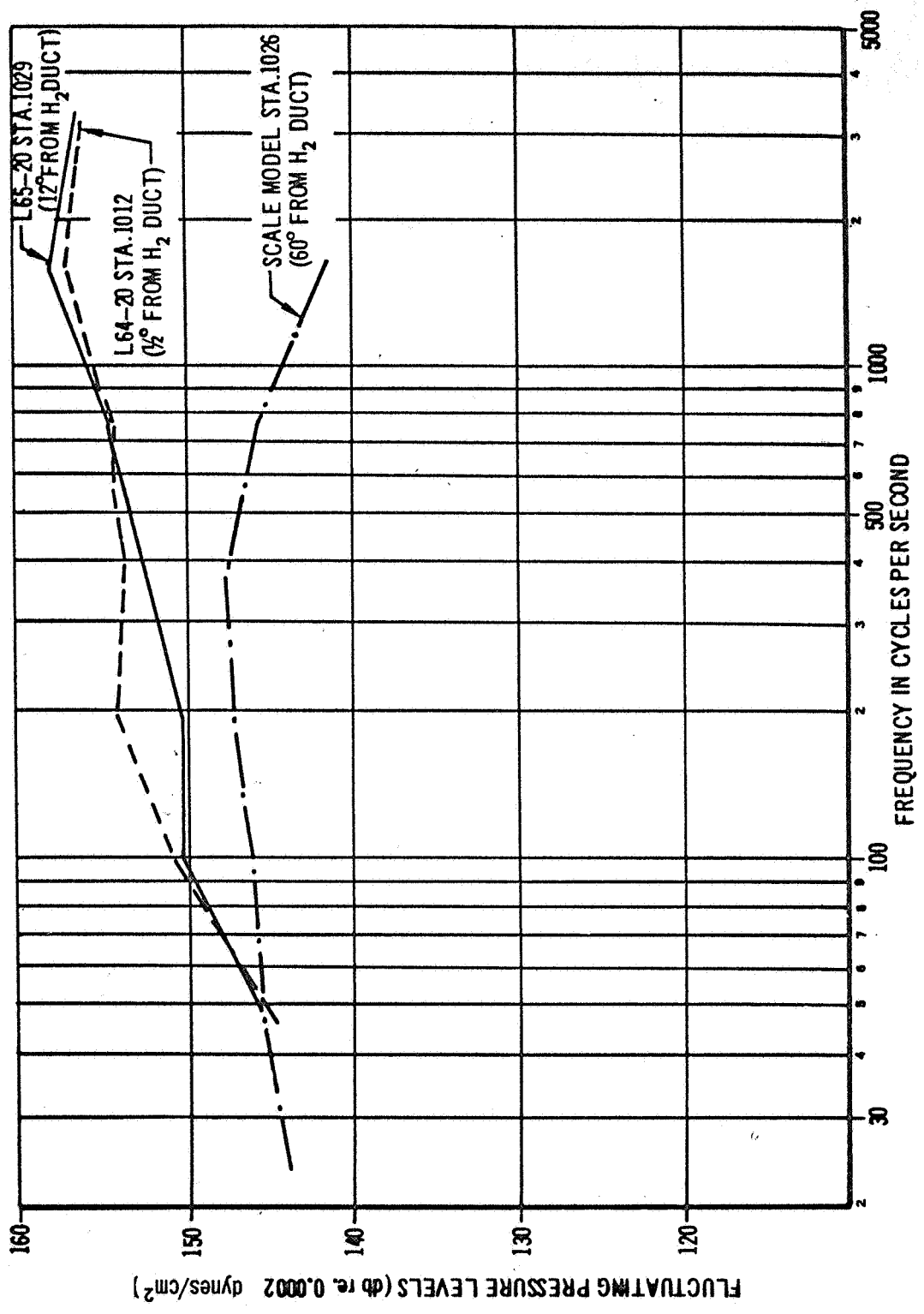


FIGURE 86

CONFIDENTIAL

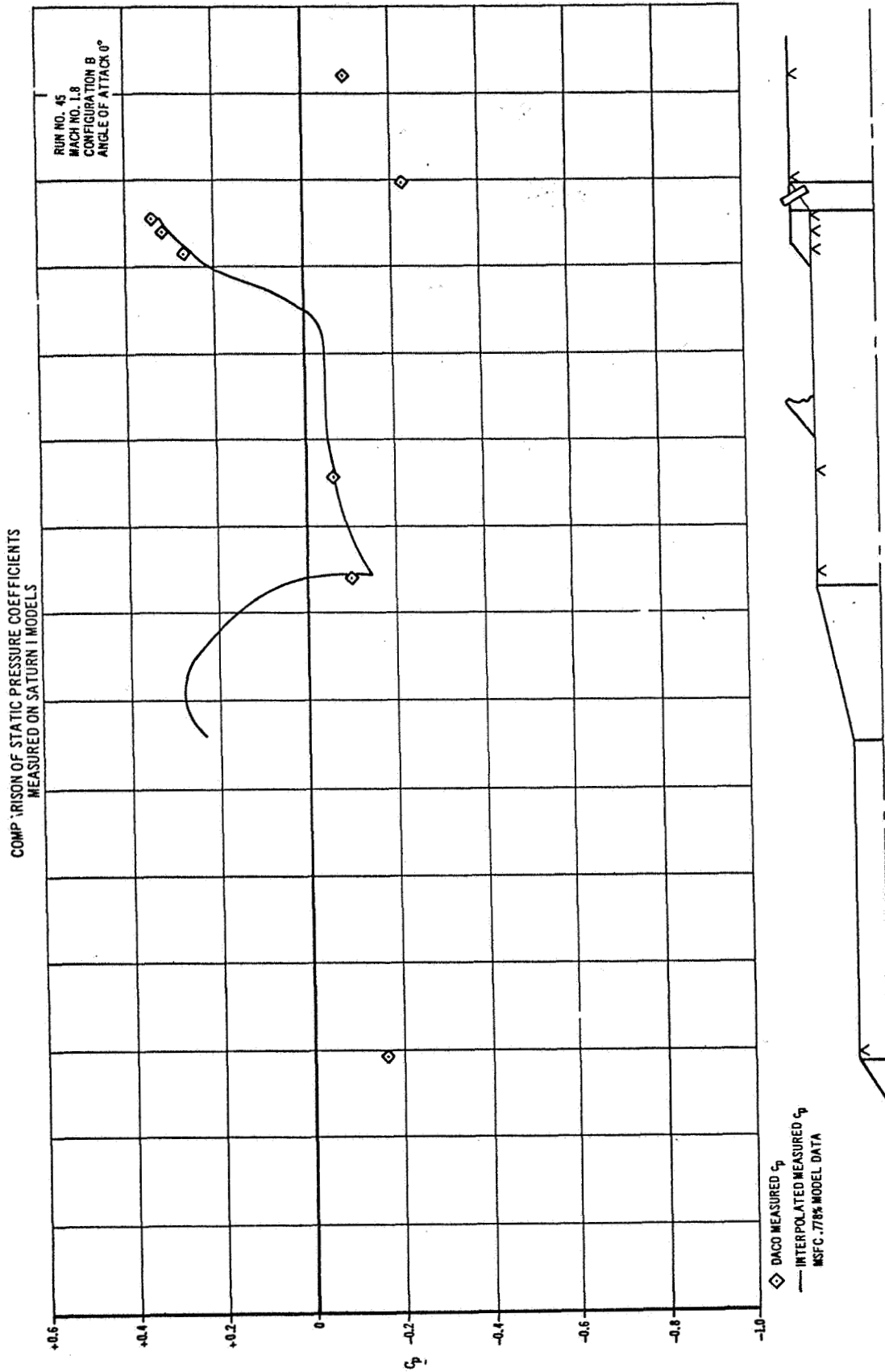


FIGURE 87

CONFIDENTIAL

CONFIDENTIAL

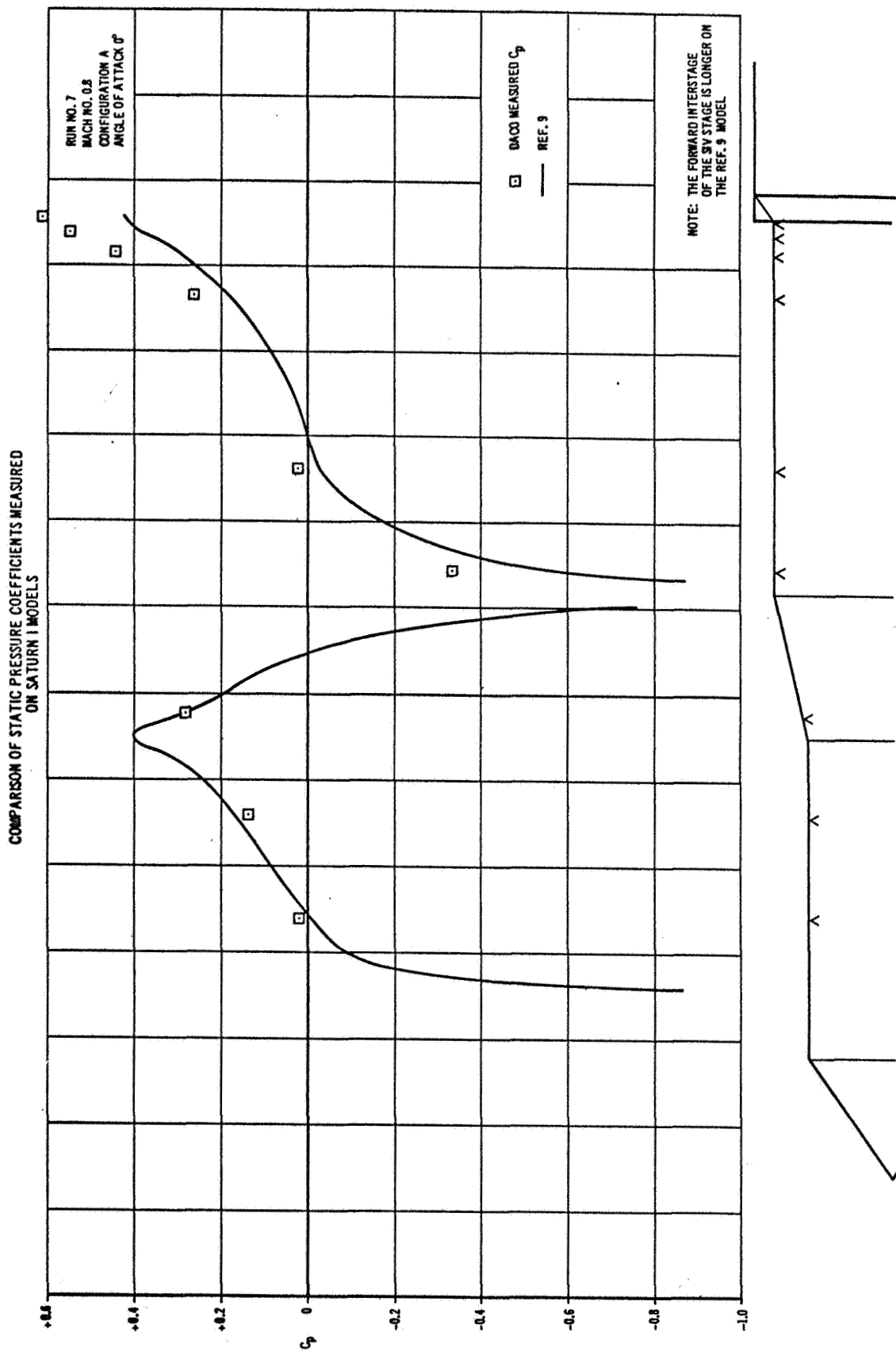


FIGURE 88

CONFIDENTIAL

COMPARISON OF STATIC PRESSURE COEFFICIENTS MEASURED
ON SATURN I MODELS

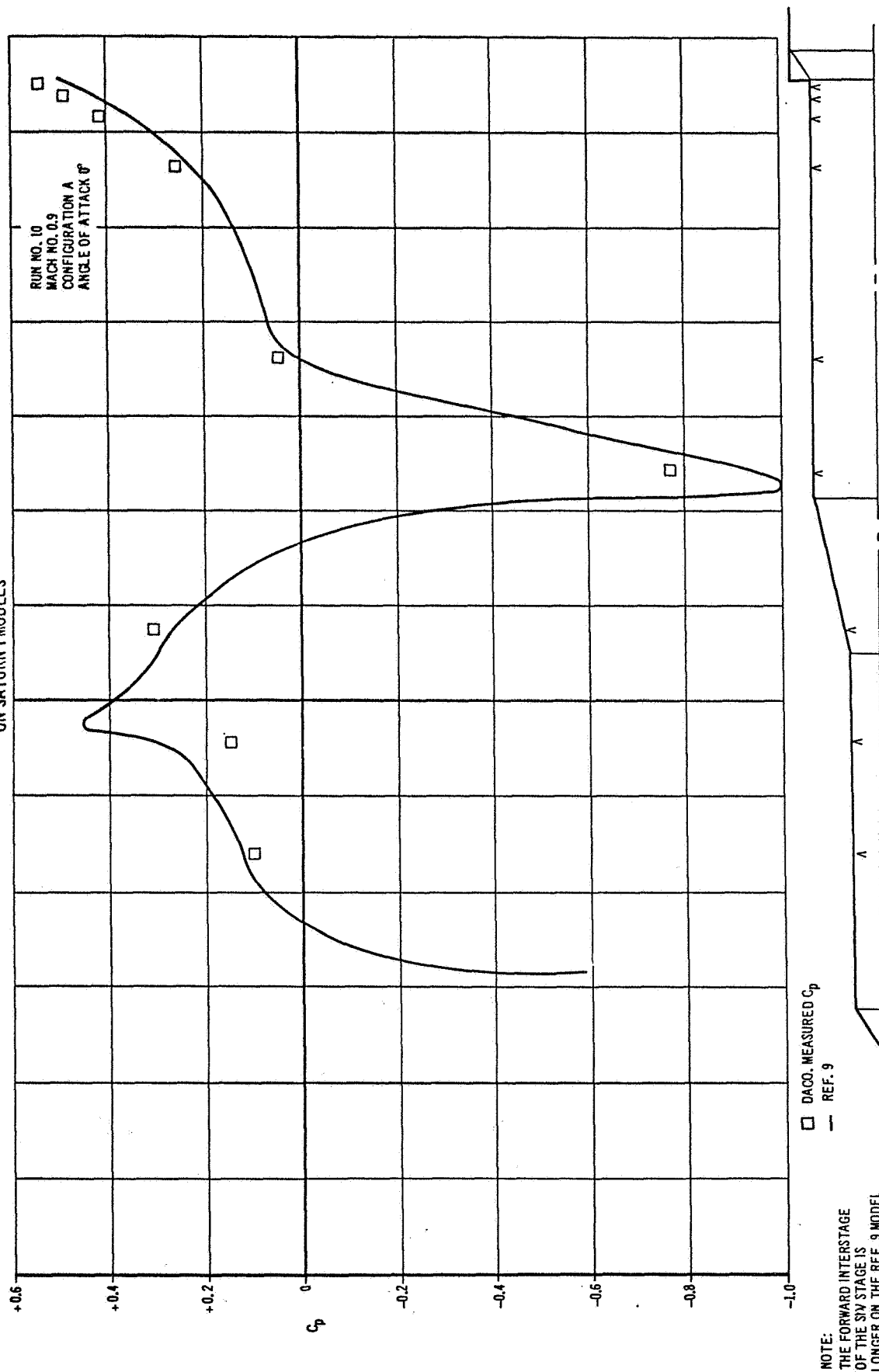


FIGURE 89

COMPARISON OF STATIC PRESSURE COEFFICIENTS MEASURED
ON SATURN I MODELS

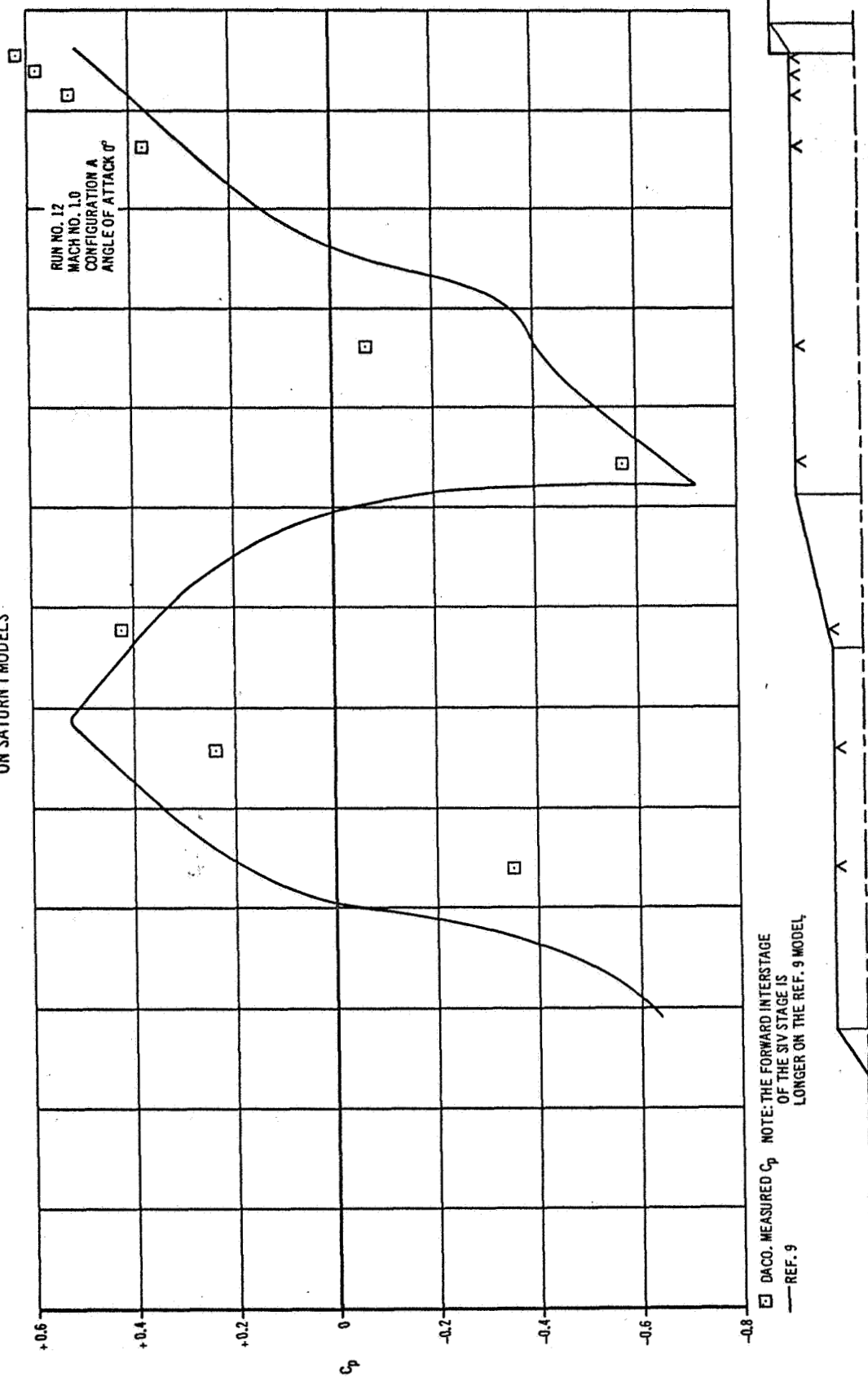
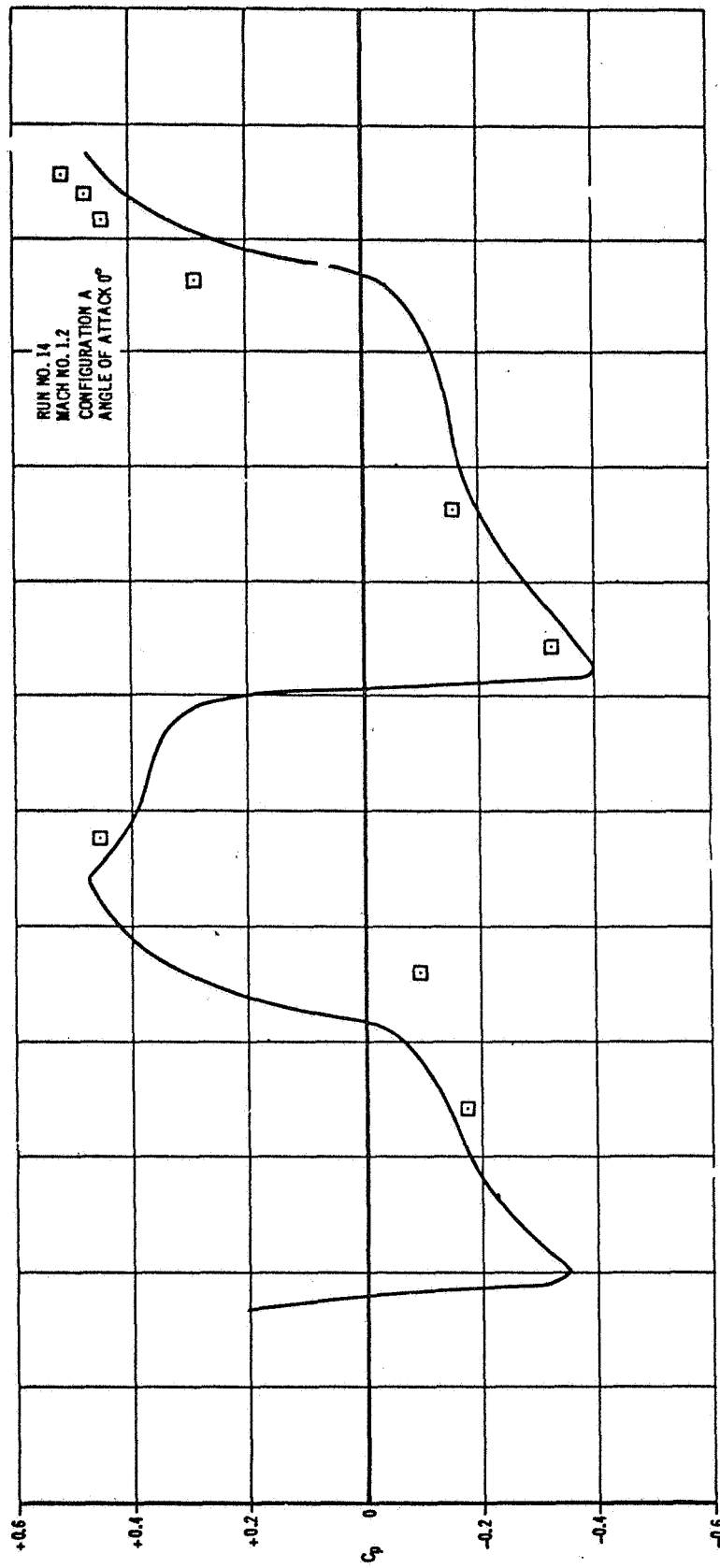


FIGURE 90

CONFIDENTIAL

COMPARISON OF STATIC PRESSURE COEFFICIENTS
MEASURED ON SATURN I MODELS



NOTE: THE FORWARD INTERSTAGE
OF THE SIX STAGE IS LONGER
ON THE REF. 9 MODEL

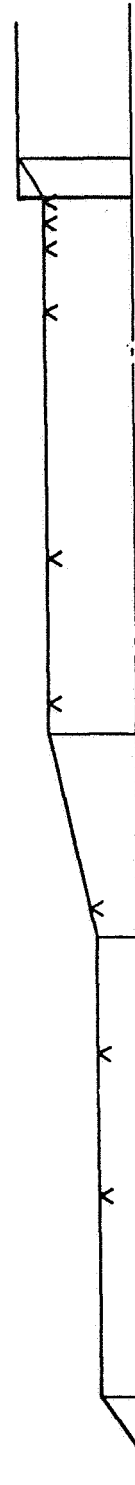


FIGURE 91

TYPICAL PRESSURE CALIBRATION OF AN LD 80-M1

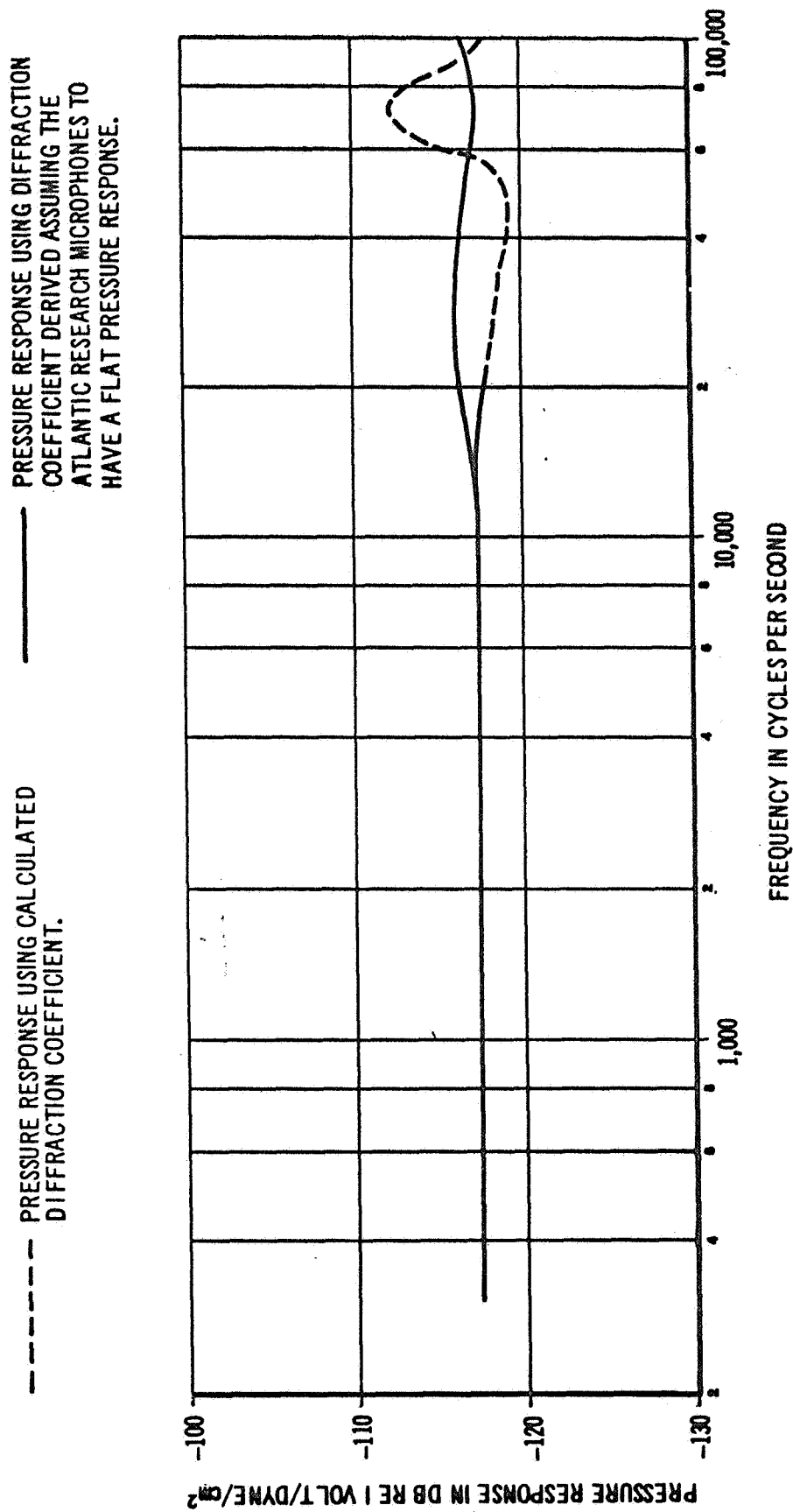
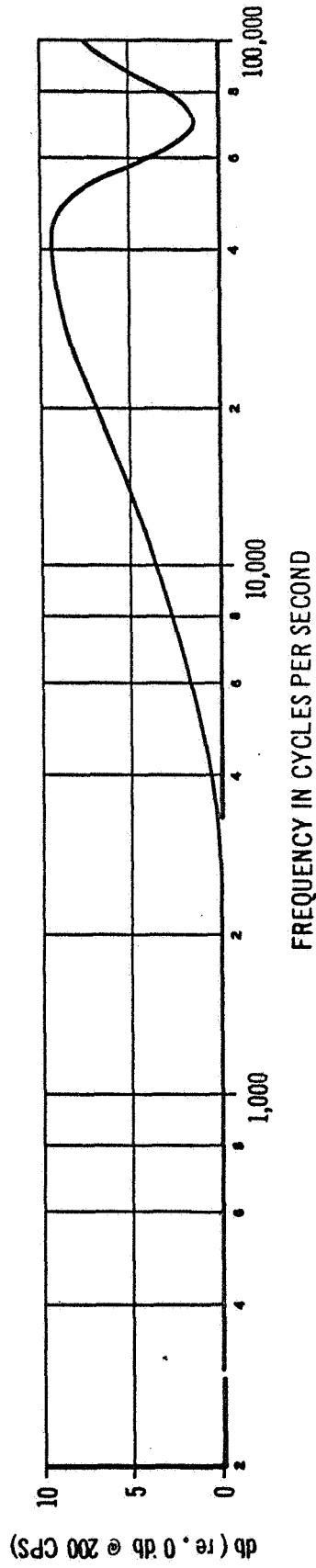


FIGURE 92

DIFFRACTION CORRECTION CURVES

CALCULATED DIFFRACTION COEFFICIENT OF THE ATLANTIC RESEARCH PRESSURE
TRANSDUCER TYPE LD80-MI



MEASURED DIFFRACTION COEFFICIENT ASSUMING THE "AVERAGE" ATLANTIC RESEARCH
TRANSDUCER HAS FLAT PRESSURE RESPONSE

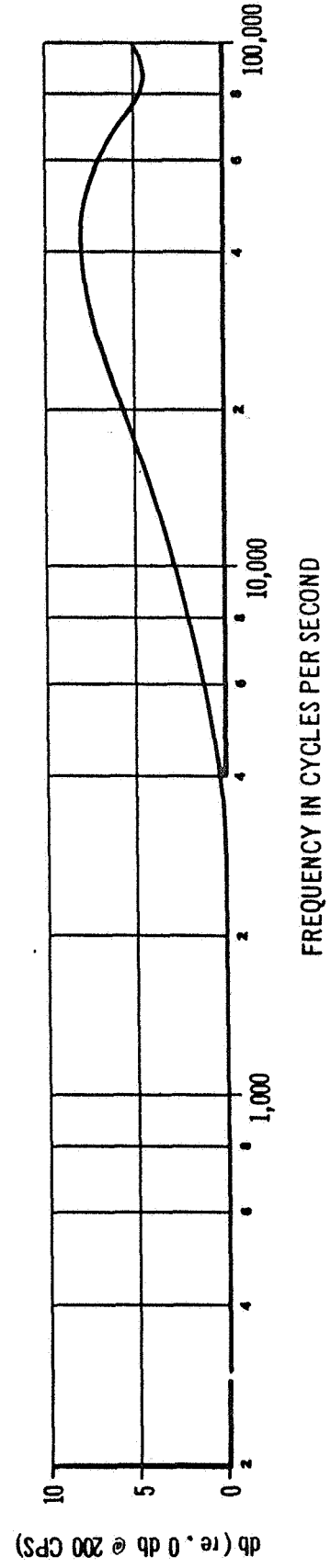


FIGURE 93

~~CONFIDENTIAL~~

DISTRIBUTION LIST

15 copies	NASA, Huntsville - Attention E. May, Aeroballistics
1 reproducible	
1 copy	DAC Aerophysics Lab
1 copy	Dr. J. S. Murphy
1 copy	J. K. Manhart
1 copy	C. M. Ailman
1 copy	Missile A2-260 Library
1 copy	File

~~CONFIDENTIAL~~



**MISSILE & SPACE SYSTEMS DIVISION
DOUGLAS AIRCRAFT COMPANY, INC.
SANTA MONICA, CALIFORNIA**